UNIVERSITA' DEGLI STUDI DI PADOVA

DIPARTIMENTO DI SCIENZE CHIMICHE

CORSO DI LAUREA MAGISTRALE IN CHIMICA INDUSTRIALE

TESI DI LAUREA MAGISTRALE

INVESTIGATING A SCALED-UP ELECTROLYSER FOR ACIDIC ELECTROCHEMICAL CO_2 REDUCTION TO FORMIC ACID

Relatore: Prof. Christian Durante

Correlatore: Prof. Dr.-Ing. Elias Klemm

Controrelatore: Prof. Valerio Causin

LAUREANDO: Carletto Alberto

ANNO ACCADEMICO 2022/2023

To my parents and my whole family.

Padova, 2023

Acknowledgements

Foremost I would like to express my gratitude to Prof. Dr.-Ing. Elias Klemm who allowed me to join the research group at the Institute of Technical Chemistry. I would like also to thank Prof. Christian Durante for allowing me to carry out this Erasmus+ experience.

I wanted to sincerely thank Marvin Oβkopp for helping me during my time in the lab and for supporting me in writing this work.

I also very much appreciate the kindly offered help of the ITC staff. In particular, I wanted to sincerely thank Andrea Loi who gave me numerous suggestions and hints for my work.

Last but not least I would like to thank my whole family for supporting me through my stay abroad, my studies and my entire life.

1. Contents

Table of symbols

Symbol	Unit	Meaning
a	$mol \cdot L^{-1}$	Activity
A	m^2	Surface area
C	F	Capacity
c	$mol \cdot L^{-1}$	Concentration
ρ	mS/cm	Conductivity
φ	V	Potential
φ^0	V	Standard potential
E or (EMF)	V	Electro motive force
F	$C \cdot mol^{-1}$	Faraday constant (F= 96.485 $C \cdot mol^{-1}$)
f	1	Excess factor
FE	1	Faraday efficiency
H	J	Enthalpy
I	A	Current
j	$A \cdot m^{-1}$	Current density
K_m	$m \cdot s^{-1}$	Mass transfer coefficient
m	g	Mass
n	mol	Mole number
Q	C	Charge
R	$J \cdot (mol \cdot K)^{-1}$	Molar gas constant (R=8.314 $J \cdot (mol \cdot K)^{-1}$)
R	Ω	Electrical resistance
S	$J \cdot K^{-1}$	Entropy
T	K	Temperature
t	s	Time
U	V	Tension
V	L	Volume
V_m	$L \cdot mol^{-1}$	Molar volume
X	1	Number
Z	1	Charge number
Δ	Variable	Difference
ε	$A \cdot s \cdot (V \cdot m)^{-1}$	Dielectric constant
ε	$A \cdot s \cdot (V \cdot m)^{-1}$	Electric field constant
υ	1	Stoichiometric coefficient
$Ø$	m	Diameter

List of abbreviations

AB	Acetylene Black
CCE	Constant Current Electrolysis
CD	Current Density
CE	Counter Electrode
CEM	Cation Exchange Membrane
CO_2RR	CO_2 Reduction Reaction
CP	Clamping Pressure
DG	Double gap
DLR	German Aerospace Centre (German: Deutsches Zentrum für Luft- und Raumfahrt)
E	Potential
ECSA	Electrochemically Active Surface Area
ECE	Energy Cathode Efficiency
EE	Energy Efficiency
EMF	Electromotive Force
FA	Formic Acid
FE	Faraday Efficiency
FF	Flow Field
FR	Flow Rate
GC	Gas Chromatography
GDE	Gas Diffusion Elecrode
GDL	Gas Diffusion Layer
HER	Hydrogen Evolution Reaction
HPLC	High Performance Liquid Chromatography
IHP	Inner Helmholtz Plane
ITC	Institute of Technical Chemistry
LCR	Linear Current Ramp
MEA	Membrane Electrode Assembly

MFC	Mass Flow Controller
MFM	Mass Flow Meter
MPL	Microporous Layer
NHE	Normal Hydrogen Electrode
OER	Oxygen Evolution Reaction
OCP	Open Cell Potential
OHP	Outer Helmholtz Plane
PTFE	Polytetrafluoroethylene
RDS	Rate Determining Step
RE	Reference Electrode
SHE	Standard Hydrogen Electrode
TC	Three-Compartment
TGA	Thermogravimetric Analysis
TZG	Total Zero Gap
U	Undivided
WE	Working Electrode
ZGA	Zero Gap Anode
ZGC	Zero Gap Cathode

2. Introduction

Carbon dioxide is a very stable molecule with limited applicability and a main role as waste product, for these reasons it is often entitled as 'carbon graveyard'. Nevertheless, it still finds applications in several industrial branches such as beverages, oil & gas or chemicals production.

In the last decades, CO_2 has been increasingly known also for its central role in climate change and nowadays, the main contributors to its emissions can be identified as the energy production and the industry sector.[1]

With the predicted increase of human population, energy demand is expected to rise from the current 22536 TWh to 35407 TWh in 2040.[2] In anticipation of this, it is important to limit the increase of greenhouse gas emissions which could lead to a global average temperature up to 2°C and catastrophic effects on the environment. Different countries are moving towards the carbon neutrality, but great strides still need to be made both in developed and developing countries.

In 2019 over 70% of the European energy stemmed from non-renewable sources, of which 48% represented by solid fuel and oil, mainly imported by the Russian federation.[3] Also, with the 2022 Ukrainian war, the necessity of an EU energetic independency was put in the spotlight again. For these reasons, a switch from fossil fuels to alternative sources is highly necessary. Different paths could be taken into consideration in order to reach such target. A possible convenient and efficient solution is adopted by France where in 2016 more than 70% of the energy demand was satisfied using nuclear power plants. Moreover, the definition of nuclear as renewable source could be debated due to its radioactive threat and waste products. In addition, the nuclear fission still involves the supply of uranium of which France, as well as most of the EU countries, are not in possession, thus hindering the energetic autonomy.[4]

Raw material availability and absence of toxic waste make renewable sources such as wind and solar very promising. On the other hand they do not deliver a constant energy output, unlike nuclear and fossil sources. Their energy production is strictly correlated with the presence of wind, light and so characterized by the weather variability. To overcome this problem, energy storage could be a decisive solution as it would allow to manage the intermittencies, through the accumulation of energy when supply is higher than demand. Different technologies are nowadays being studied for that reason. Energy storage technologies could take advantage of gravity, kinetic or pressure. A common example is the use of dams where water can be pumped from valley to higher altitudes in order to let it gain potential energy, eventually converted into electricity whenever needed through the use of turbines. On the other hand, to reach high energy amounts, dams usually necessitate big areas which could represent a problem both from a practical and an environmental point of view. As a result of that, different solutions are proposed in order to avoid the need of such big spaces. Some interesting ones are given by Gravity power and ARES where an underground system and a mass-lifting crane are used with the goal of accumulating potential energy and avoid the encumbrance of the dam.[5] Gravity storage systems are nowadays already on the market with storage capacities up to 25 MWh.[6]

Concerning the chemical-based accumulators, common Li-ion batteries could not be used for such amounts of energy, due to extremely high costs and flammability dangers that arise from Li itself. Because of that, alternative batteries are studied. An example is represented by the Ambri® technologies which uses liquid metals such Ca alloy and Sb particles to create big scale batteries that could store up to 1000kWh, 250 kW. The use of such metals is revolutionary both from an economic and safety point of view.[7]

Beyond that, industries such ammonia or concrete production cannot limit their CO_2 emissions since the processes themselves make use of carbon containing species and innovative routes are still too expensive either not possible.[8,9] To meet the new environmental policies a possible strategy would be to change the role of carbon dioxide from a harmful waste to a valuable resource by reducing it into alternative products which could be eventually used as long-term energy storage. This approach could be employed to store otherwise wasted energy excesses from renewable sources when supply exceeds demand. For that purpose the main products of carbon dioxide reduction reaction (CO_2RR) could be listed as: syngas ($CO+H_2$), ethylene (C_2H_4), methane (CH_4), ethanol (C_2H_5OH) and formate/formic acid ($HCOO^-/HCOOH$).[10] The higher the exchange of electrons required to obtain a certain product, the more complex is the reaction pathway.

Currently, many studies are conducted on this topic due to the recent stance against the global warming threat. Proof of this, is the recent European Horizon funding which allows the leading of different research for future innovations.

This work itself aims to give a small contribution to one of these European projects, entitled eForFuel (*Figure 2.1*) and conducted at the Institute of Technical Chemistry (German: Institut Für Technische Chemie - ITC) department of the Stuttgart University. In detail, the programme attempts to develop an alternative to fossil based fuels. This entails the necessity of combining different disciplines such chemistry, biology and engineering to design a competitive and sustainable process from which industries, distinguished by high CO_2 emissions, could take advantage in order to decrease their carbon footprint.

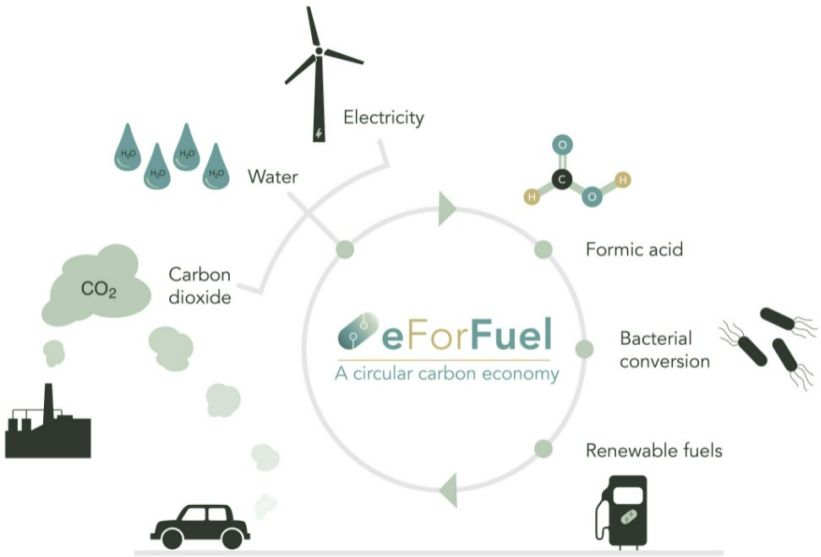

Figure 2.1. eForFuel project scheme. The image was taken form web.[11]

While the state of the art already shows an increase of interest towards the CO_2RR, in order to reach the industrial application, further studies need to be conducted. The subject areas which need to be deepened for future larger scale applications can be grouped in three main points:

1) Catalyst: the derivation of more active, selective and cheap catalysts to decrease high activation barriers
2) Scalability of the process
3) Higher production rates with the possibility to operate at continuous modality[12]

As part of the project, the present work wants to investigate these three topics with a focus on the acidic electrochemical CO_2 reduction to formic acid (FA). It is essential to operate at low pH since, when an alkaline environment is adopted, formate salts are obtained instead and an additional acidification process would be necessary. Furthermore, at high hydroxide concentrations, the CO_2 is largely converted into carbonate by-products which necessitate of an ulterior acidification step in order to remove them. Such supplemental operations would, most likely, lead to a product loss with an overall lower efficiency of the process.[13]

Previous publications demonstrated the possibility to operate at pH lower than the pK_a of FA (pK_a=3.77) using an electrolyser with a geometrical surface area of 1 cm^2.[13] Devices of this size are still used in this work to investigate the properties of several catalysts. However, the central part of this thesis is the investigation of a scale up electrolyser with a geometrical surface area of 25 cm^2. This electrolyser was developed to investigate design parameters such as the cathode-membrane distance, the membrane-anode contact and the cation exchange membrane (CEM). Furthermore, various operation conditions such as concentrations, temperature and flow rate of the catholyte as well as the current density are varied. Both the design and operation parameters were examined with a batch mode as the electrolyte was recirculated. Finally, it was examined the possibility to operate with a continuous single-pass electrolyte as it could be of relevant importance for future industrial applications.

3. Electrochemistry basics

Electrochemistry is a broad field that has assumed more importance in the last years due to the spreading of electrical devices and the switch from fuel-based machine into electrical ones. In this chapter, electrochemistry basics will be summarised and explained in order to clarify some fundamental concepts.

3.1 Electrochemical reactions

The electrochemistry is a physical chemistry discipline which considers the processes where an electronic transfer is involved. As a first introduction, these aspects will be approached both in a thermodynamic and kinetic way.

The reactions taken into consideration when speaking of electrochemistry are the so-called 'redox reactions', characterised by an exchange of electrons. The general formula can be described as:

$$v_o O + ne^- \leftrightharpoons v_R R \tag{3.1}$$

Every redox reaction has a defined standard reduction potential which was defined by comparing it with the Hydrogen standard electrode, considered 0.00 V by definition.

These potentials are used in order to foresee how a reaction will proceed. Every potential can vary depending on the conditions in which we operate. This dependence is expressed by the Nernst equation:

$$\varphi = \varphi^\circ + \frac{RT}{nF} ln \frac{{a_o}^{v_o}}{{a_R}^{v_R}} \tag{3.2}$$

Where φ is the potential under the defined conditions, φ^0 is the equilibrium potential, R is the molar gas constant, n is the number of electrons exchanged during the process, F is the Faraday constant, T is the temperature, α_R and α_O are respectively the chemical activity of the reduced and oxidised species while υ indicate the stoichiometric coefficient of the involved species.

There are different type of cells but the underlying principle is always the same. The simplest cell which can be considered is composed by two connected electrodes positioned in two different compartments defined semi-cell (*Figure 3.1*). The electrodes are immersed into an electrolytic solution which can be either watery or not (the solution can be different in the two semi cell). In every case it is necessary to have a separator in order to make the mechanical separation possible and avoid the electrical separation. The most common separators are a saline bridge, a ionic conductive membrane or a diaphragm.

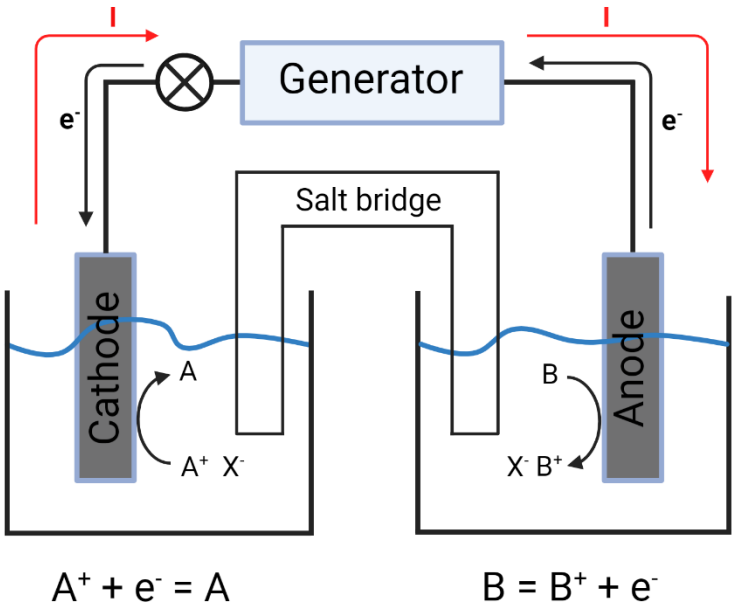

Figure 3.1 General scheme of a electrochemical cell.

When connected, the two electrodes are distinguished into cathode, where the reduction reaction happens, and anode, where the oxidation reaction happens. Because of that, the electrons flow from the anode to the cathode and the current I is defined as the number of electrons per unit of time:

$$I = \frac{dQ}{dt} \tag{3.3}$$

Where Q is the total charge and t is the time.

By convention the current flows in the opposite direction of the electrons.

In electrochemistry it is very common to use the current density j instead of the current value as it allow to more easily compare cells with different electrode areas.

$$j = \frac{I}{A} \tag{3.4}$$

3.2 Principle of Electrolytic and Galvanic cells

From the fundamental thermodynamic Gibbs equation:

$$\Delta_r G = T\Delta S - \Delta H \tag{3.5}$$

Where $\Delta_r G$ is the free Gibbs energy, T is the temperature, ΔS is the entropy and ΔH is the enthalpy.

It is known that a process can be considered spontaneous when $\Delta_r G$ is negative.

The free Gibbs energy can be expressed also through the formula

$$\Delta_r G = -nFE \tag{3.6}$$

Where n is the number of electrons, F is the Faraday constant and $\boldsymbol{E}$ is the electro motive force (EMF), which can be theoretically expressed as:

$$\boldsymbol{E} = \varphi_{cathode} - \varphi_{anode} \qquad (3.7)$$

The EMF value can be determined only at open circuit. A reaction is considered spontaneous when $\boldsymbol{E} > 0$.

In this case the system is able to produce energy work and the cell is defined a galvanic cell (*Figure 3.2b*).

The cell can run in the opposite direction too. Through a generator it is possible to apply an external potential ($\Delta\varphi_{ext}$) between anode and cathode. Depending on the voltage, the cell can operate in different ways:

- $\Delta\varphi_{ext} = \boldsymbol{E}$ in this case the system is in equilibrium. This determines a total current $I=0$
- $\Delta\varphi_{ext} > \boldsymbol{E}$ when the external potential is higher than E, the cell is an Electrolytic cell (*Figure 3.2a*)

The main features of the two cells are listed in the table below.

Table 3.1. Summary of the galvanic and electrolytic cell working conditions.

Characteristics	**Galvanic cell**	**Electrolytic cell**
Polarization	- Anode + Cathode	+ Anode - Cathode
Potential	$\Delta\varphi_{ext} < \boldsymbol{E}$	$\Delta\varphi_{ext} > \boldsymbol{E}$
Reaction	Spontaneous	Non spontaneous

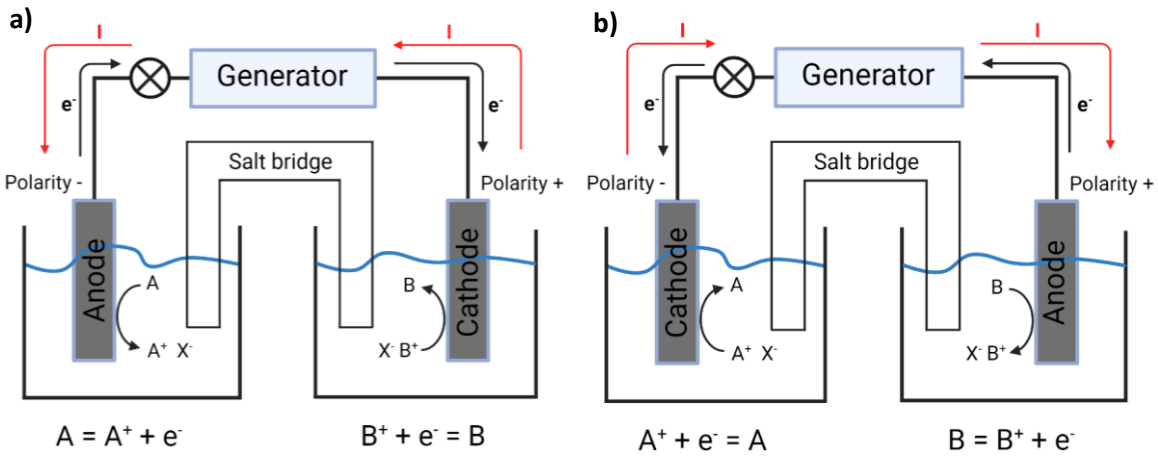

Figure 3.2 Schematic representation of a) a galvanic and b) an electrolytic cell.

3.3 Overvoltage

During the passage of current, the potential that we observe in a galvanic cell, either the potential that we have to apply in a electrolytic cell, is always higher (in absolute value) than the *EMF*. That implies: a higher potential needs to be applied in an electrolytic cell in order to make the reaction happen; a lower potential is generated by a galvanostatic cell.

The overvoltage is the result of many effects. A big part of it is the consequence of the resistance of the solution and the semi-reaction at the electrodes (it can be denoted as the resistance of the cell, R_{cell}).

It has been experimentally noticed that the potential which needs to be applied is much bigger than the sum of *EMF* and the total cell resistance (R_{cell}). This can be shown by an ideal polarization curve (*Figure 3.3*). It is noticeable that the observed curve does not reflect the theoretical one:

$$\Delta\varphi_{ext} = \boldsymbol{E} + IR_{cell} \rightarrow \quad I = \frac{\Delta\varphi_{ext}}{R_{cell}} - \frac{\boldsymbol{E}}{R_{cell}} \tag{3.8}$$

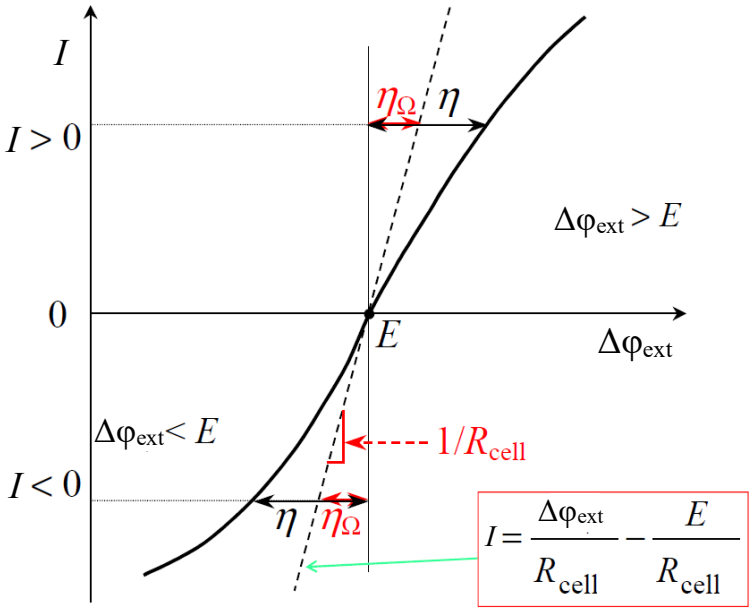

Figure 3.3 The polarization curve follow a different path from the one defined considering just the emf(E) and the resistance of the cell.

This indicates that the overall electrochemical reaction, which takes part on the surface of the electrode, can be very complex to define. In fact, it generally consists of different steps which, depending on the specific reactions, could be the cause of a process slowdown. (*Figure 3.4*)

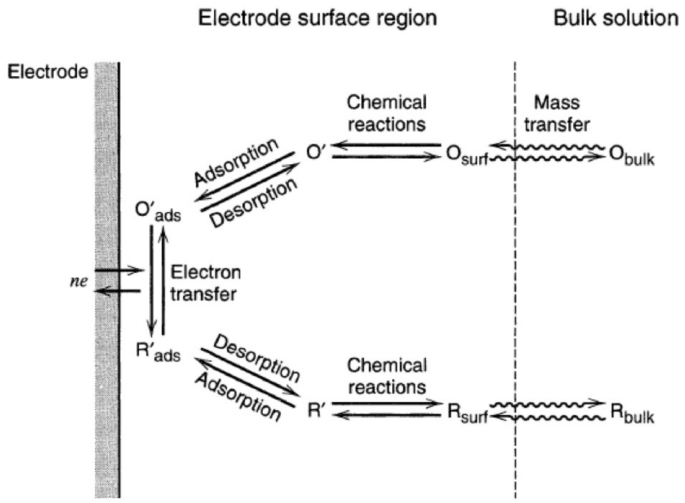

Figure 3.4 Processes which take part in the electrode surface. This image was taken from literature.[14]

Many aspects need to be considered, however in most cases, the additional overpotential (besides R_{cell}) is caused by: mass transport and charge transfer overpotential (or electron transfer). The complete overpotential equation can be rewritten as:

$$\eta = \eta_{\Omega} + \eta_{\mathrm{mt}} + \eta_{\mathrm{ct}} \tag{3.9}$$

Where:

a) η_{Ω} is the overpotential of the cell resistance R_{cell} (includes the resistances of solution, separator and electrodes materials).

b) η_{ct} describes the charge transfer overpotential and it is connected to the necessity of activating the species which take part in the reaction.

c) η_{mt} represents the slow mass transport - from the bulk to the electrode surface or vice versa - of the species involved. It can be depicted by three factors:

- diffusion, the motion of the particle is caused by a concentration gradient
- migration, the particles are moved by electrical field
- convection, the movement of the overall solution caused by the temperature or the movement of the electrode.

3.4 Butler-Volmer equation and Tafel slope

The overpotential and the total current are connected through the general formula η-I:

$$I = I_a + I_c = I_0 \times \left[\frac{C_R(0,t)}{C_R{}^*} exp\left(\frac{(1-\alpha)nF\eta}{RT}\right) - \frac{C_O(0,t)}{C_O{}^*} exp\left(-\frac{(\alpha)nF\eta}{RT}\right)\right] \tag{3.10}$$

Where I_0 is the exchange current (the current flowing on the system when $\eta=0$), n is the number of e^- taking part in the reaction, α is the transfer coefficient (values $0<\alpha<1$), $C_R(0,t)$ and $C_O(0,t)$ are the concentration of R and O species in proximity of the electrode surface and $C_R{}^*$ and $C_O{}^*$ are the concentration of O and R in the bulk.

Generally, one of the before mentioned processes is slower than the others and since its velocity will define the overall process speed, it is defined rate determining step (RDS). The most common RDS are depicted by mass transport and electronic transfer.

In the case RDS correspond to an electronic transfer, the concentration of *R* and *O* on the electrode surface are the same of the bulk. Consequently, the equation can be rewritten as:

$$I = I_a + I_c = I_0 \times \left[exp\left(\frac{(1-\alpha)nF\eta}{RT}\right) - exp\left(-\frac{(\alpha)nF\eta}{RT}\right)\right] \quad (3.11)$$

This equation is known as Butler-Volmer equation, and it is valid only for an electron-transfer controlled process.

For high values of $|\eta|$, either the anodic and cathodic contribution can be removed thus obtaining the cathodic and anodic Tafel equations respectively:

Anodic $$\eta = -\frac{2.303RT}{n(1-\alpha)F} log\ I_0 + \frac{2.303RT}{n(1-\alpha)F} log\ |I| \quad (3.12)$$

Cathodic $$\eta = \frac{2.303RT}{n\alpha F} log\ I_0 - \frac{2.303RT}{n\alpha F} log\ |I| \quad (3.13)$$

It can also be described as:

$$\eta = a + b\ log\ |I| \quad (3.14)$$

Where a is a constant and depends only by the equilibrium current while b represent the actual slope gradient of the Tafel curve.

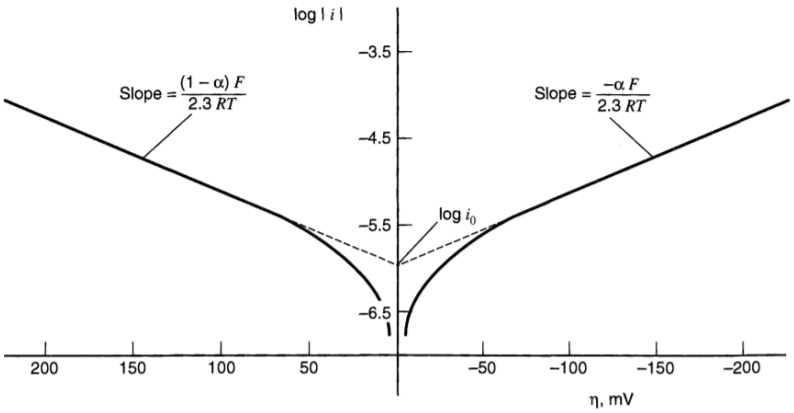

Figure 3.5 Representation of a generical Tafel slope.[14]

It is possible to obtain information regarding the mechanism and the kinetic of the process only if the reaction meets determined prerequisites such electron transfer control, high values of overpotential and a single step mechanism.

Observing the slope value it is possible to obtain information regarding RDS reaction's mechanism such the number of electrons exchanged during the RDS process.[15]

3.5 Electrochemical double layer

As previously mentioned, the electrode-solution interface is a complex structure which influences the mass transport, kinetic and mechanism of the reaction which take place.

Different models were presented in order to have a wider view on the reaction limits. Nowadays the most accurate one was defined by Bockris, Devanathen and Muller.[16] The peculiar aspect of this model is that the presence of a polar solvent on the electrode surface is taken into consideration (*Figure 3.6*).

In the electrode surface, a layer of properly polarised solvent molecules is present. Some of them can be replaced by specifically adsorbed ions with the same electrode charge, partially or not solvated. This first layer is defined as Inner Helmholtz Plane (IHP). More externally, solvated ions are positioned forming the so called Outer Helmholtz Plane (OHP). Unlike IHP ions, they have an opposite charge to that of the electrode. IHP and OHP together represent the compact double layer: an area in which the particles are positioned at a fixed distance from the electrode. It can be schematised as a capacitor with a capacitance (C) of:

$$C = \frac{Q}{\Delta\varphi} \qquad (3.15)^{17}$$

Where Q is the charge at the interface and $\Delta\varphi$ is the interface potential difference.

Outside the OHP, the ions can diffuse freely while being subjected both from the thermic agitation and the electrical field. As consequence of such ions distribution, the interface area potential is not homogeneous but, as indicated in *Figure 3.6*, it varies linearly inside the double layer while it gradually decreases outside the OHP.

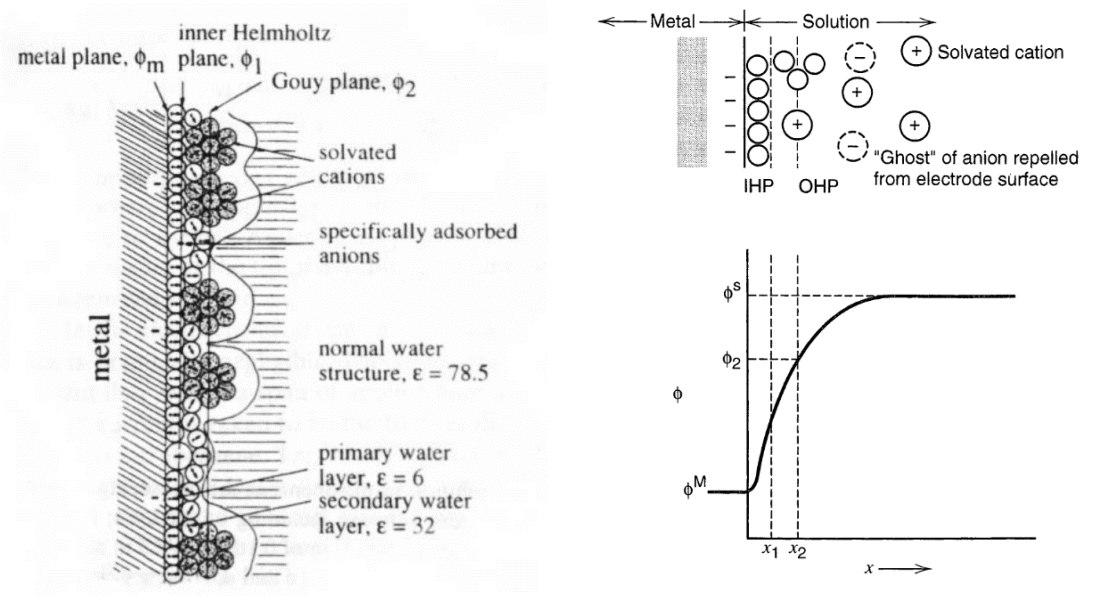

Figure 3.6 Bockris, Devanathen and Muller model sketch and potential profile in proximity of the interface electrode-solution in absence of specific adsorption ions. The images were taken from literature.[14,18]

3.6 Two and three electrode system

On the previous cell illustrations, only the total cell voltage could be measured.

In order to measure a semi-cell potential only, a third electrode need to be connected. This system takes the name of three-system electrode, and it is composed by: Working electrode (WE), Counter Electrode (CE) and Reference Electrode (RE). (*Figure 3.7*)

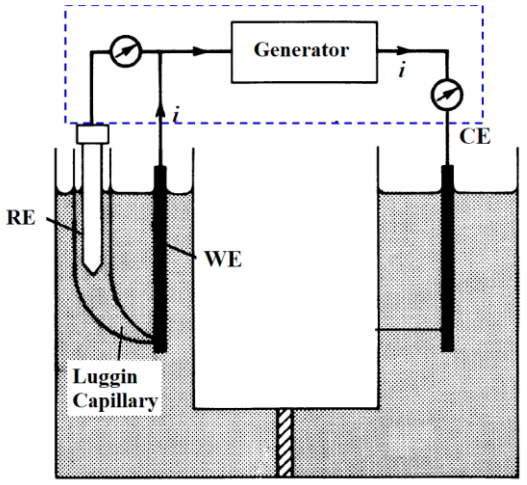

Figure 3.7 General scheme of a three-system electrode. The WE and the RE need to be positioned very close in order to reduce the resistance of the solution. Sometimes particular tools as the Lugging Capillary are used for that purpose.

Between WE and CE a certain potential is applied in order to ensure the reaction of interest, mostly located at the working electrode. In that case, the RE is dipped in the same WE solution and it is not crossed by any current. Because of that, RE potential is constant, making any variation attributable to the WE. As consequence:

- if $I=0$, the potential measured between WE and RE represents the WE equilibrium potential against RE ($\varphi^0_{cath\ vs\ RE}$)
- if $I\neq0$, the potential measured between WE and RE represents the WE potential at a non-equilibrium condition ($\varphi_{cath\ vs\ RE}$)

Now, considering the semi-reactions to happen separately, the total overpotential could be rewritten as:

$$\eta = \eta_{\Omega,S} + \eta_a + \eta_c \tag{3.16}$$

Where $\eta_{\Omega,S}$ refers to the solution and separator contribution while η_a and η_c are the anodic and cathodic contributes which consider the global processes and electrodes materials resistances.

By using the three-electrode system, η_a and most of $\eta_{\Omega,S}$ contributes could be excluded allowing to measure η_c only:

$$\eta_c = \varphi_{cath\ vs\ RE} - \varphi^0_{cath\ vs\ RE} \tag{3.17}$$

Nevertheless, a small amount of solution between WE and RE is still present and act as a resistance *(Figure 3.8)*. For this reason, WE-RE distance need to be reduced in order to decrease its ohmic drop $\eta = IR$. This can be achieved by using specific tools such the Lugging Capillary *(Figure 3.7)*. Generally, in more recent instruments (e.g. Gamry® potentiostat) a current interrupt method could be used instead. That can be conducted only by using a potentiostat equipped with a circuit which can rapidly turn on and off the current flow. This method consists in measuring the cell voltage immediately before and after the current interruption. While the WE could be conceived as a capacitor, the WE-RE solution is the equivalent of a single resistance ($R_{WE\text{-}RE,solution}$). Therefore, since the WE capacitor can hold the voltage, the difference between the voltage before and after the current interruption corresponds to the overpotential caused by the solution.[19]

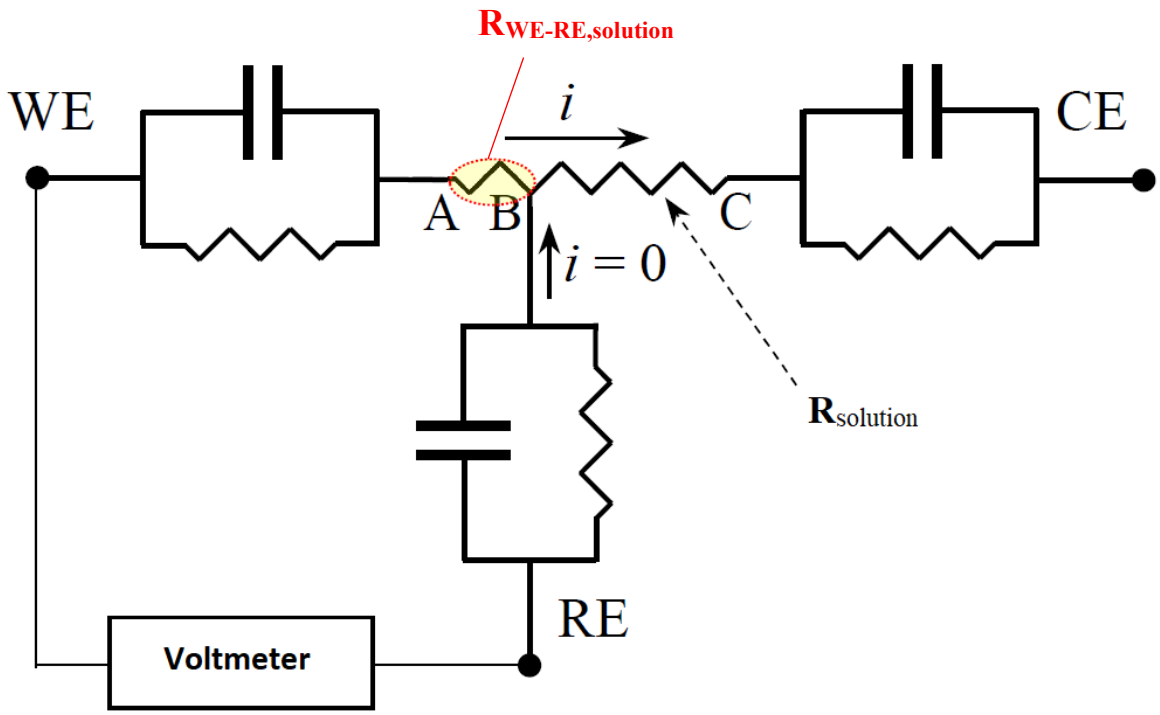

Figure 3.8 The three electrodes are represented as a resistance and a capacitor in parallel. The solution is represented as a resistance. Part of this resistance (yellow one) affect the potential measured between the WE and RE.

3.7 Faraday efficiency and Energy efficiency

The efficiency of the cell is generally described through different parameters, among which the Faraday Efficiency (FE) also called current efficiency.

For CO_2RR as for other electrochemical reactions, the Faraday efficiency (FE) 'is defined as the ratio of the experimentally detected amount of objective product to the amount of theoretically generated product'.[20] It can be calculated through different formulas depending on the analysis conducted. The generic formula could be expressed as:

$$FE = \frac{n \cdot z \cdot F}{Q} \quad (3.18)^{21}$$

Where n is the moles of product detected; Q is the total charge passed through the system, recorded during the electrochemical operation; F is the Faraday constant; z is the number of electrons required to obtain 1 molecule of the product.

However, the Faraday efficiency does not take in account the energy needed to make an electrochemical reaction happen. For that reason, it might be important to take into account the energy efficiency (EE) defined as:

$$EE = \frac{\varphi^0_{cell}}{\varphi_{cell,actual}} FE \quad (3.19)^{12}$$

Where φ^0_{cell} is the standard potential given by thermodynamics and $\varphi_{cell,actual}$ is the actual cell voltage.

When a three-electrode system is used, the energetic cathode efficiency (ECE) can be used instead as it allow to focus on the cathodic compartment independently of the anode reaction. In this case the equation is described as:

$$EE = \frac{\varphi^0_{cathode\ vs\ RE}}{\varphi_{cathode\ vs\ RE}} FE \quad (3.20)^{9}$$

Where $\varphi^0_{cathode\ vs\ RE}$ is the standard cathode potential given by thermodynamics and $\varphi_{cathode\ vs\ RE}$ is the measured cathode potential.

4. State of the Art

4.1 CO_2RR

4.1.1 Mechanism

Due to the high potential needed to reduce CO_2, the absence of a metal catalyst generally lead to parasite electrochemical reactions.[22] Also, the CO_2 thermodynamic stability and kinetic inertness, make its reduction energetically expensive.[23,24] For these reasons, a catalyst is essential in order to shift the reaction towards the desired products and lower the energy costs of the process.

CO_2RR can lead to different products depending on the operating conditions and catalyst. The main products and their relative standard potential φ^0 (pH 7 and T=25°C) are listed hereby:

$$CO_2 + H_2O + 2\,e^- \rightleftharpoons HCOO^- + OH^- \qquad -0.43 \text{ V vs SHE}^{25} \quad (4.1)$$

$$CO_2 + H_2O + 2\,e^- \rightleftharpoons CO + 2\,OH^- \qquad -0.53 \text{ V vs SHE}^{25} \quad (4.2)$$

$$CO_2 + 6\,H_2O + 8\,e^- \rightleftharpoons CH_4 + 8\,OH^- \qquad -0.25 \text{ V vs SHE}^{25} \quad (4.3)$$

In accordance with their product selectivity, the catalyst metals can be grouped as showed in *Table 4.1*.

Table 4.1. CO_2RR catalysts grouped by product formation.[25]

Catalyst metal	Main product from CO_2RR
Cu	alcohols and hydrocarbons
Au, Ag, Zn, Pd and Ga	Carbon monoxide (CO)
Pb, Hg, In, Sn, Cd, Tl and Bi	$HCOOH/HCOO^-$ with small amounts of H_2
Ni, Fe, Pt and Ti	No or little amounts of product

In addition to the mentioned reactions, a hydrogen evolution reaction (HER) could also occur. It represents the main parasite reaction as its potential falls within the CO_2RR potential range.

$$2H^+ + 2e^- \rightleftharpoons H_2 \qquad -0.41 \text{ V vs SHE}^{25} \quad (4.4)$$

In order to improve the catalyst performances, it is essential to understand the mechanistic aspect of the reaction and which species interact with the carbon dioxide. Regarding the HCOOH formation, we can classify three groups of catalyst according to the action performed by their relative oxide species[26]: oxide active catalysts (Sn, In, Tl, Cd, Hg)[25]; oxide buffered materials (Pb) and oxide-independent (Bi).

Tin and Bismuth based catalysts are of particular interest, due to their low toxicity and price compared to the others.[9,28,29]

Table 4.2 List of the current metal prices (2021-2022)[28]

Metal	Price $/Kg
Bismuth	8.04
Tin	34.17
Indium	215.00
Lead	2.30
Cadmium	2.49

a) Tin based catalyst

When there is no CO_2 limitation, Sn exhibits a ~90% and ~10% product selectivity towards HCOOH and CO, respectively.[25] In more recent analysis it has been observed that the reaction occurs on its oxide layer instead of metallic Sn, since the metal tends to form a passivation oxide layer when exposed to atmospheric oxygen.[30] The passivation layer is generally composed of Sn(II)O and Sn(IV)O_2 species indicated as SnO_x (where x=1, 2).[31,32]

The established mechanism for the CO_2RR was the formation of a $CO_2^{\bullet-}$ radical with a single electron transfer as first reaction and RDS, catalysed by the metallic Sn.[33] Most of the time this consideration was done by looking at the Tafel slopes. As mentioned in *Chapter 3.4*, the number of electrons exchanged during the RDS can be extracted from the slope of the Tafel curve when the prerequisites of: electron transfer control, high values of overpotential and single step mechanism are met. Nevertheless, the slopes observed in different researches showed divergent values of 60 or 120 mV/dec for the $HCOO^-$ production via SnO_x catalyst. At 60 mV/dec the RDS is described as the protonation of the $CO_2^{\bullet-}$ radical after a reversible transfer of one e^- to CO_2[34] while a 120 mV/dec slope define the RDS as the electron transfer to CO_2.[33] In addition, it has to be noticed that the number of exchanged electrons could actually indicate several reactions making the Tafel slope analysis frivolous.[35]

Further research was conducted to investigate the role of Sn and SnO_x during a CO_2RR catalytic process.[32,36,37] A metallic Sn surface was obtained by chemically etching the SnO_x surface through a strong acid (HBr or HCl).[32,38,39] At a potential range from -0.5 to -0.7 V (vs Ag/AgCl) a maximum formic acid faraday efficiency (FE_{FA}) of ~40%, for the SnO_x and ~20% for the Sn, was reached.[32,39] Zhang et al.[38] analysed it at a more negative range of potential, from -1.6 to -2.0 V (vs Ag/AgCl), observing a higher selectivity towards FA with FE_{FA} values >90% with the SnO_x and ~40% with the Sn. Such results demonstrated the central role of SnO_x for the HCOOH selectivity.[9,22,37,39,40]

This research was later deepened by Baruch et al.[31] where, in their analysis, a thin layer of mixed Sn/SnO_x was deposited into a ZnSe optical disk and in situ analysed through an ATR-IR in order to describe the mechanism of the CO_2 reduction reaction. The results showed a voltammetry peak at -1 V vs SHE without the presence of carbonate. This, was attributed to the reduction of SnO_2 into SnO/Sn(II) oxyhydroxide through the acceptance of 2 e^-. After that, the CO_2 could easily get adsorbed into the surface of the electrode, creating a tin-carbonate bond. The tin oxyhydroxide was then able to transfer the two electrons to the carbon in order to obtain formate which, followed by a protonation, led to a desorption of formic acid into the solution (*Figure 4.1*).

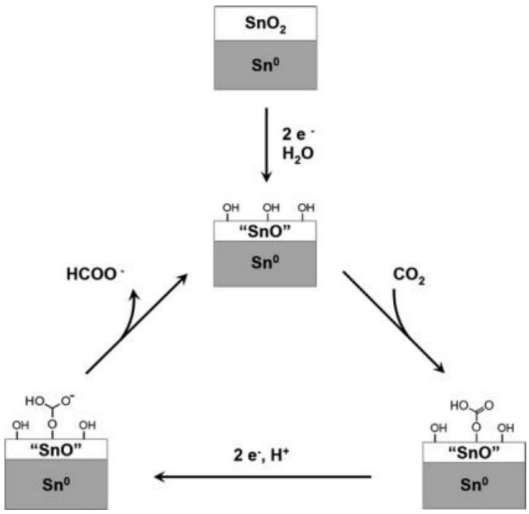

Figure 4.1 Mechanism of CO_2RR mechanism on SnO_x. The image taken from literature.[31]

b) Bismuth based catalyst

As for Bi-based catalyst, the product selectivity is shifted towards 91 to 100% FA depending on the Bi oxidation state and the applied voltage.[29]

It was noticed that the amount of Bi oxide species does not play a key role in the HCOOH formation. This was proved by Pander et al.[26] who conducted an ATR-IR measurement on a ZeSe crystal.[31] The presence of different quantities of Bi_2O_3 on the electrode surface caused no variation on the FE_{FA}.[26,41] In addition, no intermediate was observed, indicating that the CO_2RR process follows a different pathway than Sn. In detail, it appears that Bi_2O_3 get quickly oxidised to metal Bi^0 where the CO_2RR actually occur.[26]

Concerning the mechanism of CO_2 reduction in presence of Bi-based catalyst, it did not receive the same attention as for the Sn. C.C. Miao[42] and Qiu et al.[41] sought an interpretation through a Tafel slope analysis. Still, the slopes showed different trends depending on the catalyst morphologies. That made the interpretation of the mechanism misunderstandable over this path. In parallel, ATR-IR analysis proposed an alternative CO_2RR mechanism[26]:

$$Bi^0 + H^+ + e^- = Bi^0\text{-}H_{ads} \quad (4.5)^{26}$$

$$Bi^0\text{-}H_{ads} + CO_2 + e^- \rightarrow Bi^0 + HCOO^- \quad (4.6)^{26}$$

Competing with HER:

$$Bi^0\text{-}H_{ads} + Bi^0\text{-}H_{ads} \rightarrow 2\ Bi^0 + H_2 \quad (4.7)^{26}$$

A RDS was not defined.

4.1.2 Catalyst oxide layer degradation and pH dependence

Both Sn- and Bi-oxides are subjected to degradation during the CO_2RR process. The degradation rate depends by different factors, in particular: the pH, the potential, and the temperature at which the reaction is conducted. As we can see from the Pourbaix diagrams *(Figure 4.2),* per each condition, we can identify a more thermodynamically stable species. Nevertheless, this does not necessarily involve a relevant transformation since the reaction could be kinetically slow.

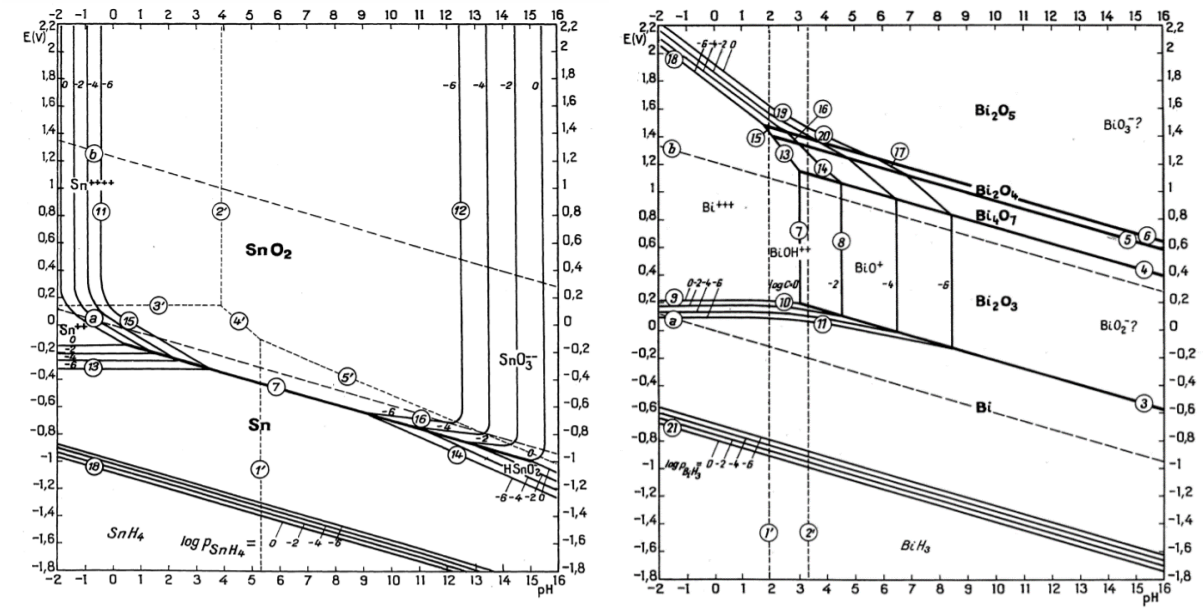

Figure 4.2 Pourbaix diegram of Sn and Bi. The images were taken from literature.[43]

The range of potential in which the majority of CO_2RR experiments are conducted varies from -0.4 to -2.0 V (vs SHE). In this region, the Pourbaix diagram shows that the SnO_2 is not stable and tends to get reduced into its thermodynamically stable form Sn^0 through the reaction:

$$SnO_2 + 2H_2O + 4e^- = Sn^0 + 4\ OH^- \qquad (4.8)^8$$

Since the SnO_2 is the only active specie for the FA production, its degradation implies a decay of FE_{FA} and an increase of HER.[32] This results in a limitation for SnO_x electrodes, especially in long-term experiments.[8]

Bi_2O_3 is subjected to degradation too, since the thermodynamically stable species in the CO_2RR voltage range, are the metallic Bi and the BiH_3. Nevertheless, 'the gaseous hydride BiH_3 appears to be a compound which is thermodynamically unstable and which tends to decompose into bismuth and hydrogen; this is actually observed in practice.'[43]

Bi_2O_3 get quickly reduced to Bi^0 through the reaction:

$$Bi_2O_3 + 3H_2O + 6\ e^- = 2\ Bi^0 + 6OH^- \qquad (4.9)^{44}$$

Nevertheless, this does not represent a limit for the FA production as the CO_2RR appears instead to occur in metallic Bi.[26] Because of that, experiments with Bi_2O_3-GDE can proceed with stable FE_{FA} values in the long-term experiments too (from 12 to 24 h).[8,45] However, an increase of HER over time is inevitable also in this case.

Bienen et al.[8] supposed that the increasing HER could be caused by:

- a blockage of the GDE gas pathways with electrolyte or precipitated carbonate salts.

- an increase of the GDE wetting which translates in longer electrolyte pathways and increasing local pH as well as formate concentrations. During a galvanostatic experiments (*j*=constant) this could determine a shift of the potential to less negative values which promotes the development of side products such as H_2.

Nevertheless, 'the approach to use Bi_2O_3 GDEs was not able to completely deconvolute the impact of catalyst alteration and GDE wetting onto the degradation mechanisms to safely identify the mainly responsible phenomenon.'[8]

4.2 GDE

The CO_2 is characterised by a limited solubility of ~34 mmol/L (at T=20°C and P=1 atm) in aqueous electrolyte which could eventually translate into a mass transport limitation when high current densities are applied.[46] Since the CO_2 diffusion generally plays a role of *RDS,* it is possible to define the maximum current density (CD_{max}) that could be applied before observing an excessive evolution of parasite reactions such HER. This is derived from the combination of the Faraday law and the 1st Fick law:

$$j = \frac{C_{CO_2}}{\delta} \bullet D_{CO_2} \bullet z \bullet F \qquad (4.10)^9$$

Where D_{CO2} is the diffusion coefficient of CO_2, δ is the diffusion layer thickness and C_{CO2} is the concentration of CO_2 into the bulk solution. Depending on the electrode type, the diffusion layer thickness could vary considerably with a significant impact on the CD_{max} and product selectivity. For the planar electrodes δ assume a value of ~50 µm[10] from which it can be derived the relative limit CD_{max} of just ~10 mA/cm^2 (at standard conditions).

4.2.1 Multiple- and single- layer electrodes

To overcome the solubility limits of CO_2, a gas diffusion electrode (GDE) can be used in order to replace planar electrodes. GDEs can be grouped as multi- and single-layer.[13,47] The latter is a 3-phase boundary model with only one interface. The first is a thin film model characterised by the presence of two different interfaces: gas/liquid film and liquid film/solid.

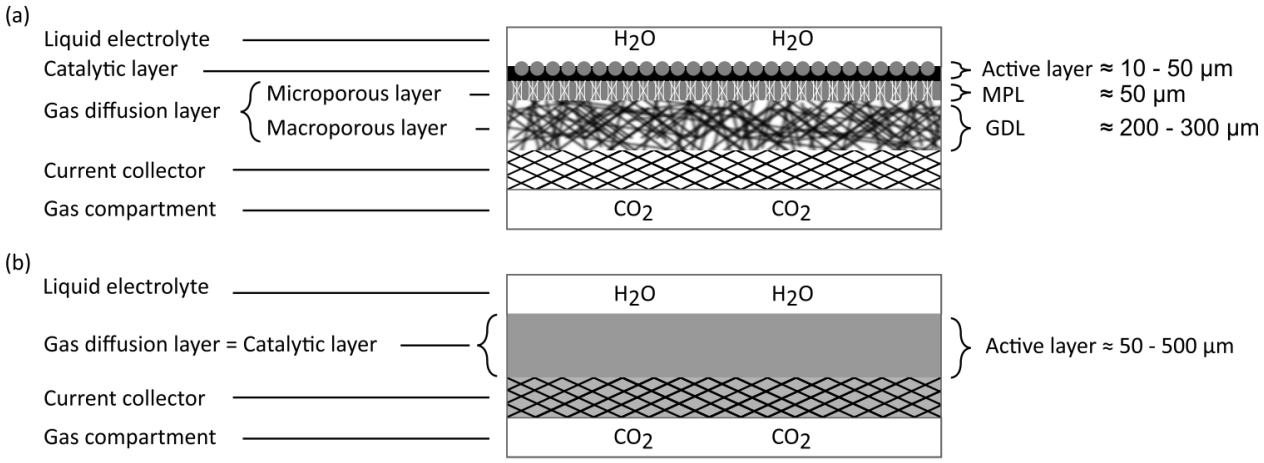

Figure 4.3 a) Schematic representation of a multi-layer GDE b) schematic representation of a single-layer GDE. This image was taken from literature.[47]

In the multi-layer configuration, a gas diffusion layer (GDL) is combined with a catalyst layer (CL). The GDL consists of a porous carbon fibers substrate (usually carbon paper) with the purpose of providing mechanical support, electrical conductivity and improving

the transport of CO_2. In some cases it can be coated with a microporous layer (MPL).[48,49] 'The purpose of the microporous layer is to minimize the contact resistance between the macro-porous and catalyst layer, limit the loss of catalyst to the GDL interior and prevent water accumulation within the pore volume of the micro-porous layer thus gases can freely contact the catalyst sites.'[48] Concerning the CL, it is generally made by two main components: the catalyst and the binder (a hydrophobic polymer).[50,51]

In recent years, an alternative GDE model was developed and it comprises the functionalities of GDL and CL in one single layer, hence the name homogeneous single-layer GDE. The term 'homogeneous' refers to the catalyst and pores distribution. This property is essential for the improvement of the process as, unlike the multi-layer GDE, it allows to reach current densities up to 1 A/cm^2.[47] The catalyst is thereby deposited on a support, which is later mixed with the binder, pressed and heated, rendering the pore system highly hydrophobic.[9] The support consists of a porous and electrically conductive material such as carbon black. Besides being conductive, the carbon black performances are determined by its channel network and pore distribution which allow the gas to flow through the carbon matrix in order to reach the catalyst.[22] The pores can be divided into two main sizes: large-macropores (Ø>10 µm) and small-macropores (Ø<0.1 µm). The former are formed after the binder has melt. This is the reason of their high hydrophobic behaviour which prevents them from being clogged by the electrolyte and ensures effective transport of CO_2. Small-macropores, on the other hand, are an intrinsic property of the substrate and allow the passage of water as they show a hydrophilic behaviour when an electrical field is applied between electrode and the electrolyte.[52] In detail, the presence of an electrical field could induce a reduction of the surface energy of the electrode-electrolyte interface with a consequent continuous capillary penetration.[53] Such phenomena is referred as electrowetting and it can take place at both electrically conductive and dielectric materials. Nevertheless, the wettability is more sensitive over the first ones.[54]

4.2.2 Binder and catalyst ratios

The previously mentioned binder consists of a polymer such as polytetrafluoroethylene (PTFE) or Nafion® which is typically used to increase both hydrophobicity and mechanical stability to the overall GDE as the carbon material alone would be very brittle.[55] On the other hand, adding a binder could reduce the conductivity of the GDE and its active surface area due to less electrolyte intrusion. For that reason, it is important to find an appropriate catalyst@AB/binder ratio depending on the specific catalyst and carbon composition. At the ITC department of the University of Stuttgart, it was possible to achieve a maximum wetting, without a complete flood of the electrode, by using a single layer GDE with 35 wt.% of binder (composed by 56 wt.% PTFE and by 44 wt.% Nafion). However long-term stability is lacking presumably due to the continuous electrowetting over time.[47] Besides the binder balance, an analysis for the catalyst load was carried out for the Sn-based GDE.[22,47] The loading is usually referred to the Sn^0 as its oxidation state is uncertain. Thereby different Sn wt.% were tested in order to obtain the best compromise on FE_{FA}, current density and φ_{cell}. The optimal performances were reached at 11.6 wt.% of Sn^0.[47] Lower Sn-loadings determined less catalyst surface and so little active sites while higher amounts showed lower overvoltage at a given current density but worse performances in terms of selectivity due to higher H_2 evolution. Such HER increase was most likely due to a less particle-particle distances and lower metal-support interactions.[47]

4.2.3 GDE preparation

In conclusion, there are two main techniques used for the GDE preparation. A common one is the ink-based method for catalyst deposition, which is used for making the multi-layer GDE. It consists of the dispersion of catalyst and PTFE into an organic solvent (usually isopropanol or ethanol).[55] The solution (ink) is then sprayed directly on the GDL surface. Nevertheless, the spraying process could take long time since the organic solvent needs to evaporate between every sprayed layer. In contrast, homogeneous single-layer GDEs can be obtained through a dry pressing technique. This method was tested to avoid the necessity of a solvent, which allows to have more reproducible and faster electrodes production.[52,55] They are particularly important for the acidic operations due to their higher intrusion depth, which allows for higher local pH next to the electrode. This aspect will be deepened later in *chapter 4.4*.

4.3 Cell configurations

The objective of this chapter is to provide an overview of the cell configurations used today for CO_2RR. Brief summaries are given by *Table 4.3* and *Table 4.4*.

4.3.1 GDE-free cells

The oldest and simplest cell for the CO_2RR is represented by the H-type cell whose name derives from its typical "H" shape as illustrated in *Figure 4.4.* It has a wide variety of applications such as screening analysis, potentiometric studies, microbial electrolysis, and any other process which requires a separation of the WE form the CE.

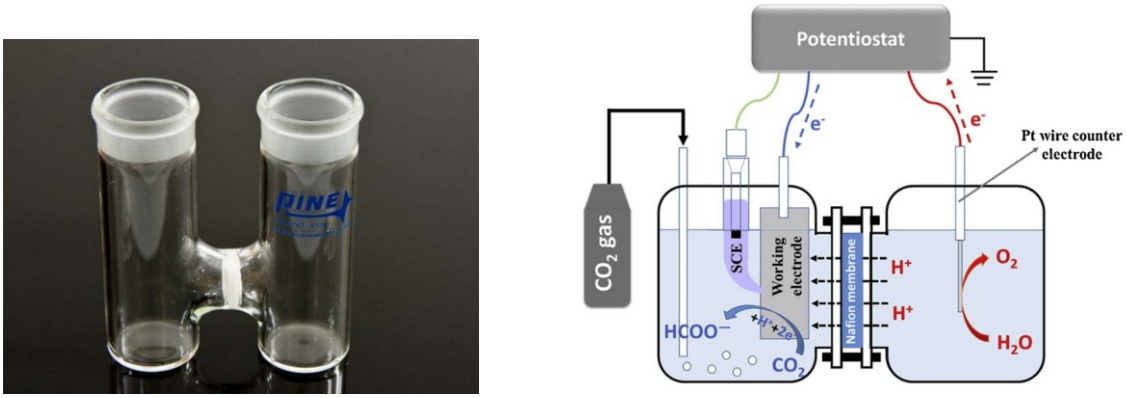

Figure 4.4 Photo and schematic representation of an H-type cell in a batch configuration.[49,56]

The overall design consists of two compartments, filled with the appropriate solution, separated by a fine frit (an ion exchange membrane can be used instead). WE and CE are positioned at the cathodic and anodic side respectively. In order to determine the φ_{WE} without the anodic contribute, a RE is usually added in the cathodic compartment. When a CO_2RR is conducted, the frit separation is essential, since it makes the product collection easier and it avoids its oxidation at the anode.[56] In the H-type cell, the cathode generally consists of a planar electrode and, because of that, the CO_2 is bubbled into the electrolyte. Nevertheless, as mentioned on *Chapter 4.1*, the CO_2 solubility in water solutions is very low and hinders the application of H-type and the other GDE-free cell since CD higher than 100 mA/cm^2 could not be reached making them not relevant for industrial applications.[13,49,57,58]

4.3.2 GDE-based cells

Alternatively, CO_2RR could be conducted with a GDE as cathode in order to improve the CO_2 diffusion. An example is given by Mahmood et al.[59] back to 1987. The cell structure was created for the synthesis of formic acid and is reported in the picture below.

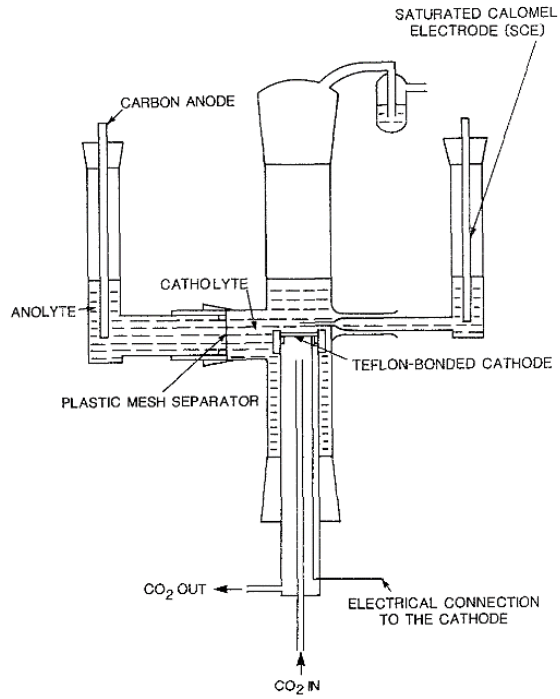

Figure 4.5 Representation of Mahmood cell design. This figure was taken from literature.[59]

Beside the use of a GDE, the cell is characterised by a vertical structure where the cathode was pointing upwards to avoid bubble accumulations on the active area surface. Experiments were conducted under acidic conditions (pH 1-5) with a Sn-based catalyst, allowing to reach FE_{FA} of 58% and φ_{cath} of -1.8 V (vs SHE).[59]

In recent electrolysers, a flowing catholyte is usually adopted in order to improve the electrolyte homogeneity. Such design evolved from fuel cell and water electrolyser.[49] Nowadays, different configurations of GDE-based flow cell are used for carbon dioxide reduction. The main ones will be presented here to get a better view on the actual progress and determine which of these could be considered for a future scale up. *Table 4.3* shows a list of flow cells from literature with their main characteristics. Most of the efforts observed so far have focused on the materials and conditions (e.g. catalyst, electrolyte,..) and no effective upscale has yet been tested. For this reason, most of the electrode surface area present little dimensions with limited CD, generally not relevant for industrial application.

a) DOUBLE GAP CELL (DG)

A first flow cell configuration is the double gap cell (DG). As stated by its name, a gap is left between electrodes and membrane allowing the electrolyte to flow in between. An electrolyte solution is required on both electrodes, as the water itself would not provide enough conductivity.

Kopljar et al.[22] used a DG cell in order to analyse the metal loading effects on faraday efficiency under alkaline conditions. The final results showed excellent performances with FE_{FA} up to 90% at CD of 200 mA/cm^2 and φ_{cath} of -1.57 V (vs SHE). Moreover, it was stated that CO_2 availability could become less when operating under alkaline conditions since, in basic aqueous media, dissolved CO_2 is converted into the HCO_3^-/CO_3^{-2} equilibrium by the OH^- species, making it inactive. For this reason, the influence of different alkaline pH gradients (8, 10 and 12) was examined observing no relevant improvements.[22]

Lower pH operability of a DG cell was investigated some years later by Oβkopp et al.[13] In this case, it was reported a FE_{FA} up to 86% and CD of 200 mA/cm^2 by using a neutral solution both as catholyte and anolyte (*figure 4.6 a*).

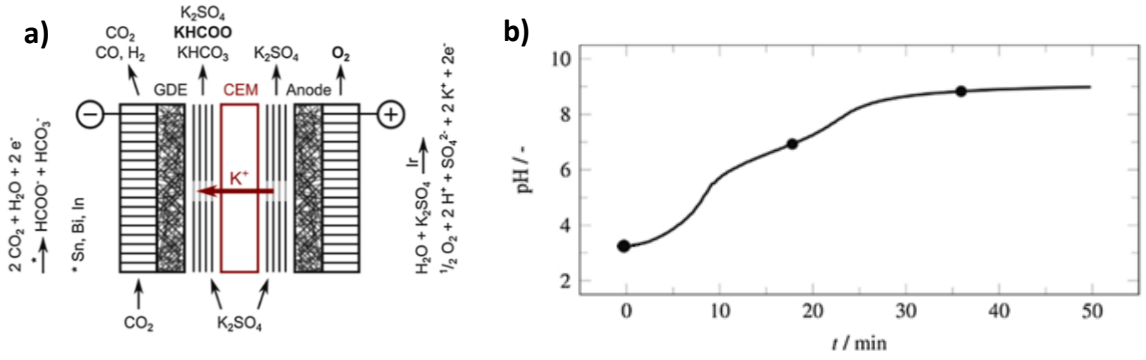

Figure 4.6 a) Schematic sketch of the DG cell configuration b) pH variation over time while using a pre-acidified catholyte (pH=3.4) with a DG configuration. The images were taken from literature.[13]

On the other hand, this configuration presented an increase in pH over the time which hindered the conduct of experiments under acidic conditions with a pre-acidified catholyte of pH=3.4 (H_2SO_4 was added to a 0.5 M K_2SO_4 solution). This is showed in *figure 4.6 b* where the curve displays the presence of two buffer zones which represent the HCO_3^-/CO_3^{-2} and H_2CO_3/HCO_3^- equilibriums. Such behaviour was even more pronounced when operating at natural pH, where the lower concentration of carbonates resulted in a more rapid increase in pH with no visible buffer zones.

Evidence of this trend has also been given by Dufek et al.[60], where a neutral pH catholyte (0.5 M K_2SO_4) combined with an alkaline anolyte (2 M KOH) were used in a DG cell to produce syngas ($CO+H_2$). After 40 min, the catholyte solution evolved from pH 6.5 to pH of 13.5 with an increase of carbonate concentration of 0.11 M as well. This description matches the outcomes previously mentioned suggesting that this is an intrinsic behaviour of the DG configuration.

Such pH increase could be justified as ‘it is more likely that potassium cations rather than protons migrate through the cation exchange membrane, even though the potassium ion mobility in water and through the membrane is far lower than the one of protons.’ As consequence, the OH^- generated at the cathode cannot be neutralized leading to a rise of the pH.[13] Also, the presence of a direct contact between electrolyte and GDE is more likely to cause a catalyst degradation in the long-term.

b) UNDIVIDED CELL (U)

An alternative flow cell for CO_2RR was presented by Kenis et al.[61] in 2010 and takes the name of undivided (U) cell. Unlike most of the configurations, it does not present any membrane since the intersection of reactants and products was controlled by an ultrathin channel (<1 mm thickness) of buffer electrolyte (*Figure 4.7*). The lack of any membrane significantly reduced the cell expenses.[58,61,62]

Such configuration allowed to operate under acidic conditions without an overwhelming HER. It also demonstrated flexibility with regard to the operating conditions such pH and composition due to the slow diffusion of products.[58]

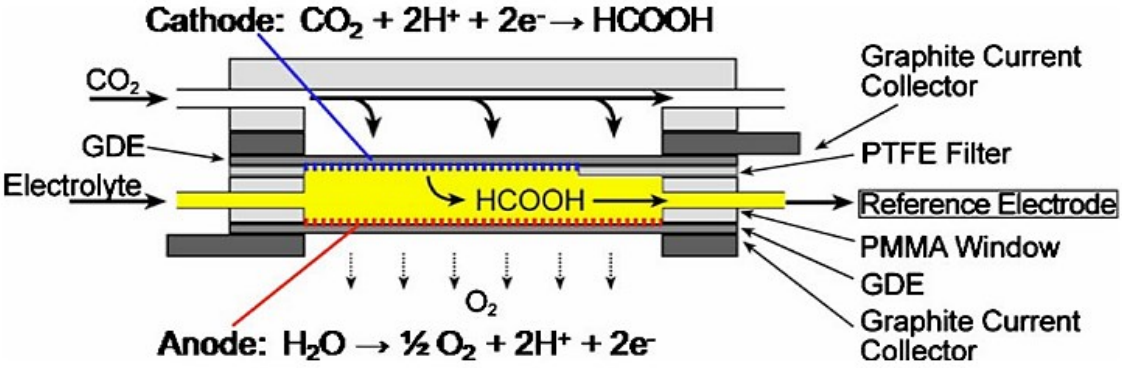

Figure 4.7 Microfluidic cell scheme. This figure was taken from literature. [61]

Lu et al.[63] even stated the possibility to use a pH differential technique by adding 0.01-cm-thick PVC sheet ('insulating separator') with a 0.1 cm^2 window between the cathodic and anodic flow channels in order to allow an ion exchange between anode and cathode. By employing a double laminar flow with pH of 14 and 2 for anolyte and catholyte respectively, it was possible to decrease the cathodic potential from -2.1 V to -0.81V (vs NHE) while allowing the OER at lower potential (from 1.7 to 1 V). Peaks of 96% in FE_{FA} were reached at CD=146 mA/cm^2 and -0.8 V (vs SHE).

Experiments up to ~8 h could be performed noticing a decrease of FE_{FA} from 95 to 81% with a relevant GDE degradation which led to a decrease of 41% in reactivity rate.[62]

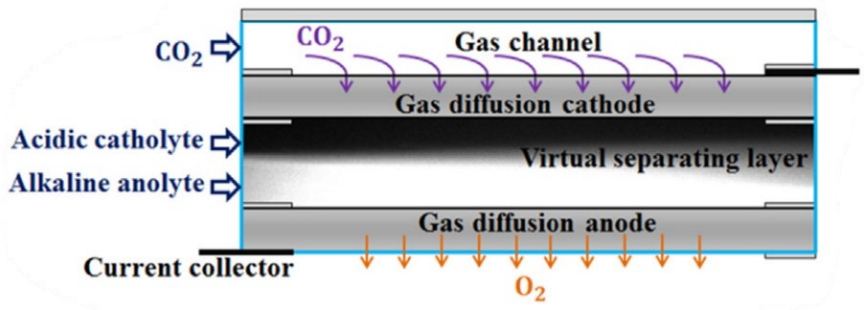

Figure 4.8 representation of the differential pH cell in proximity of the insulating separator window. This picture was taken form literature.[63]

A not negligible advantage of the U cell is given by the extensive knowledge already acquired on it. Such wide quantity of information allowed to develop a mathematical model by considering all the variable parameters, in particular: mass transfer constraints, kinetic losses, overpotentials, neutralisation energy dissipation and electrical resistance losses.[64]

Besides its high efficiency, the U cell could only operate through a single pass-design since the electrolyte recirculation (batch mode) would lead to a product oxidation. FE_{FA} achieved values up to 89%, with CD in the order of 100 mA/cm^2 and φ_{cell} of 3.0 V.[61]

c) TOTAL ZERO GAP CELL (TZG)

The presence of both electrolyte and membrane generally lead to high φ_{cell} making the process inefficient. The analysis of the undivided cells established that the presence of a membrane is essential to avoid oxidation of the product. For this reason, it was considered the possibility to remove the electrolyte layer instead. The configuration adopted in this case is named full membrane electrode assembly (MEA) or total zero gap (TZG). Here, anode, GDE and membrane were pressed together, while gaseous CO_2 was supplied to the cathode by a bubble humidifier in order to control the amount of water vapor. The latter has the purpose of carrying the dissolved CO_2 to the catalyst surface by forming a CO_2-saturated thin liquid film on the catalyst surface. The CO_2 consumed by the reaction in the film was immediately replenished from the bulk gas stream.[65]

The cell configuration is represented in *Figure 4.9*.

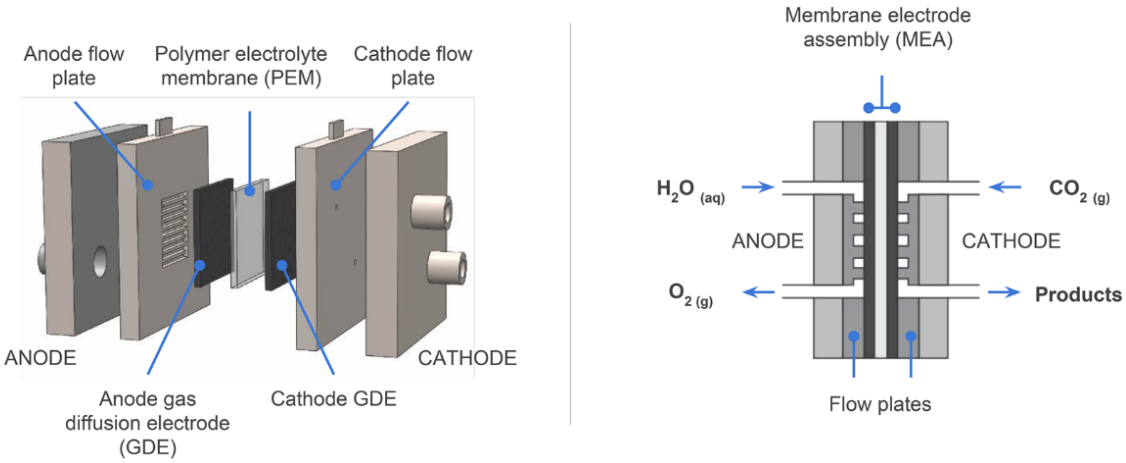

Figure 4.9 General representation of a TZG.[57]

Lee et al.[65] stated that the absence of catholyte made the CO_2 solubility less of a limiting factor, allowing the production of high formate concentrations.

Under long-term experiments (48 h), FE_{FA} up to 93% (at CD=40 mA/cm^2) with a total cell voltage of 2.2 V could be achieved. Also, because of the lower potential, it was observed a higher stability of the catalyst layer (Sn) with almost no changes in structure, surface's composition, and morphology. On the other hand, the full MEA high efficiency seemed limited in the total cell voltage range 2.1 - 2.2 V since at higher values, the FE_{FA} dropped at 60%. Because of that, CD was relatively limited with a maximum of 52 mA/cm^2 at 2.2V.[65]

Also, the absence of electrolyte could accelerate the ion exchange rate with a consequent acidification of the water condense in the GDE which promote the HER. In conclusion, as for the catholyte-based cells, the formation of a liquid product such as FA, could still flood back to the gas diffusion electrode with a consequent obstruction of its CO_2 transport pores. This makes the absence of catholyte no longer convenient.[58]

d) ZERO GAP ANODE CELL (ZGA)

More recent cells still involve the use of catholyte for a better pH control and so HER mitigation. However, in order to lower the potential of the cell, the anode is attached to the membrane forming a MEA. A recent example of such cell type was presented by Oβkopp et al.[13] (*Figure 4.10)*.

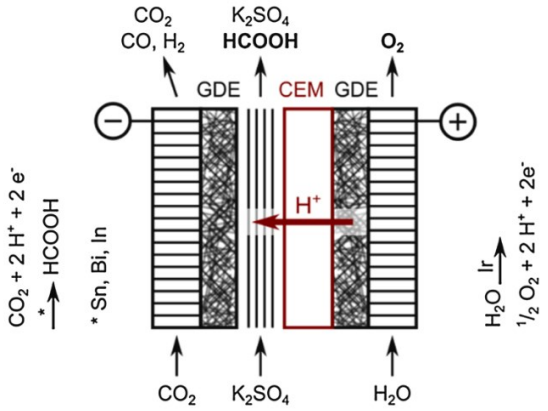

Figure 4.10 Schematic representations of the ZGA cell.[13]

Compared to the U cell, the ZGA showed better formic acid yield due a lower FA crossover. Also, it allowed to work under acidic conditions (*figure 4.11*) with a consequent drop of CO_2 loss caused by the non-faradaic reactions of carbonate formation. As it will be described in *chapter 4.4*, this is one of the fundamental problems in CO_2RR as it could traps large amounts of CO_2. In addition, the positioning of the anode next to the membrane made possible to avoid the need of salts on the anolyte. Because of that, no other cationic species, other than protons, could cross the membrane and reach the cathode. Most likely, that could explain why the pH could be held constant.

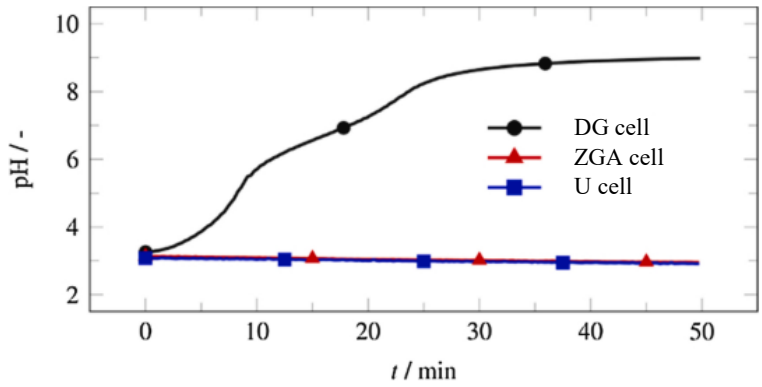

Figure 4.11. Graphic of DG, ZGA and U cell's pH variation over time. The image was taken from literature.[13]

A similar cell design was also adopted by Sen et al.[37], where an alkaline catholyte was used. Here a single-pass mode was suggested since the batch system showed a high cross-over under alkaline conditions. FE_{FA} up to 90% could be achieved at CD of 110 mA/cm^2 and -1.65 V (vs Ag/AgCl). Also CD peaks up to 358 mA/cm^2 were observed with cathodic potential of -1.8 (vs Ag/AgCl).

Still, this configuration presents some limitation, especially in the long-term runs: as for U and DG cells, the CL erosion is generally the main limiting factor since it leads to a deactivation of the catalyst particles. Also, the recirculation of catholyte in batch mode could lead to an excessive product concentration which could eventually flow through the membrane and/or – if FA is produced – cause an excessive acidification and so HER. To bypass such limitation, different solutions could be considered, such the adoption of a single-pass electrolyte.[37]

e) GAPLESS CELL WITH A CENTRAL ELECTROLYTE FLOW (THREE-COMPARTMMENT CELL)

Finally, the three-compartments cell (TC) configuration could be considered as an alternative to ZGA cells. Its main structure is depicted in *Figure 4.12* and shows the presence of three compartments delimited by two different membranes: an anion exchange membrane (AEM) and a cation exchange membrane (CEM). Anode and cathode are in contact with the CEM and AEM respectively while deionised water is made flow in between the two membranes. Due to the low conductivity of water and FA, the use of an electrolyte or an ion exchange resin is crucial.

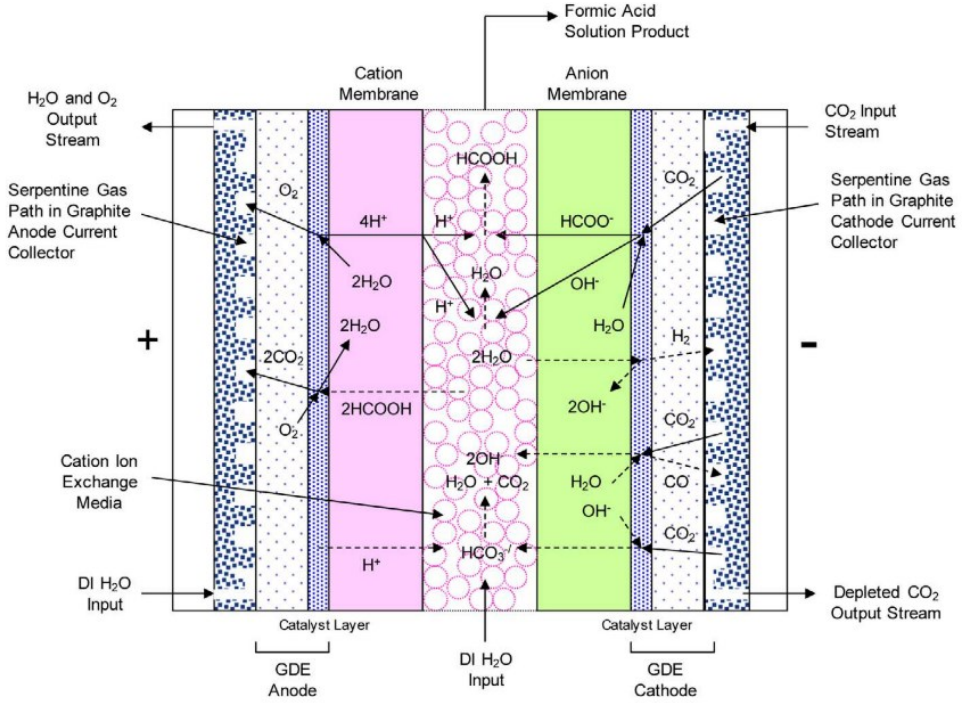

Figure 4.12 2D scheme of a three-compartment cell. The image was taken from literature.[66]

The innovative aspect of this cell was the addition of an anionic membrane in order to avoid a direct contact between electrolyte and cathode. This type of membrane allows the passage of negative ions only. Because of that, HER is minimised since the flow of protons to the electrode is impeded. Finally, in the centre compartment FA will be formed.

The TC cell allowed to reach FE_{FA} up to 94% at CD of 140 mA/cm^2 and 3.5 V (-1.5 for the cathodic compartment). In terms of durability it displayed some of the best results maintaining a FE_{FA} of 70% after 1000 h with a Bi-based GDE and a total cell potential of 3.7 V.[66] Nevertheless, such long-term experiment was actually made possible by using a reverse polarisation technique which aim to remove the graphitic form of carbon on the electrode surface during electrolysis. In detail, the potential was reversed at 1.7 V for 30s every 120-150h allowing to maintain decent FE_{FA}.[67] This technique could also be considered for the analysis of other configurations.

Overall the TC cell demonstrated very good performances and could be considered one of the most promising configurations for a future scale-up, allowing to work at pH lower

than ~3. Still, excessive acidic conditions led to a FE_{FA} drop of 38% when the electrolyte changed from pH~2.0 to pH~1.7 in batch mode.[67]

For the same reason, with a single-pass mode, the water flow rate played a fundamental role since it was inversely proportional to the concentration of FA and therefore to the pH of the solution. However, a single-pass electrolyte allowed to produce solutions with 11 wt.% (2.4 M) in FA, maintaining an average FE_{FA} of 78%.

During the process, the exit of gas bubbles from the central compartment was observed: GC investigation revealed the CO_2 was the predominant gas component, with small, equimolar amounts of CO and H_2. That may be occurring because of FA decomposition, most likely on the CEM interface due to strongly acidic properties. The reactions considered were:

Decarboxylation $$HCOOH \rightarrow CO_2 + H_2 \quad (4.11)$$

Dehydration $$HCOOH \rightarrow CO + H_2O \quad (4.12)$$

However, FA losses to decomposition have been claimed to be ~10% or less.[66]

Lastly, TC cell configuration needs to face elevated costs due to the presence of an additional membrane. The Sustanion™ AEM used in this configuration is generally characterised by high prices which could become a problem for its economical viability. In conclusion, the crossover through the anodic membrane to the cathode surface is still a problem that need to be solved.

f) Today's application

Nowadays, GDE based flow cell are used at industrial scale for different chemical processes. An example is given by the chlor-alkali synthesis. Landmark in this sector is the German company Covestro® which stated the use of an oxygen depolarized cathode (OCD) technology for the $O_{2(g)}$ reduction into OH^-. The benefits brought by this system are witnessed by a reduction of 30% in energy consumption.[68]

Concerning the CO_2RR, the cell scale is still quite limited and under study. Only in 2019, Siemens® and Evonik® launched the project Rheticus which aim to convert carbon dioxide into butanol and hexanol. For that purpose, Siemens® developed the world's first industrial electrolyser to reduce CO_2 into syngas as intermediate product: it comprises 10 cells with a total surface area of 3000 cm^2 and because of that it is the biggest cell stated by literature so far.[69] Unfortunately, no further detailed information are given by the company.

Table 4.3. Summary of the cells performances found in literature and considered.

Name	Initial pH	Final pH	Product /Catalyst	Type	Area (cm^2)	FE_p%	CD (mA/cm^2)/Voltage (V)	Operation mode
Mahmood[59] **(1987)**	Acidic	acidic	FA / SnO_x	DG (GDE-free)	<3.2	58	n/a / -1.8 (vs SCE)	-
Oβkopp[13] **(2021)**	Acidic-Neutral	alkaline	FA / SnO_x	DG	1	86	200 / n/a	Batch
Kopljar[22] **(2014)**	Alkaline	alkaline	Formate / SnO_x	DG	1	90	200 / -1.57 (vs SHE)	n/a
Dufek[60] **(2011)**	Neutral	alkaline	Syngas / Ag	DG	10	90	30 / -1.9 (vs Ag/AgCl) / 3.2 (total cell)	Batch
Whipple[61] **(2010)**	Acidic	acidic	FA / Sn(commercial)	U	1	89	100 / 3.0 (total cell)	Single-pass
Lu (2016)[63]**;**	Acidic	acidic	FA / Pb-PtRu	U	0.1	96	146 / -0.81 (vs SHE)	Single-pass
Oβkopp[13] **(2021)**	Acidic	acidic	FA / SnO_x	U	1	87	200 / n/a	Batch
Lee[65]	-	-	Formate / Sn	TZG	25	93	40 / 2.2	Single-pass
Oβkopp[13] **(2021)**	Acidic	acidic	FA / SnO_x	ZGA	1	89	200 /-1.4 (vs SHE)	Batch
Sen (2019)[37]	Alkaline	Alkaline	Formate / SnO_x	ZGA	0.25	90	110 /-1.65 (vs Ag/AgCl)	Single-pass
Sen (2019)[37]						<70%	385/-2.0 (vs Ag/AgCl)	
Yang[67] **(2020)**	Acidic (center compartment) Neutral (cathodic compartment)		FA Bi_2O_3	TC	5	90	200 / 3.7 (total cell)	Single-pass (1000 h)
Yang[66] **(2017)**			FA Sn			94	140 / 3.5 (total cell)	Single-pass (142 h)
Siemens[69]	n/a	n/a		n/a	3000	n/a	n/a	n/a

Table 4.4. Summary of the cell configurations main features.

Cell configuration	Description	Pros	Cons
GDE-free cell			
BATCH/H-TYPE CELL	Anode and cathode are dipped in two different solutions separated by a frit/membrane	Easy to build	Limited CO_2 solubility; limited mass transport and so current density; difficult to scale-up
GDE-based cell			
DOUBLE GAP (DG)	Similar to a batch cell with the addition of flowing electrolytes between electrodes and membrane.		The presence of an electrolyte layer between electrodes and membrane (both for the cathode and the anode) could determine higher φ_{cell}; Impossibility to conduct experiment under acidic conditions; Catalyst degradation; GDE excessive flooding risk;
UNDIVIDED (U)	Membrane-free cell where anode and cathode are separated by a thin film (<1mm) of electrolyte in order to avoid the crossover of the products.	no need of expensive membranes; the absence of membrane makes the proton/ion transport more efficient; flexibility in pH conditions with the possibility to employ a pH differential technique.	Impossibility to recirculate the electrolyte without removing the product since it would get oxidated at the anode; limited operability time due to catalyst degradation and GDE excessive flooding risk; limited current density and cell voltage operability.
TOTAL ZERO GAP (TZG)	Anode, membrane, and cathode are pressed together forming a full membrane electrode assembly (MEA). H_2O flows behind the anode and humidified CO_2 is sent at the cathodic compartment.	Very efficient mass transport due to the absence of electrolyte; reduced ohmic loss; possibility to operate at acidic conditions	HER problem due to the easy flow of H^+ into the cathodic compartment; cathode flooding risk due to electrolyte flooding back to the GDE.
ZERO GAP ANODE (ZGA)	Anode is pressed against the membrane by forming an half MEA. It could be considered an half way between DG and ZGA cell configurations.	Better control over pH and temperature; lower φ_{cell} compared to DG configuration; possibility to work under acidic conditions.	Catalyst degradation; GDE excessive flooding risk;
THREE COMPARTMENTS (TC)	Consists of three compartments outlined by two different membranes: a cation exchange membrane (CEM) and an anion exchange membrane (AEM). Anode and CEM are attached together similarly to the ZGA configuration while on the cathode surface an AEM is laid down; between the two membranes a water is made flow (central flow compartment).	High CO_2 diffusion; Limited HER due to the presence of an anion exchange membrane; High CD and FE_{FA} at relatively low potential; Long-term experiment achievable without relevant GDE damages; Possibility to work under very acidic conditions (pH<3).	High costs due to the presence of two membranes; an ion exchange resin is required; possible FA decomposition in the centre compartment; the presence of a double membrane could cause an excessive voltage increase; risk of an excessive flooding in the GDE.

4.4 pH & Temperature

4.4.1 pH

As mentioned, HER is the main parasite reaction when it comes to CO_2RR. It is therefore logical to think that the pH has an important influence on the selectivity of the process. In the case of formate/FA production, CO_2RR can deviate to different paths depending on the pH of the environment as showed in *figure 4.5*.[13]

Table 4.5 List of the main reactions in acidic and alkaline conditions. This table was taken form literature.[13]

	Acidic		Alkaline	
Faradaic reactions:				
Reduction:	$CO_2 + 2H^+ + 2e^- = HCOOH$	(4.13)	$CO_2 + H_2O + 2e^- = HCOO^- + OH^-$	(4.1)
	$CO_2 + 2\,H^+ + 2e^- = CO + H_2O$	(4.14)	$CO_2 + H_2O + 2e^- = CO + 2OH^-$	(4.2)
	$2H^+ + 2e^- = H_2$	(4.15)	$2H_2O + 2e^- = H_2 + 2OH^-$	(4.21)
Oxidation:	$H_2O = 2H^+ + ½O_2 + 2e^-$	(4.16)	$2OH^- = H_2O + ½O_2 + 2e^-$	(4.22)
Non- Faradaic reactions:	$HCOO^- + H^+ = HCOOH$	(4.17)	$HCOOH + OH^- = HCOO^- + H_2O$	(4.23)
	$CO_3^{2-} + H^+ = HCO_3^-$	(4.18)	$CO_2 + OH^- = HCO_3^-$	(4.24)
	$HCO_3^- + H^+ = CO_2 + H_2O$	(4.19)	$HCO_3^- + OH^- = CO_3^{2-} + H_2O$	(4.25)
	$H^+ + OH^- = H_2O$			(4.20)

The Pourbaix diagram in *Figure 4.13* shows that the equilibrium slope H^+/H_2 has a less negative potential compared to the $CO_2/HCOO^-$ at acidic pH. This indicates that the reduction of protons to molecular hydrogen is the favoured reaction. Therefore, most of the CO_2RR researches are conducted under alkaline conditions, where the $\varphi^0_{H+/H2}$ present more negative values instead.[8,9,22,27,47,70]

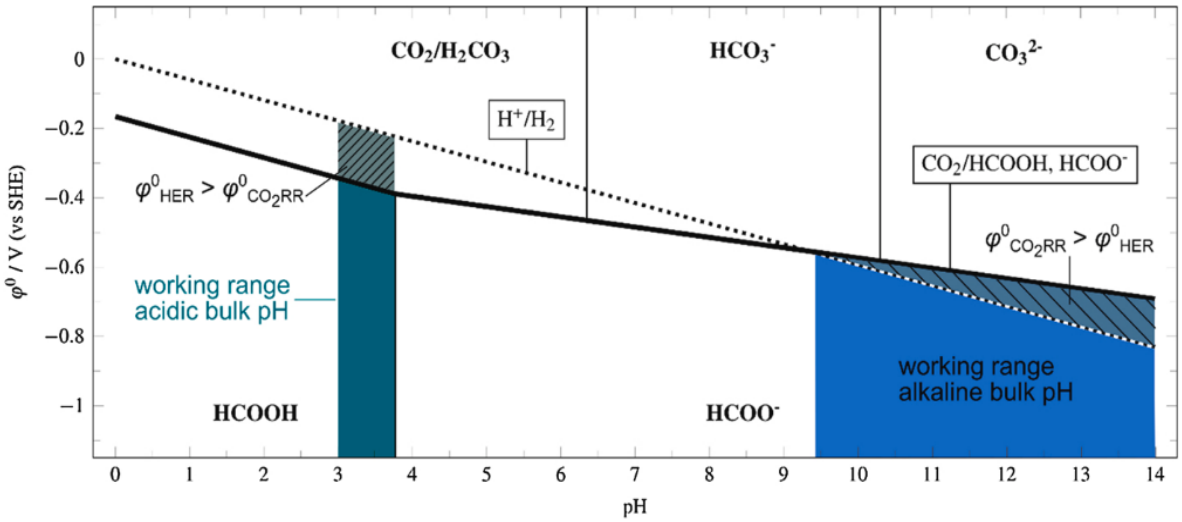

Figure 4.13 Pourbaix diagram of CO_2 products. The $HCOO^-$ formation happens at higher pH. The image was taken from literature.[13]

Nevertheless, working under alkaline conditions determine the production of formate salts which require an additional acidification process in order to obtain the FA. Also, high pH could cause the generation of carbonate by-products (*reaction 4.24* and *reaction 4.25*) which determine the need of an ulterior acidification step in order to remove them.[13] For these reasons alkaline reactions could be not so effective, with a consequent interest in acidic operability.

Some researches witnesses the possibility to conduct CO_2RR experiments also under low pH obtaining FE_{FA} in the same range - or even better[61] - as those obtained using an alkaline electrolyte.[8,30,39] Bondue et al.[71] proved it by analysing the CO_2 reduction into CO under mildly acidic conditions with a gold electrode. The amounts of H_2 and CO were quantified via an electrochemical mass spectrometry (DEMS) within it was declared the protons to react with OH^- ions before they could reach the electrode surface (*reaction 4.20)*. This mechanism can justify the possibility to conduct experiments under acidic conditions. An essential requirement is to balance the concentrations of bulk H^+ with the OH^- next to the surface. It should be noted that this is particularly true when GDEs are used: here the alkalinity is higher due to the microporous surface which trap the OH^- ions, inhibiting their diffusion into the bulk and preventing the proton reduction into H_2.

Oβkopp et al.[13] also demonstrated the presence of an alkaline pH in proximity to the GDE surface which leads to a bicarbonate/carbonate species formation (*reaction 4.27*) independently from the bulk pH:

$$2CO_2 + H_2O + 2e^- = HCOO^- + HCO_3^- \qquad (4.27)^{13}$$

Nevertheless, considering the pK_a (=6.4) for the $HCO_3^- \rightleftharpoons H_2CO_3$ reaction[72], when an acidic bulk (pH<6.4) is adopted, the high concentration of H^+ allow the bicarbonate to eventually shift back to carbon dioxide:

$$HCOO^- + HCO_3^- + 2H^+ = HCOOH + H_2O + CO_2 \qquad (4.28)$$

Because of that, the actual CO_2 loss, caused by the carbonate formation, was observed to be negligible.

On the contrary, when alkaline bulk pH were used, the presence of high quantities of hydroxide resulted in an increase of the bicarbonate and carbonate species (*reactions 4.24 and 4.25*). Both HCO_3^- and CO_3^- could eventually react with potassium ions and precipitate if their concentration exceed the solubility limit. This could prevent the shift back to carbon dioxide. In detail, a loss of one molecule out of two could be observed in case of a sole bicarbonate formation and one molecule out of three in case of a sole carbonate formation. Sole bicarbonate or carbonate formation only occurs at the relative pK_a value (equal to 6.4 for the $HCO_3^- \rightleftharpoons H_2CO_3$ acid reaction and 10.3 for the $CO_3^{2-} \rightleftharpoons HCO_3^-$ one)[72]. Between these pK_a there can be a mixture of both.

4.4.2 Temperature

Temperature is an important factor to consider when it comes to CO_2RR since it can affect several features such as:

- CO_2 diffusion (from the bulk to the electrode surface)
- CO_2 solubility
- Kinetics of the CO_2 conversion at the active site
- Electrochemically active surface area (ECSA)[9]

Its impact could either vary differently depending on the operating conditions such, current density, electrode type (cathode) and pH conditions. These parameters were observed to be particularly linked to each other.

Besides its importance, the temperature effect was rarely studied. In fact, most of the CO_2RR researches operates at room temperature[22,59,73] (20°C) as cooling or heating would have required providing additional energy to the entire system.

With regards to the GDE-free cells, Kim et al.[74] analysed different temperatures at a potential of -1.4 V (vs Ag/AgCl) under acidic conditions. The cathode was a solid electrode (Sn foil) which implied a limited CO_2 diffusion. The FE_{FA} values at different temperatures are portrayed in *Figure 4.14*.

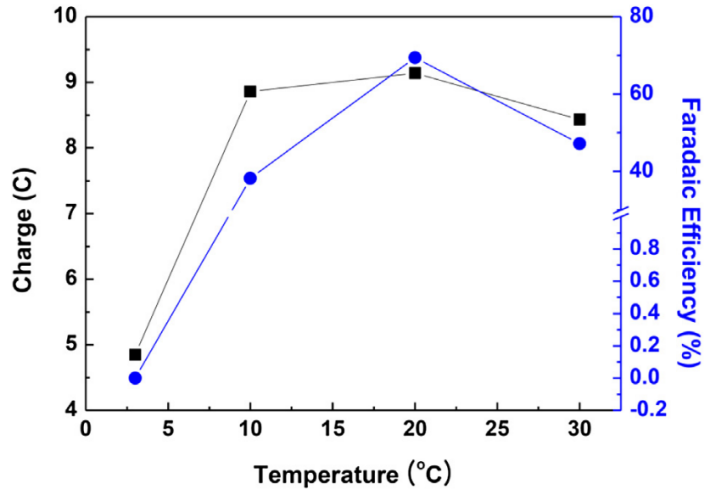

Figure 4.14 Faraday Efficiency of formic acid at different temperatures. This image is taken from literature.[74]

From its analysis it was demonstrated that T~20°C shows superior FE_{FA} compared to $T \geq 30$°C. Analogue results were recorded in other H-type cell analysis at j <200 mA/cm^2.[75,76] This trend is caused by the characteristic low CO_2 solubility of the GDE-free cells (*chapter 4.3*) which is eventually lowered by increasing the T of the electrolyte (*figure 4.15)*. That limit the amount of CO_2 available with a consequent lower FA production.

As mentioned in *chapter 4.3*, the GDE-based cell can improve the CO_2 concentration in the electrolyte. For that reason they allow to reach higher T of analysis without an excessively low carbon dioxide concentration and so faraday efficiency.

The effect of *T* on GDE flow cell were studied in Löwe et al.[9] work, where the CO_2RR was conducted under alkaline conditions (2 M $KHCO_3$) with a 1 cm^2 SnO_x GDE.

The optimal cell efficiency was observed at *T*=50°C since it falls within the range of best *T* compromise (35-50°C) between CO_2 solubility *S* and bulk-electrode diffusion *D* (*figure 4.15*). *T* lower than 50°C showed higher HER because of CO_2 diffusion limitation and low formate diffusion with an increasing electrolyte resistance in the pores. On the other hand, *T* > 50°C led to a lower CO_2 solubility.

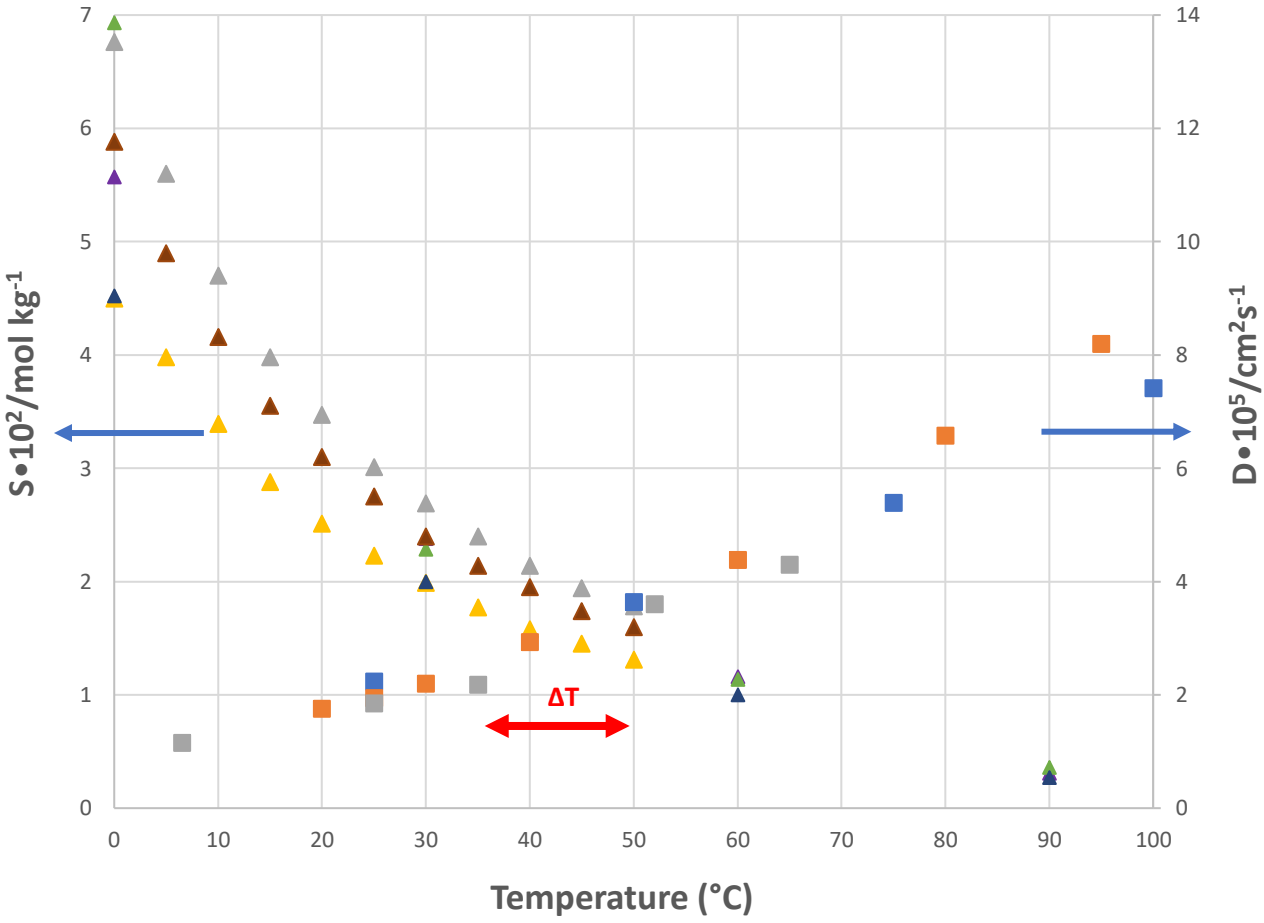

Figure 4.15. Graphic reconstruction of CO_2 solubility (S) and diffusion (D) over temperature. The squares represent the CO_2 diffusion in pure water (orange[77], blue[78], grey[79]). The triangles represent the CO_2 solubility in 2M NaCl (yellow[80], black[81]), 1 M NaCl (purple[81],brown[80]), 0.5 M NaCl (grey[80]) and pure water (green[81]). The images were reconstructed by data found in the literature.

Nevertheless, the analysis showed that below a diffusion limited current density of *j*=200 mA/cm^2 the temperature variation has little effect on the efficiency of the process (*Figure 4.16a*).[9]

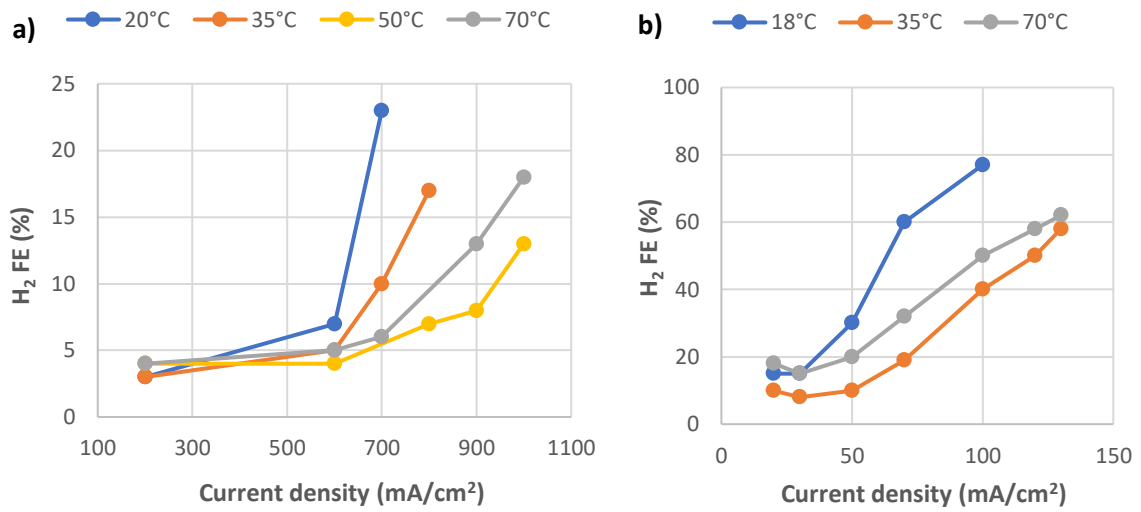

Figure 4.16. Graphic representation of the H_2 FE over CD at different T. The images were reconstructed by data found in the literature.[9, 60]

Analogue result are displayed by Dufek et al.[60] where it was analysed the temperature effect with a lower *j* range of 10-130 mA/cm^2.[58] In detail, it was reported a FE change by testing different temperatures effect on syngas ($CO+H_2$) production via an Ag based GDE. *T* of 18, 35 and 70°C were analysed under neutral conditions (0.5 M K_2SO_4). In this case higher FE_{CO} were observed at 35°C. Such results are in agreement with previous studies since at CD lower than the diffusion limited current density (in this case ~50 mA/cm^2) the *T* has no effect (*figure 4.13b*).

4.5 Cation exchange membrane

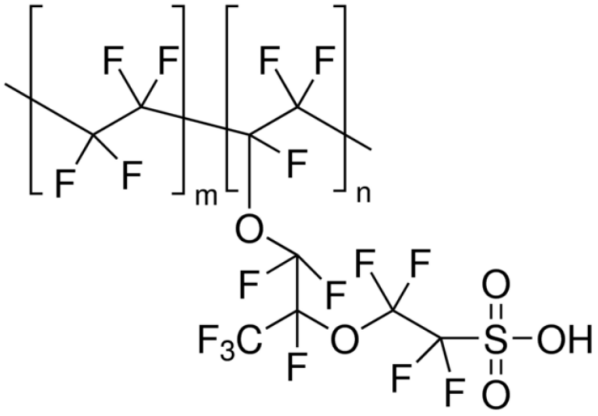

Figure 4.17. Nafion® membrane structure.

Cation exchange membranes must allow the passage of cationic species while blocking or limiting the passage of the final products - such FA or methanol - from cathode to anode. The main requirements of the membranes can be listed as: high ionic conductivity and resistance to decomposition in order to prevent the product permeation. The Perfluorinated sulfonic acid membranes (PFSA by Nafion®) shows the best performances both in terms of membrane durability and conductivity.[66] Also, literature states that the PFSA membranes present a smaller FA crossover compared to other fuels. This is probably attributable to the negative or neutral charge of FA (it can become neutral forming dimers at high concentrations) which makes difficult its approach to the sulphonic groups of the membrane. For these reasons they are largely used in the fuel cell and flow cell sectors.

In 2007, Jeong et al.[83] presented a study conducted on the crossover of FA on different PFSA membranes. Nafion® 112, 115 and 117 were analysed using a fuel cell equipped with a gas chromatograph. In this study, it was observed that the crossover is mainly related to membrane thickness, working temperature and FA concentration.[83]

As regards the thickness, the state of the art considers it crucial for the permeability of the products. In detail, the membrane thickness is supposed to be inversely related to the crossover.[66,83,84] However, Rhee et al.[84] proved that the relation between FA crossover and membrane thickness is not so linear: the research was conducted on Nafion® 112 and 117 with a house-built permeation measurement device. The latter was made of two chambers separated by the membrane (under analysis) in absence of an electric field. It was demonstrated how the thickness does not actually lead to major discrepancies in FA loss. In fact, besides the thickness ratio of Nafion®117 and Nafion®112 was 3.5, the flux of FA with the 112 was only 2 times higher than the 117. This was in agreement with Jeong et al.[83] research which showed that Nafion®112 has a crossover CD just 2 times higher than Nafion®117 in a fuel cell when applying CD in the range 50<CD<150 mA/cm^2.

In the same CD range, Jeong et al.[83] declared that also *T* do exert an important effect as crossover CD increased from 60 mA/cm^2, at 30°C, to 160 mA/cm^2, at 90°C.[83] The explanation for such trend is still unclear.

Finally, FA concentrations needs to be considered too when analysing the membrane permeability. Higher crossovers were observed when increasing FA concentrations from 1

to 10 M. Nevertheless, at concentrations ~20 M a trend reversal was noticed. Such phenomena was suspected to be caused by a dehydration of the superficial layer of the membrane with a consequent inhibition of the FA permeation as it is hydrophilic. Alternatively, as expressed by Yang et al.[66], particular CEM could present a membrane polymer characterised by the presence of low water quantities itself (e.g. Nafion® 1100 EW) which limit the transport of FA to the anionic compartment.[66,85] On the other hand, the absence of water causes a decrease of the membrane conductivity with an increase in electrical resistance and so φ_{cell}.[86]

5. Experimental Methods

5.1 List of Chemicals

Table 5.1 List of the used chemicals.

Chemical name	Formula	Purity	Brand
Potassium sulphate	K_2SO_4	≥99%	Carl Roth
Acetylene Black	C	100%	Alfa Aesar
Sodium Dodecyl sulphate (SDS)	$NaC_{12}H_{25}SO_4$	≥99%	Carl Roth
Maleic Acid	$C_4H_4O_4$	≥99%	Carl Roth
Formic acid	CH_2O_2	≥98%	Carl Roth
Bismuth nitrate pentahydrate	$Bi(NO_3)_3•5H_2O$	≥98%	Carl Roth
Sodium hydroxide			
Tin(II) chloride dihydrate	$SnCl_2•2H_2O$	≥99.99%	Aldrich
Urea	CH_4N_2O	≥99.5%	Carl Roth
TF 2053Z PTFE powder (450 µm)	-	-	3M Dyneon

5.2 Preparation of Gas Diffusion Electrodes

5.2.1 Preparation of SnO_x@Acetylene Black

The preparation of the SnO_x@Acetylene Black (SnO_x@AB) is based on the deposition precipitation method published by K.C. Song and Kopljar et al.[22] In a 500 mL round flask, 29.47 g of acetylene black and 1.87 g SDS were suspended by vigorous stirring in bi-distilled water (520 mL). The reactants were mixed by a magnetic stirrer overnight. After, the flask was put under ultrasonication for 1 hour. 1.47 g of $SnCl_2•2H_2O$, 19.52 g of urea and 130 mL of bi-distilled water were later added and heated at 90°C under reflux for 4 h. The final product was filtered through a Buchner funnel and washed with at least 2500 mL of bi-distilled water. After the filtration, the product was dried in the oven for 24 h at 100°C.

5.2.2 Preparation of Bi_2O_3@Acetylene Black

The preparation of the bismuth catalyst was done considering the procedure followed by Bienen et al.[8]

13.59 g of acetylene black were mixed overnight in 300 mL of bi-distilled water through a magnetic stirrer. The solution was sonicated for at least 1 h before slowly pouring 22.5 mL of 37% $HCl_{(aq)}$. 5 min later, 2.91 g of $Bi(NO_3)_3 \cdot 5H_2O$ were added, followed by a 15 min of stirring. Finally, a 1 M NaOH solution was poured until pH=12 was reached. After that, the mixture was stirred for 2 h and then refluxed for 3 h at 80°C. In the end the product was washed with 2500 mL of distilled water and dried for 24 h.

5.2.3 Preparation of Gas Diffusion Electrodes

a) Preparation of round dry-pressed electrodes (Ø=3.3 cm) for the 1 cm^2 geometrical surface area cell

To achieve a suitable mechanical stability and hydrophobicity, the catalyst powder was mixed with PTFE powder (450 µm) followed by heat treatment.[22,52]

The pressed material consisted of catalyst@AB and PTFE combined in a 65:35 mass ratio and mixed using a knife mile. Due to the limited mixer scale, a maximum of 4.3 g of material could be mixed per time as it was noticed higher amount of material would not ensure an optimal mixing.

For a single GDE, 422 mg of catalyst@AB and PTFE were weighted and poured into a circular metal die with a diameter of 3.3 cm. The die was then compressed by a hydraulic press with 3.5 t of weight for 60 s followed by 7 t for 180 s.

Finally, the GDEs were sintered to ensure a good compactness and porosity of the material. This process was conducted by increasing the temperature up to 340°C with a heat rate of 5 K/min and then held for 10 min, all under N_2 atmosphere.

c) Preparation of dry-pressed electrodes (10 cm x 10 cm) for the 25 cm^2 geometrical surface area cell

The preparation of the rectangular electrodes for the 25 cm^2 cell was conducted by the partner department German aerospace centre (in german: Deutsches Zentrum für Luft- und Raumfahrt, DLR).

The GDEs are formed using a pair of compressing rollers which compact the catalyst@AB and the stainless-steel mesh (type 1.4404, 0.5 mm mesh size, 0.16 mm wire thickness) together in order to end with a dry pressed electrode with an integrate current collector. The catalyst mixture is the same as that previously described for the dry pressed round electrode with Ø=3.3 cm (catalyst@AB:PTFE=65:35).

At the end of this process a 30x15 cm^2 piece GDE is formed. The final 10x10 cm^2 electrodes were cut out using a hydraulic press and an appropriate stencil.

c) Preparation of spray-coated electrodes (10 cm x 10 cm) for 25 cm^2 geometrical surface area cell

In order to avoid material waste - with particular reference to the stainless steel meshes - a spray coated method was tested.

These GDEs were made using a carbon fiber-based gas diffusion layer (Sigracet 39 BB where BB indicate the presence of a MPL) that serve both as structural support and as gas diffusion layer (GDL) in order to improve the diffusion of the CO_2 into the solution. In this case, it is preferably to use a carbon paper endowed with a micro porous layer (MPL) in order to improve the GDE hydrophobicity in case of macroscopic cracks on the catalyst@AB layer.

Concerning the preparation, a solution - defined as ink - was made mixing 1.4 g of catalyst@AB and 0.753 g of PTFE (450 μm) in 100 mL isopropanol. The quantities of catalyst and PTFE were calculated in such a way as to have 1 mg/cm^2 of Sn^0 in the electrode. The quantity of isopropanol was not precise since it was used as solvent.

The spray coating process was conducted using an air gun, a capillary tube (Ø 1 mm) and a hot plate. The ink, stored in an external reservoir, was made to flow in the Ø 1 mm tube and at its exit it was volatilized through the air jet coming from the air gun nozzle.

In that way, the ink could be sprayed and deposited to the GDL. Also, the isopropanol evaporated leaving just the PTFE and the catalyst@AB layer. In order to make the process faster, the GDL was usually laid in a heated plate maintained at 80°C with the purpose of allowing the isopropanol to evaporate faster. Since the whole process may take a long time, the procedure could be done automatically by using an automatic spray coating machine. The machine used was a Nadetech ND-SP Ultrasonic Lab Spray Coater and it was designed to produce electrodes with areas up to 100x100 mm.[87]

5.3 Electrolyser Cells

5.3.1 Cell with 1 cm^2 geometrical surface area

The 1 cm^2 geometrical active area cell is the same used by Oβkopp et al.[13] The schematic drawing is represented in the following image.

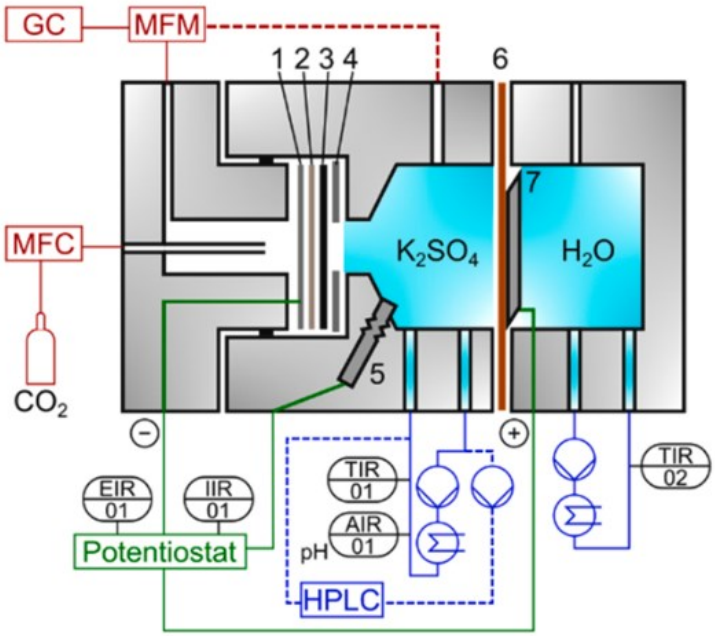

Figure 5.1 representation of the 1 cm^2 cell. 1) current collector. 2) carbon paper. 3) gas diffusion electrode (GDE). 4) 1 cm^2 mask (ABS). 5) screw type RE (Ag/AgCl). 6) membrane (Nafion 117). This image was taken from literature.[13]

It is important to distinguish between active and geometrical surface area of the electrode: the former is provided by a the three phase boundary. Instead, the geometrical surface area represent the surface area in contact with the catholyte and it is provided by using masks and/or sealings proper of the cell (e.g. point 4 of *figure 5.1*), as the total electrode surface would be even greater. Therefore when referring to the 1 cm^2 cell, '1 cm^2' indicates the geometrical surface area.

As shown in the picture, the cathodic compartment can be divided into two regions, delimited by the GDE itself. On the outermost side, CO_2 is flowed, and a gas diffusion layer has been used to help the gas reach the three-phase boundary zone. Also, a stainless-steel mesh is positioned behind the GDL serving as current collector improving the current passage. On the other cathode half, the GDE is in direct contact with a 0.5 M K_2SO_4 catholyte. The FA obtained at the three-phase boundary get desorbed and stored into the solution. Here, a reference electrode (Ag/AgCl electrode) is also positioned. Finally, Nafion® 117 is the only membrane used to divide the anodic from the cathodic compartment.

Besides the liquid FA, also parasite gases such CO and H_2 are developed. In order to have a good quantification of them, the head space of the cathode chamber is combined with the gas outlet of the electrolyser (red lined in *figure 5.4*)

Finally, at the anodic compartment, bi-distilled water is made flow. An IrO_2/Ti is used as anode and eventually positioned on a Pt mesh which acted as current collector. Additionally, the cell operated with a ZGA configuration, therefore the anode was pressed against the membrane.

5.3.2 Cell with 25 cm^2 geometrical surface area

The 25 cm^2 cell design is shown in *Figure 5.2.* The overall structure matches the 1 cm^2 cell with the addition of some new features.

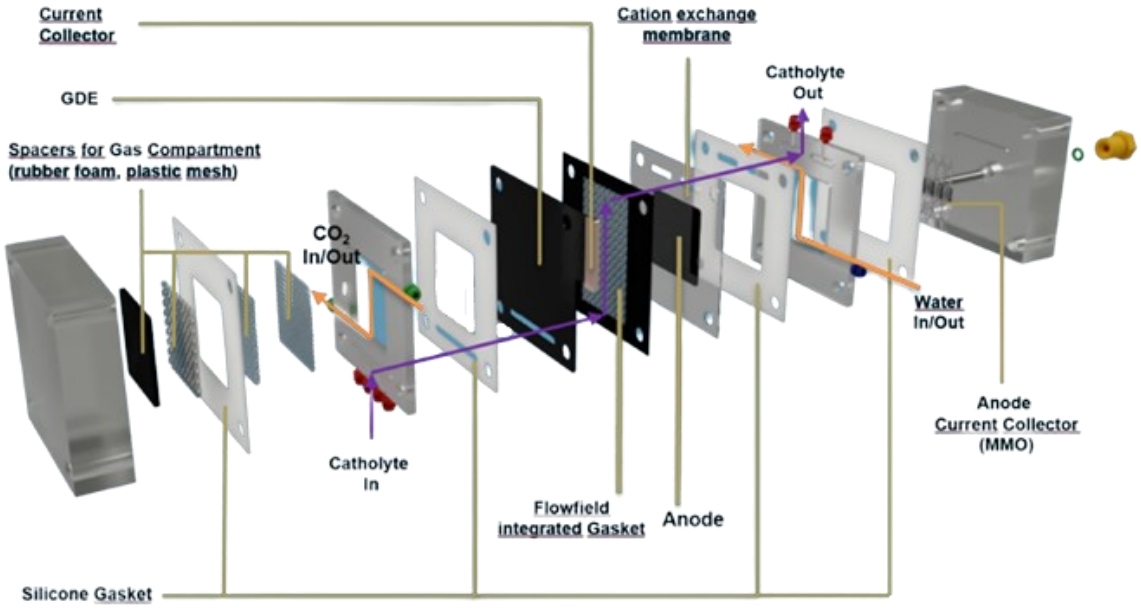

Figure 5.2 Exploded-view drawing of 25 cm^2 electrolyser cell (image received from Marvin Oвkopp).

Also in this case, it has to be distinguished the difference between active and geometrical surface area previously described for the 1 cm^2 cell. Therefore when referring to the 25 cm^2 cell, '25 cm^2' indicates the geometrical surface area, as the total electrode surface would be even greater.

This cell presents a two-electrode configuration, implying that only the full potential of the cell can be measured. The cathode side is split into two compartments by the GDE. On the cathode outermost side, a rubber foam and a plastic mesh act as spacers with the aim of avoiding the electrode deformation and facilitate the CO_2 flow. On the opposite side, a 0.5 M K_2SO_4 catholyte circulates between the GDE and the membrane thanks to the presence of a polypropylene mesh which take the name of flow field (FF). By changing its thickness, the electrode-membrane distance could be varied and so the electrolyte layer thickness.

Moreover, the anode consists of a porous Titanium transport layer coated with IrO_2 and it is laid upon a MMO coated titanium current collector. As in the cathode side, the anolyte (bi-distilled water) recirculates from an external reservoir to the cell. In addition, the pressure between the anode and the membrane could be varied using an external clamp and a torque wrench. In this way, it is possible to control the so-called clamping pressure (CP).

The two-cell compartment were separated using a CEM. Some of the membrane used in this work and their relative thicknesses are listed in *table 5.2*.

Table 5.2. List of the membrane analysed with their relative thicknesses.

Membrane	Thickness (µm)
Nafion 115	127[66]
Nafion 117	178[66]
Nafion 324 (reinforced)	150[85]
FKBPK130	110-140[88]

Finally, in both the cell design, gases are collected in the catholyte chamber which means that no leakage somewhere should happen. While the 1 cm^2 cell was designed for having a complete sealing, for the 25 cm^2 cell there was the necessity to have a sealed reservoir. For this reason, a threaded 250 mL bottle was used in order to properly collect the gases.

Figure 5.3 Photo of the catholyte reservoir.

5.4 Experimental setup

The complete structure of the system is schematised in *Figure 5.4*. The dashed lines indicate the setup modifications when the 1 cm^2 cell is used. The analysis was conducted with the Gamry® reference 3000 potentiostat. When total current I exceeded values of 3 A, a

Gamry® Reference 30k Booster was connected. Since the 1 cm^2 cell present a three-electrode configuration, the integrated current-interrupt method (*chapter 3.6*) was used to automatically neglect the *IR* loss.

Catholyte and anolyte were pumped with two peristaltic pumps which allowed to mix the solutions and maintain them at *T*~42°C by a thermostat. Catholyte pH and conductivity were measured by two Hamilton Arc Air® sensors (Polilyte Plus H Arc 120) and its inlet temperature (T_{inlet}) and outlet temperature (T_{outlet}) were measured through *T* sensors.

The CO_2 inlet flow was regulated through an EL-flow series Bronkhorst® mass flow controller (MFC) with a max capacity of 50 mL/min for the 1 cm^2 cell and 500 mL/min for the 25 cm^2 cell. To avoid the GDE breakage, the pressure was monitored through an Omega® sensor (model) and adjusted with a needle valve in the off-gas line. The out-gas flow rate was then detected with an EL-flow series Bronkhorst® mass flow meter (MFM).

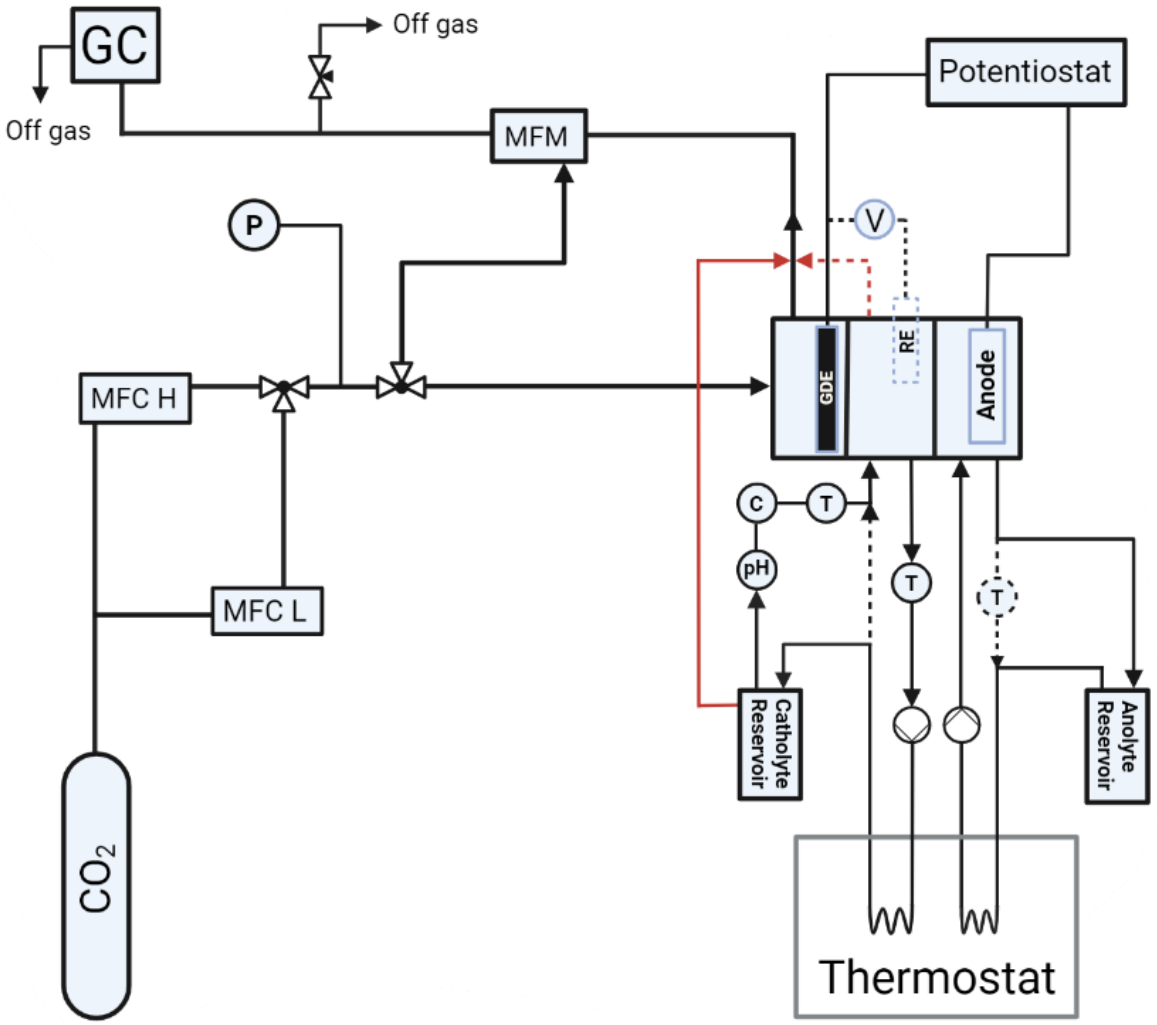

Figure 5.4 Flow diagram of the setup with the 25 cm^2cell. The dashed lines indicate the setup when the 1 cm^2cell is used. Red lines indicate the link between cathode/catholyte reservoir and MFM. Legenda: C=conductivity; T=Temperature; P=pressure; MFC H=high CO_2 flow rate (0-500 mL/min) ; MFC L=low CO_2 flow rate (0-50 mL/min)

5.5 Analysis and data treatment

5.5.1 Faraday Efficiencies and Energy efficiencies analysis

Gaseous products (H_2, CO, CO_2 and CH_4) were quantified online by a Gas Chromatography (Agilent 7890A equipped with two Hayasep Q and one Molsieve 5A columns) using Argon 5.0 as a carrier. Thermal conductivity (H_2, CO_2, CO) and flame ionisation detector (CH_4 and impurities) were used as detectors. The offline measurement was conducted using a HPLC (Agilent 1280 infinity) equipped with a Nucleogel Sugar 810H (Machery-Nagel) column, a refractive index detector, and 5 mM sulfuric acid in water as eluent. The flow rate was set at 0.6 mL/min.

The Faraday efficiency obtained through the GC was calculated considering the amount of H_2 and CO produced during the experiment. As showed in the *Chapter 4.1*, the reactions (4.2), (4.3) and (4.4) depict the main parasite reaction for the HCOOH synthesis. Considering their amount and Faraday efficiency, it is possible to estimate indirectly the FE_{FA}.

The Faraday efficiencies of H_2 and CO were calculated through an adaptation of the general FE formula (*formula 3.18*):

$$FE_p = \left(\frac{1}{V_m} \cdot \frac{1}{N} \sum_{i=1}^{N} x_{p,i} \cdot V_{out}\right) \cdot z \cdot F \cdot (I \cdot t)^{-1} \qquad (5.1)^{13}$$

With p being either H_2 or CO, V_m the molar volume, N the amount of GC measurement performed, $x_{p,i}$ the volume fraction of the respective product p, V_{out} the measured outlet flow rate at the measurement number i, z the number of electrons, F the Faraday constant, I the electric current and t the time of the experiment.[13]

From FE_{H2} and FE_{CO} is then possible to determine FE_{FA}:

$$FE_{FA} = 1 - (FE_{H_2} + FE_{CO}) \qquad (5.2)$$

The offline HPLC analysis gives the FA concentration instead. In that way it is possible to determine the FE directly through the formula:

$$FE = \frac{z \cdot c \cdot V \cdot F}{I \cdot t} \qquad (5.3)$$

Where c is the FA concentration and V is the overall catholyte volume.

Nevertheless, the total volume of catholyte may increase due to the osmotic passage of water from anode to cathode. To obtain the most accurate measurement possible, a known amount of maleic acid was injected as an internal standard at the end of each experiment. Then, through HPLC measurement, the experimental concentration of maleic acid could be determined and used to derive the actual final volume of catholyte.

While FE describe the selectivity of the CO_2RR process, it does not consider the voltage employed and so the energy required. For this reason, it is usual to find the energy efficiency (EE) in literature.[67] This parameter is described through the general *formula 3.19* which adapted for the cathodic and anodic reactions employed in this work become:

$$EE = \frac{(\varphi^0_{OER} - \varphi^0_{CO2\ to\ HCOOH})}{\varphi_{cell}} \times FE_{HCOOH} \qquad (5.4)$$

Where φ^0_{OER} (1.23 V vs NHE at 298 K) and $\varphi^0_{CO2\ to\ HCOOH}$ (-0.199 V vs NHE at 298 K) are the standard electrode potentials of oxygen evolution reaction (OER) and CO_2RR to HCOOH while φ_{cell} is the total cell voltage.

When a three-electrode system is employed and the cathode potential is measured against a RE, the energetic cathode efficiency (ECE) is generally calculated instead (*formula 3.20*). Specifically for the CO_2 reduction to HCOOH it becomes:

$$ECE = \frac{\varphi^0_{CO2\ to\ FA}}{\varphi_{cath\ vs\ RE;\ IR}} \times FE_{HCOOH} \qquad (5.5)$$

This does not represent a real energetic efficiency, since ohmic overpotentials and counter reaction are not considered in this value. Also, the ECE depends on the reference electrode chosen for obtaining $\varphi^0_{CO2\ to\ FA}$ and $\varphi_{Cath\ vs\ RE;\ IR}$. Nevertheless, it allows to observe and compare the cathodic performance only.

5.5.2 Thermogravimetric analysis

For every batch, the amount of Sn-loading or Bi-loading were measured with a thermogravimetric measurement (TGA). The metal loaded carbon sample was heated in air until a temperature of 750°C was reached and the respective mass loss was measured. The remaining mass was assumed to be pure SnO_2 or Bi_2O_3 respectively. However the relative catalyst loading is generally given for the elements Bi^0 and Sn^0 in the total mass weight (wt.%) as the exact Sn and Bi oxide species during CO_2RR operation are not known.

5.5.3 Electrochemical experiments

Every electrochemical experiment consisted of a linear current ramp (LCR) and a constant current electrolysis (CCE) in series. The LCR was employed as preconditioning step to increase the electrochemical active surface (ECSA) before conducting constant current electrolysis.

In the 1 cm^2 cell, the linear current ramp consists of an increase of the current from 0 to -400 mA/cm^2 with a scan rate of 2 mA/(s*cm^2). Instead, the following CCE was conducted at a current of -400 mA/cm^2 observing the potential variations.

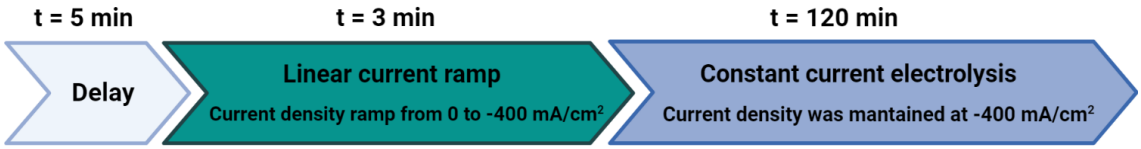

Figure 5.5 Schematic representation of the 1 cm^2 cell measurements.

In a similar way in the 25 cm^2 cell, the LCR measurement consisted of varying the current density from 0 to -100 mA/cm^2 with a scan rate of 2 mA/(s*cm^2). That was followed by

the CCE where the potential variations were observed maintaining the current density at -100 mA/cm^2.

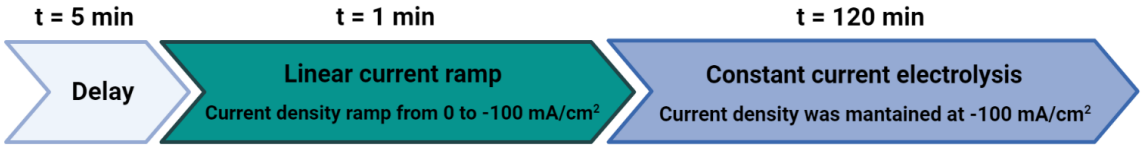

Figure 5.6 Schematic representation of the 25 cm^2 cell measurements.

6. Results and discussion

As contribution to the eForFuel project, the main scope of this work was to identify the different features that could lead to a higher efficiency of the scale up electrolyser (with a 25 cm^2 geometrical surface area). Still, the electrolyser with a 1 cm^2 geometrical surface area, was used for several catalyst analyses and single-pass operational tests. Both the cells are characterised by a ZGA configuration which allowed to operate in acidic conditions to obtain HCOOH as the final product. At batch mode, the pH trend over time showed a similar behaviour regardless of the catalyst and most of the cell features, for both the setups. *Figure 6.1* shows the pH observed in the two electrolysers in a batch mode with a 0.5 M K_2SO_4 catholyte at T~42°C. A catholyte volume of 40 mL and a CD of -400 mA/cm^2 was used for the 1 cm^2 cell; while a catholyte volume of 250 mL and a CD of -100 mA/cm^2 was used for the 25 cm^2 cell. Current density and catholyte amount were adjusted according to the geometrical electrode surface to get the same concentration and pH time curve in case that FE is the same.

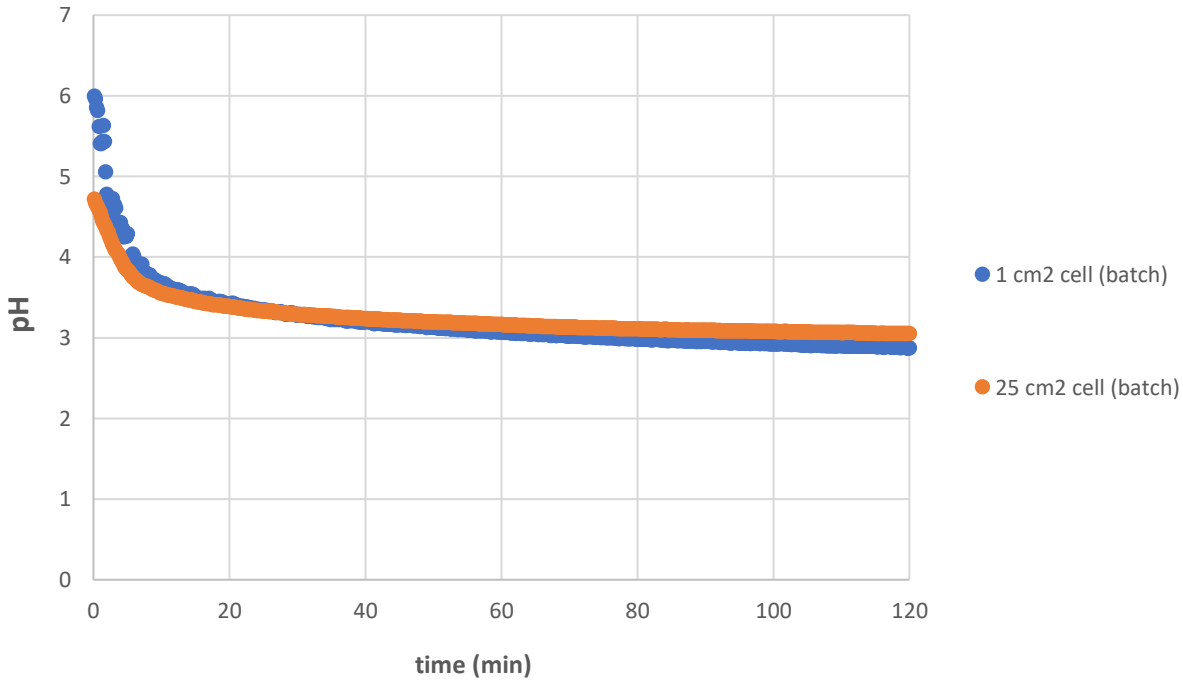

Figure 6.1. pH over time with the 1 cm^2 and 25 cm^2 geometrical surface area electrolyser at batch mode with a SnOx@AB catalyst (2.52 wt.% of Sn). 1 cm^2: CD=-400mA/cm^2; catolyte volume=40 mL. 25 cm^2 cell: CD=-100mA/cm^2; catholyte volume=250 mL;

As described in the previous chapters, most of the up-to-date research on CO_2RR shows little interest in the scalability of the process making its industrial applicability still impractical. Because of that, it was taken into account what reported by Kopljar et al. [12], for which, the analysis which need to be deepened could be rearranged into three main points:

1) Catalyst analysis

The first tests were conducted over the catalyst reproducibility in order to guarantee the validity of the results ascertained for the 25 cm^2 cell features. Only Sn- and Bi-based catalysts were used in this work. In addition, since the optimal GDE Sn-loadings were already reported in the literature[22,47], part of the analysis was conducted with the aim of defining which Bi-loading could lead to higher selectivity towards FA.

2) Scalability of the process

The main contributors to the efficiency of the scale up cell were never been established, for this reason each characteristic was analysed one by one in order to define their relative significance. The design parameters, such the distances between electrodes and membrane, were tested before proceeding with the operation parameters (temperature, flow rate, concentration and current density) investigation.

3) Possibility to operate at continuous mode

Alternatively to the batch mode, the possibility to operate with a continuous single-pass catholyte was tested in both the electrolysers as it could be of fundamental importance for future industrial applications.

6.1 Catalyst

6.1.1 Reproducibility of Sn and Bi-based GDE

In this work, only SnO_x and Bi_2O_3 catalysts were tested for the HCOOH production due to their low cost and toxicity.[9,28,29]

Scale up experiments determined the need for larger-scale catalyst synthesis. Nevertheless, the available devices allowed to obtain final quantities of 35 g and 17 g respectively for the SnO_x@AB and Bi_2O_3@AB (*Chapter 5.2*). Considering that a single 25 cm^2 GDE required ~6 g each, the amount from a single batch of synthesis was not enough to conduct a large number of experiments. For that reason, it was essential to ensure that the catalyst behaved the same for every batch. To guarantee the significance of the experiments, a 'performance test' analysis was conducted in the 1 cm^2 electrolyser since it requires less material for its GDEs and present less variable parameters (no variable cathode-membrane distance and no CP). Also, the loading of the catalyst in weight percentage (wt.%) of Sn (or Bi) on AB was monitored for every synthesis by using a TGA.

The same Sn-loading was used for the production of SnO_x@AB since previous research had already investigated the optimal one[47]. On the contrary, no studies on the different Bi-loadings were found in the literature. This suggested the need for further studies on the matter.

In summary, the product selectivity and catalyst loading reproducibility were analysed for both the catalysts. In addition, the effects of different catalyst loadings were tested for Bi-based catalyst only.

a) SnO_x@AB reproducibility

Eleven SnO_x@AB batches were produced with the same exact synthesis described in *chapter 5.2*. The product efficiency of every batch was then double checked with an online GC and, right after, with an offline HPLC measurement. In fact - as described in *chapter 5.4* - the amount of FA could be determined indirectly by measuring the amount of H_2 and CO (*formula 5.2*). In addition, a HPLC measurement was conducted after every experiment with the aim of measuring the concentration of FA in the final solution and directly deriving the FE_{FA} (*formula 5.3*).

Also, for every batch, the catalyst loading was detected through the use of a TGA. Loadings are expressed as weight percentage (wt.%) of metallic Sn related to the total mass, as its exact oxidation state during operation is not yet clear.[47] The results are reported in *Figure 6.2*.

The analysis for SnO_x showed high reproducibility on product efficiency: no CH_4 or C_2 products were detected while FE_{FA} of ~87% was achieved in nearly every synthesis. The remaining percentage was partitioned between CO and H_2 with average values of ~10% and ~3% respectively. Generally, the results presented lower FE_{FA} for the HPLC

measurement since part of the product could flow through the cation exchange membrane and get oxidised at the anode (crossover). For that purpose, different membranes were tested later in order to reduce the loss of FA by crossover. The Sn-loadings on the total weight assumed similar results ranging from 2.19 wt.% to 2.84 wt.%.

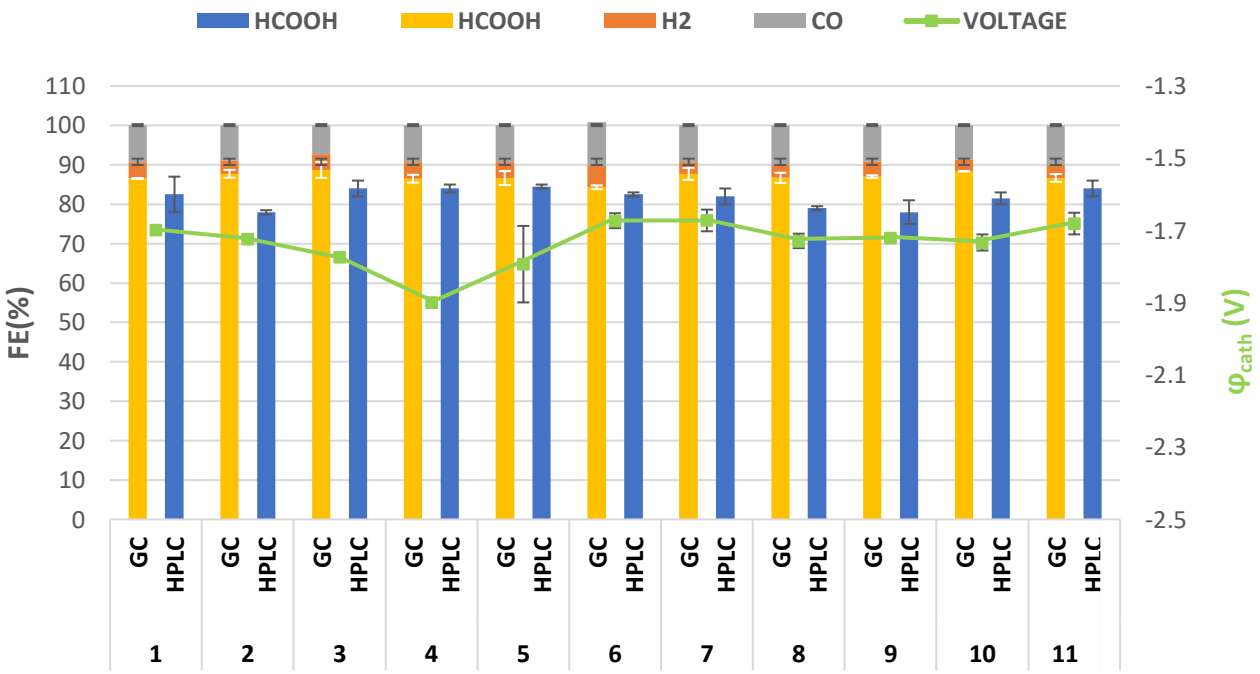

Actual Sn-loading (wt.%)	**2.19**	**2.52**	**2.82**	**2.76**	**2.84**	**2.27**	**2.76**	**2.62**	**2.67**	**2.44**	**2.32**
Experimental Sn-loading (wt.%)	2.55	2.55	2.55	2.55	2.55	2.55	2.55	2.55	2.55	2.55	2.55

Figure 6.2. Graphical representation of the Faraday Efficiencies for different SnO_x@AB batches. Every batch is characterised by two bars, the first was defined through a GC and the second through an HPLC. In the table below, the actual and experimental Sn-loadings (wt.%) are showed per every batch. CD=-400mA/cm^2; catholyte=0.5 K_2SO_4; T~42°C; anolyte=bi-distilled water; t=120 min at CCE; catholyte volume=40 mL; flow rate= 9 mL/min.

b) Bi_2O_3@AB reproducibility

The same reproducibility tests - as shown for the SnO_x - were conducted for Bi_2O_3@AB. However, just five different batches were prepared during the course of the work. Three different amount of $Bi(NO_3)_3$•$5H_2O$ amount were used, in order to obtain different catalyst loading. The loadings are referred to elemental Bi since there could be other Bi oxide species beside Bi_2O_3. *Figure 6.3* shows the Bi wt.% values for every batch and their respective product selectivity in the short term experiment (2 h).

As can be seen, no reproducibility was achieved for the Bi-loading according to the procedure described in *chapter 5.2.2*. Additionally, in some cases, an actual value higher than the experimental one was obtained (e.g. batch 4 and 1). Such phenomena was observed in a less relevant way for the Sn wt.% too but no explanation was found.

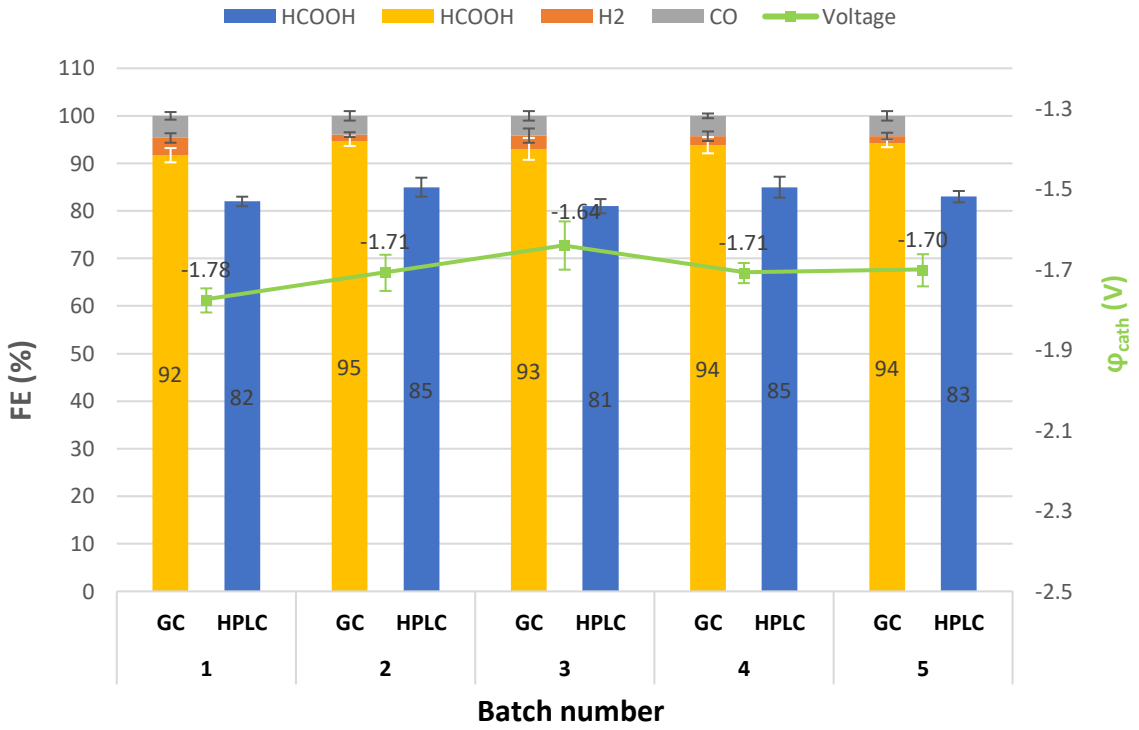

Actual Bi-loading (wt.%)	**9.9**	**17.0**	**20.6**	**23.3**	**32.3**
Experimental Bi-loading (wt.%)	8.4	22.2	22.2	22.2	35.6
Amount of $Bi(NO_3)_3 \cdot 5H_2O$ (reagent)	2.91	8.73	8.73	8.73	17.46

Figure 6.3. Effects of different Bi-catalyst loadings (wt.%) on FE and φ_{cath} in short term experiments (2 h). In the table below, the actual and experimental Bi-loadings are showed per every batch. CD=-400mA/cm^2, catholyte=0.5 K_2SO_4; T~42°C; anolyte=bi-distilled water; t=120 min at CCE; catholyte volume=40 mL; flow rate= 9 mL/min.

Higher amounts of Bi wt.% in the batch - which result in higher amount of Bi_2O_3 mg/cm^2 in the electrode - were expected to increase the FE_{FA}. Instead, no effects were observed in the 2 h experiments. For this reason, longer operation durations were conducted with the purpose to induce a more relevant FE_{FA} variation.

The comparison between 17.0 wt.% and 20.6 wt.% Bi-loading in a 8 h long experiment is shown below (*figure 6.4a*). As can be seen, also in this case, no relevant variations of FE were observed, suggesting that the Bi-based catalyst has a high reproducibility on the product selectivity regardless its loading. However, it has to be noted that a difference of ~4 wt.% may not be enough to detect a relevant FE_{FA} improvement.

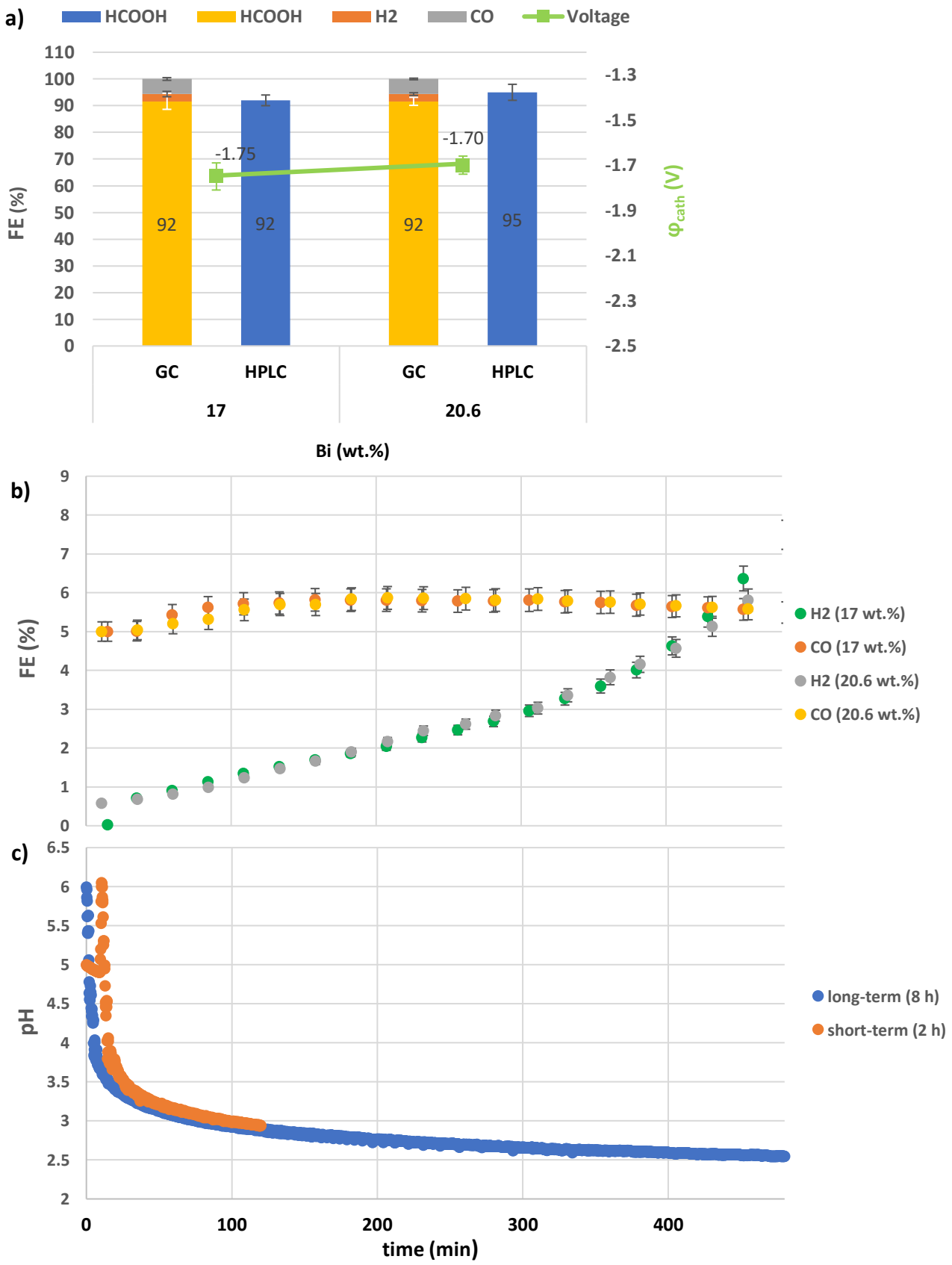

Figure 6.4.a) Effects of different Bi-loadings (wt.%) on FE_{FA} and φ_{cath} in long-term experiments (8 h). b) FE_{H2} and FE_{CO} trend over time at different Bi-loadings. c) pH trend over time for the 2 h and 8 h experiments. CD=-400mA/cm^2, catholyte=0.5 K_2SO_4; T~42°C; anolyte=bi-distilled water; t=480 min; catholyte volume=40 mL; flow rate= 9 mL/min.

As presented in *figure 6.4b*, Bi_2O_3@AB shows stable CO production even after 8 h run. On the other hand, HER displays a strong increase after ~300 min. The latter could be explained as, over time, the pH show a dynamic decrease that could lead to an excessive acidification of the electrolyte (*figure 6.4c*). Overall, the FE_{HER} presented values less than 10%.

The long-term operability of Bi_2O_3 is most likely related with its low degradation. The stability of the Bi species at different pH and voltage is reported in the Bi-Pourbaix diagram (*figure 4.2*). In this case, the operating cathodic potential ranges from -1.7 to -1.8 V (vs Ag/AgCl) while the local pH of the GDE is supposed to have a high value (*chapter 4.4*). Under these conditions, Bi_2O_3 tends to reduce to Bi^0 (*reaction 4.9*). However, while other metallic elements (e.g. Sn^0) appear to be inactive for the FA production, the metallic Bi is characterised by a high selectivity to FA.[26] In fact, it is assumed that Bi_2O_3 is rapidly reduced to Bi^0, where the CO_2RR actually happens.[26] Because of that, the Bi-based GDE are more favoured for future long-term applications.

c) Comparison of the two catalysts

In conclusion, Bi-based and Sn-based catalysts were compared. The results are shown in *figure 6.5* and represent the average result from all the batches of SnOx@AB and Bi_2O_3@AB since, despite having different loadings, they all performed very similarly in the short-term experiments (2 h). Also, the pH showed the same trend over time regardless the catalyst.

Between SnO_x@AB and Bi_2O_3@AB, the latter showed generally better performance in terms of FE_{FA} as it present a higher intrinsic product selectivity[29,89], however, it also presented a higher mismatch between the online GC and offline HPLC measurements. For both catalysts, the cathodic potential assumed values of approximately φ_{Cath} = -1.73 V (vs Ag/AgCl) so that the ECE was also similar, varying from 16% to 20%.

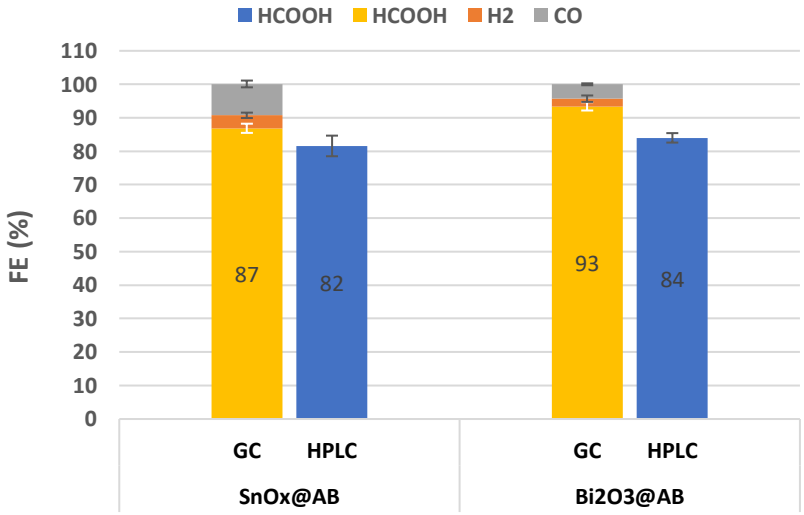

Figure 6.5.Comparison between average Faraday efficiencies of Bi- and Sn-based catalyst@AB. CD=-400mA/cm², catholyte=0.5 K_2SO_4; T~42°C; anolyte=bi-distilled water; t=120 min at CCE; catholyte volume=40 mL; flow rate= 9 mL/min.

Nevertheless, SnO_x@AB was used in most of the experiments of this work as its synthesis allowed to produce more quantity of it per batch and it also showed a higher reproducibility on Sn-loading.

6.1.2 Comparison between dry-pressed DLR and ITC GDEs

As mentioned in the *Experimental Methods*, the GDEs used in this work were produced by different departments. The 1 cm^2 GDEs fabrication could be made at the ITC department, while the 25 cm^2 GDEs needed to be pressed by the associate DLR group due to the necessity of bigger devices. To prove the likeness of the two GDE types, the respective electrodes - from the same batch of catalysis - were tested and compared in the 1 cm^2 cell.

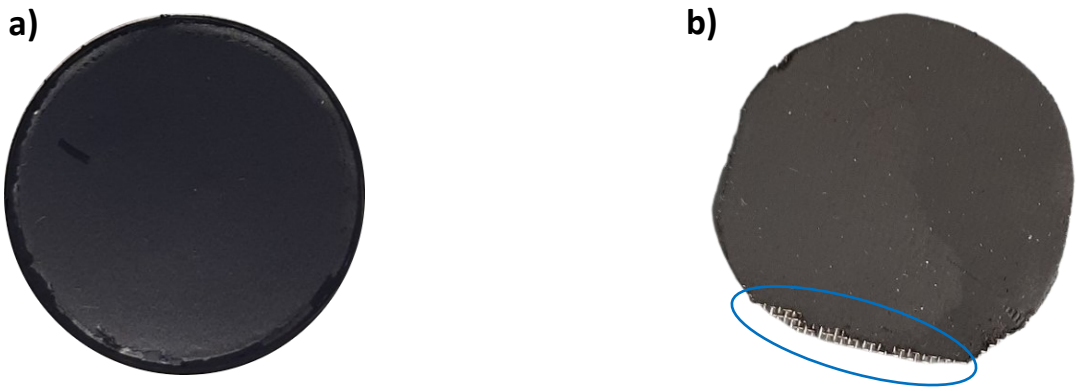

Figure 6.6 a) ITC and b) DLR gas diffusion electrodes in comparison. The blue circle evidence the presence of integrated mesh in the DLR GDE.

The DLR GDEs needed to be cut and adequately shaped. The photos above represent how the two types of electrodes looked like before the analysis. As it is possible to notice from the *Figure 6.6 b,* a visible difference is the presence of an integrated mesh in the DLR GDE which also resulted in a greater thickness than the ITC one.

The FE_{FA} graph reported below, demonstrate the good overlapping of the two GDE preparation methods. The cathode voltage showed a value of -1.73 V (vs Ag/AgCl) for both GDEs, implying a match for the ECE as well. These results demonstrated the effective reproducibility of the GDE preparation methods.

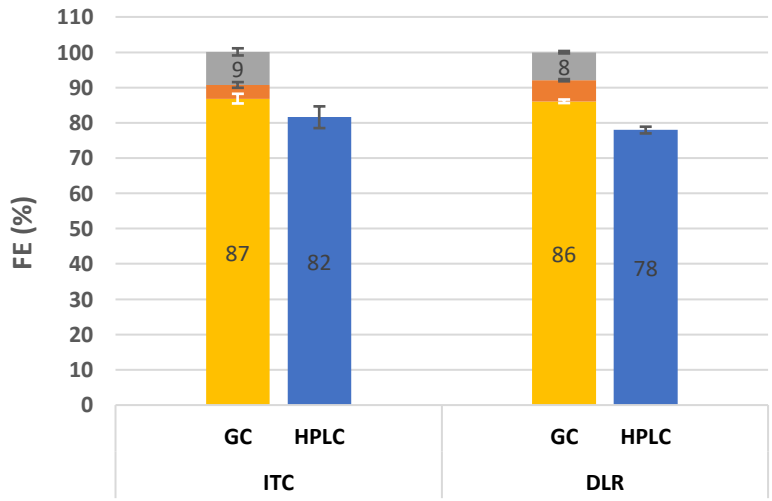

Figure 6.7 Graphic representation of the ITC and DLR GDEs performance. CD=-400mA/cm^2, catholyte=0.5 K_2SO_4; T~42°C; anolyte=bi-distilled water; t=120 min at CCE; catalyst: SnO_x@AB (2.19 wt%); catholyte volume=40 mL; flow rate= 9 mL/min.

6.2 Scale up

6.2.1 Clamping pressure & Flow field effects

The scale up setup was designed with the purpose of analysing additional aspects which could determine a relevant improvement of the electrolysis process. *Figure 5.2* shows the presence of new design parameters that could be opportunely varied: the clamping pressure (CP) and the flow field (FF). The first experiments were conducted on these parameters before proceeding with the study of other features of the cell. Also, as mentioned in *chapter 5.3.2*, the DLR GDE were used with the scale up cell.

a) Clamping pressure

The electrolyser components were held together through four bolts, each per vertex and properly tightened with a 2.5 Nm torque. It has to be clarified that the actual applied pressure, on the active area of the electrode, was not influenced by that. It could instead be varied by using an external clamp and a torque wrench which allowed to apply the desired pressure inside the cell. Such parameter takes the name of clamping pressure and it mainly influence the anode-membrane distance. The exact CP values were then monitored both during the assembly process and during the experiment. Clamps, pressure sensor and cell were kept together with the use of a plastic slab (*Figure 6.8*).

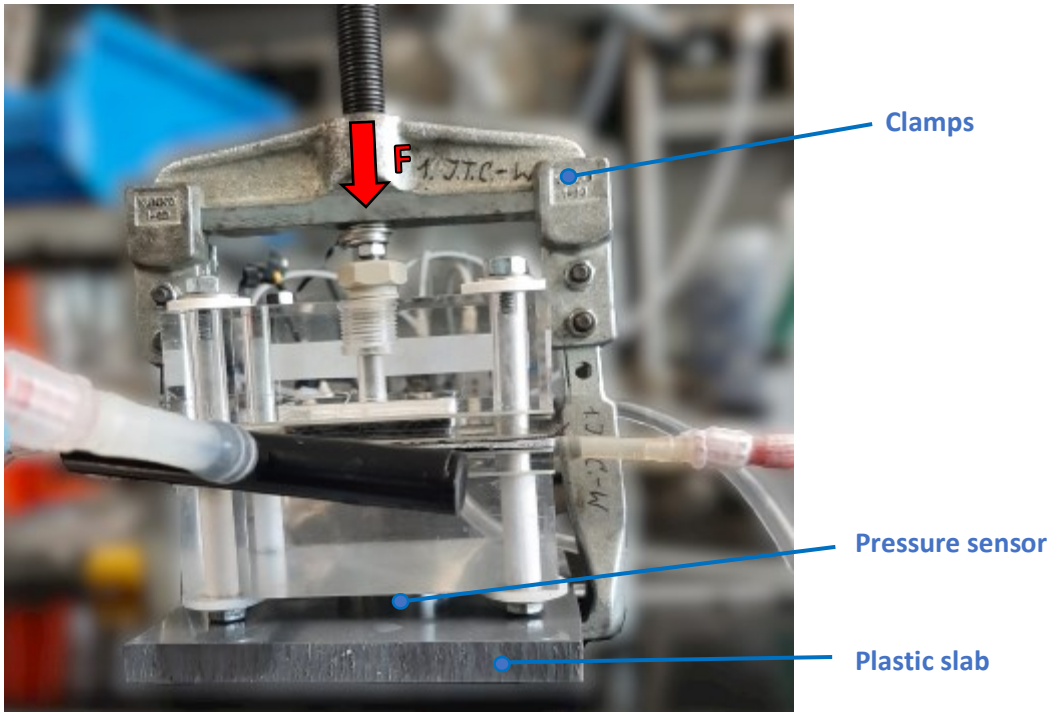

Figure 6.8 Photo of the cell, the pressure sensor and the plastic slab held together by clamps.

Clamping pressures of 0.4, 0.8, 1.6, 2.4 and 3.2 bar were tested in this work. Due to the fragility of the anode, higher pressures could not be applied.

As for the total cell voltage φ_{cell}, it is noted a lower potential when higher pressures are applied (*figure 6.9*). This is most likely induced by a better anode-membrane contact which led to a consequent decrease in R_{cell}.

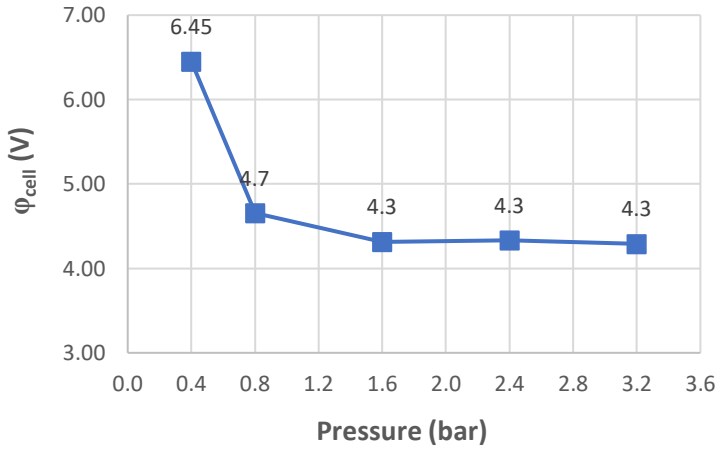

Figure 6.9 Graph of the φ_{cell} variation at different CP with SnO_x@AB catalyst. FF=0.5mm; CD=-100 mA/cm^2; T~42°C; catholyte=0.5 M K_2SO_4; flowrate=20 mL/min; anolyte=bi-distilled water; t=120 min at CCE; catalyst: SnO_x@AB (2.19 and 2.82 wt.%); catholyte volume=250 mL.

On the other hand, the following graph, shows that the FE_{FA} tend to decreases when higher pressures are applied. This is particularly evident when CP higher than 2.4 bar are used.

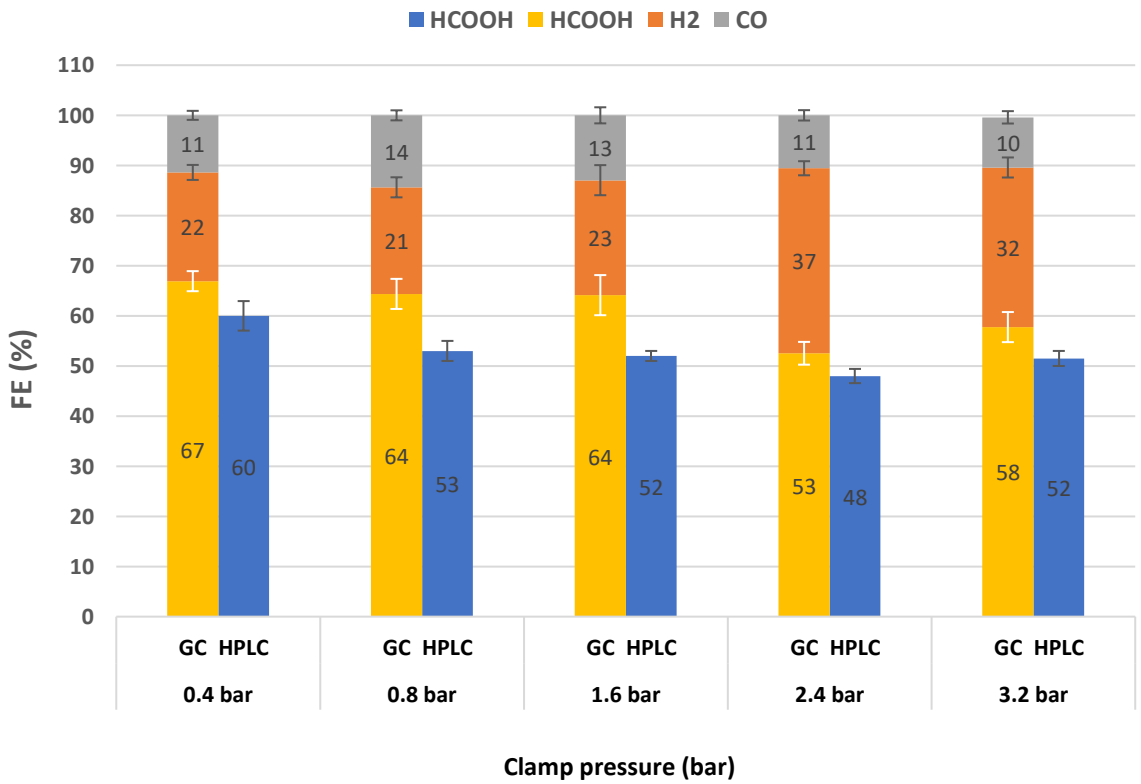

Figure 6.10 Graph of the FEs variation at different CP. FF=0.5mm; CD=-100 mA/cm^2; T~42°C; catholyte=0.5 M K_2SO_4; flowrate=20 mL/min; anolyte=bi-distilled water; t=120 min at CCE; catalyst: SnO_x@AB (2.19 and 2.82 wt.%); catholyte volume=250 mL.

The reason for such decrease in FA selectivity is not very clear but different hypothesis were considered. In detail, this trend could be justified by:

a) an actual GDE damage caused by the penetration of the flow field grid into the catalyst layer (*Figure 6.11a*).

b) an acidification of the GDE from direct contact with the membrane. This allows a direct transport of H^+ to the electrode surface with an increase in HER. Such phenomena could be particularly relevant when thin FF are used. (*Figure 6.11 b*)

Also, in both cases such effects could eventually lead to an obstruction of the catholyte flow resulting in a thinner and a less uniform flow regime.

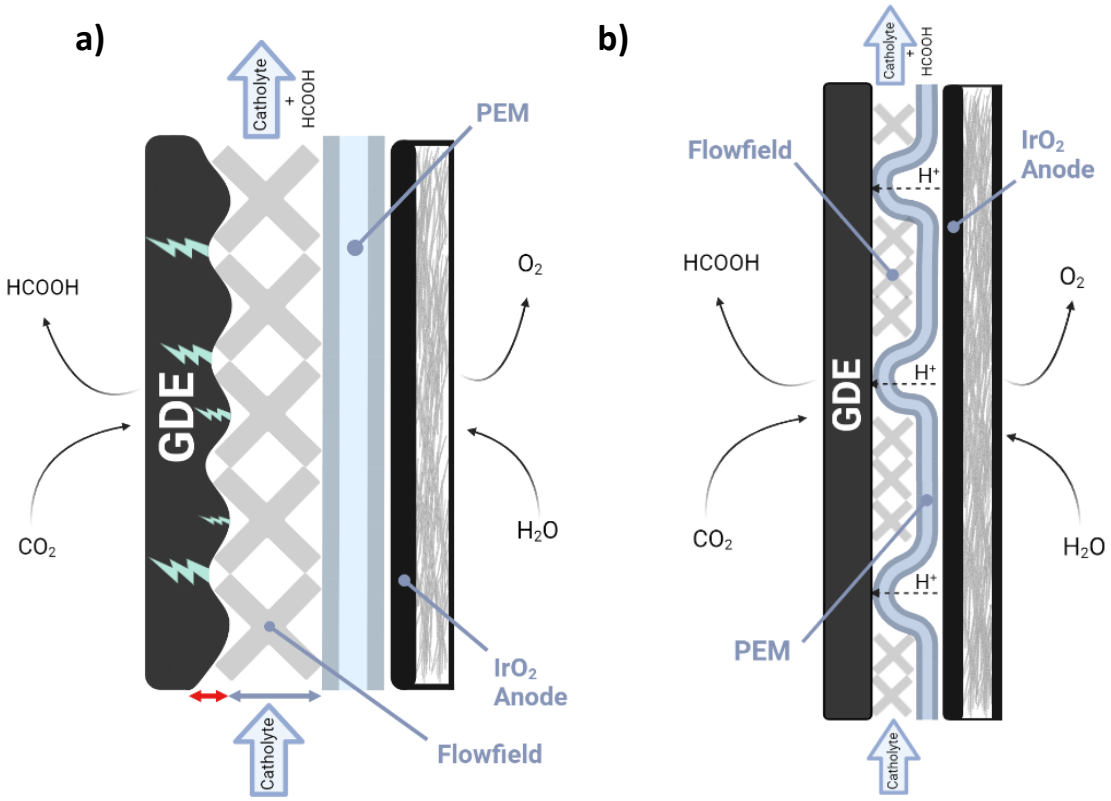

Figure 6.11 a) Lateral 2D representation of the GDE damages apported by the FF infiltration b) Lateral 2D representation of the contact between GDE and membrane when high CP are applied.

To better understand the actual cause of the FE_{FA} decrease, the CP was tested with the use of the appropriate GDE-membrane spacers (FF) described in *chapter 5.3*. FF with 0.5 and 2 mm thickness, were compared at CP of 0 and 3.2 bar. In this way it would have been possible to determine whether this decrease was caused by an effective contact between the membrane and the GDE.

The results (*figure 6.12)* show that the FE_{FA} is more influenced by CP when a thin FF is used. This behaviour could represent a proof of the possible cathode-membrane contact either the presence of an overall thinner catholyte layer.

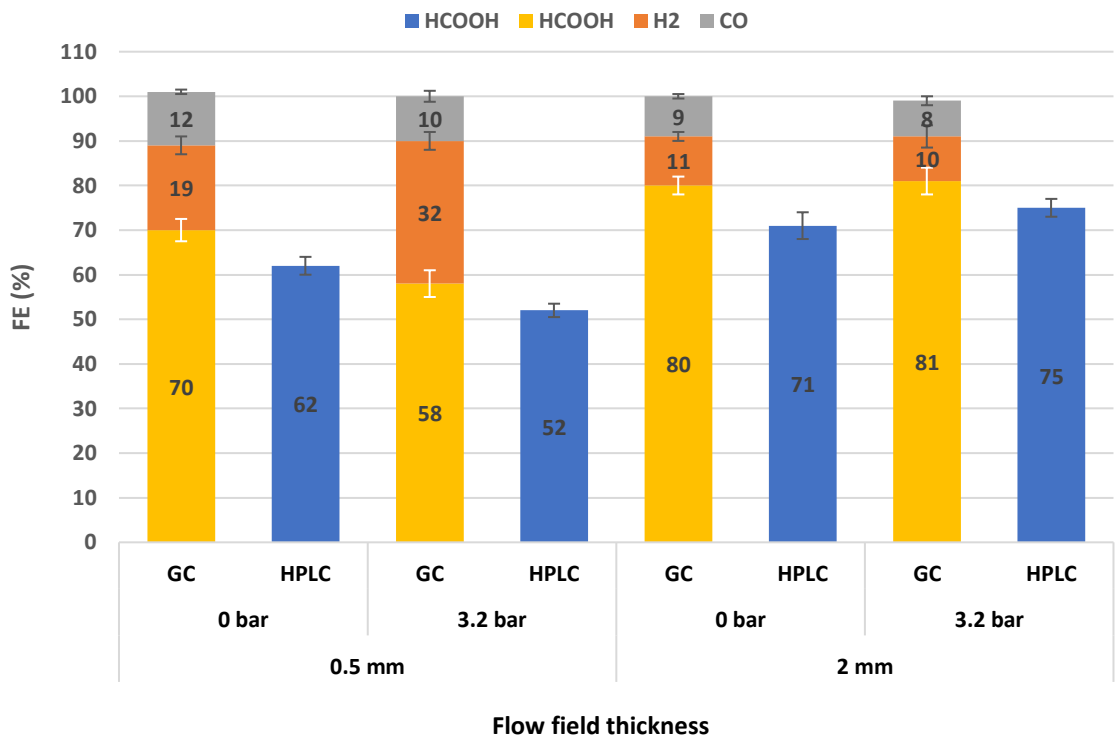

Figure 6.12. CP effect at different FF thicknesses. CD=-100 mA/cm²; T~42°C; catholyte=0.5 M K_2SO_4; flowrate=20 mL/min; anolyte=bi-distilled water; t=120 min at CCE; catalyst: SnO_x@AB (2.19 and 2.82 wt.%); catholyte volume=250 mL.

For the subsequent analysis a CP of 1.6 bar was used as it showed the best compromise between φ_{cell} and FA production.

b) Flow field

As previously mentioned, the distance between GDE and membrane could be varied using flow fields (FF) of different thicknesses. In detail, FF of 2, 1.3 and 0.5 mm were analysed.

The results are reported in the figures below and display an improvement of the FE_{FA} at greater thicknesses with an absolute difference of almost ~20% between the 0.5- and 2-mm FF. Interestingly, while pH presented the same trend, FE_{HER} showed a steeper increase with thinner FF (*figure 6.13b*).

A possible explanation for such behaviour is that the presence of a thinner catholyte layer - which result in a fewer inner cell catholyte volume - could lead to a mass transport problem of FA from electrode to bulk. This result in a higher concentration of FA in the GDE and thus a lower local pH in the electrode. As mentioned in *chapter 4.4*, the possibility to operate in acidic conditions is due to the presence of a high concentration of OH^- in the GDE which avoid the protons to reach the active sites and get reduced. Consequently, an acidification of the local pH of the GDE causes a higher evolution of H_2.

Also, with a thinner FF there could be a possible GDE-membrane contact as observed previously (*figure 6.12*).

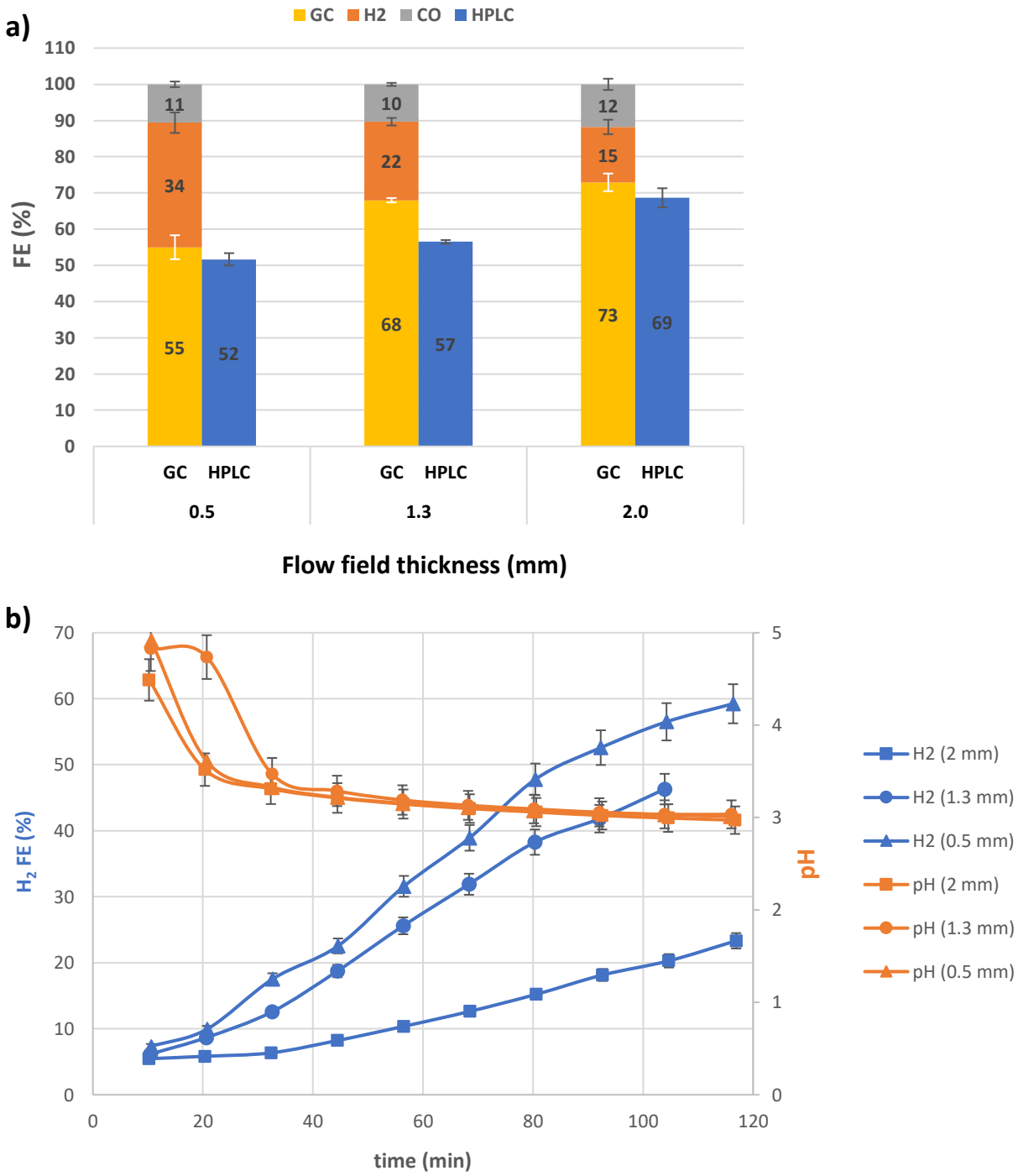

Figure 6.13. Flow field effects on a) product selectivity b) pH and FE_{HER} over time. CP=1.6 bar; CD=-100 mA/cm^2; T~42°C; catholyte=0.5 M K_2SO_4; flowrate=20 mL/min; anolyte=bi-distilled water; t=120 min at CCE; catalyst: SnO_x@AB (2.27 and 2.76 wt.%); catholyte volume=250 mL.

A conductivity of ~69 mS/cm was measured for the catholyte solution (0.5 M K_2SO_4). Therefore, considering the other cell resistances as constant, it was possible to calculate the expected increase in $R_{solution}$ and cell voltage (ΔV) (*figure 6.14b*). As it can be seen, the voltage increase should be negligible but a much higher ΔV was observed instead when switching from the 0.5 mm to the 1.3 mm FF (*figure 6.14a*). The reason for such lower cell

voltage with a 0.5 mm FF is still unclear. Overall, as showed in *figure 6.14a,* all the different FF presented a similar EE ranging from 16% to 19%.

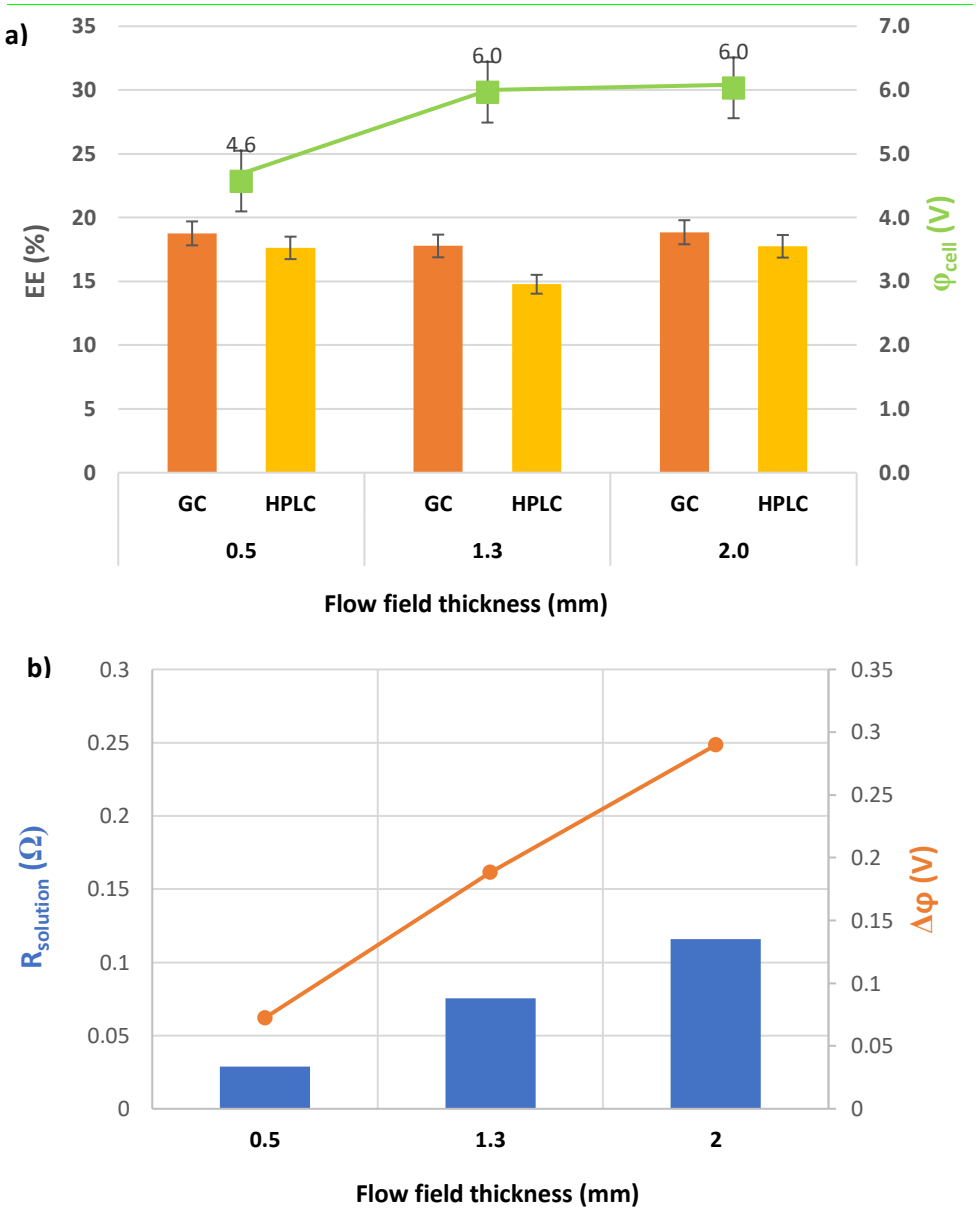

Figure 6.14. Flow field effects on a) Energy efficiency and φ_{cell}. b) $R_{solution}$ and $\Delta\varphi$. CP=1.6 bar; CD=-100 mA/cm^2; T~42°C; catholyte=0.5 M K_2SO_4; flowrate=20 mL/min; anolyte=bi-distilled water; t=120 min at CCE; catalyst: SnO_x@AB (2.27 and 2.76 wt.%); catholyte volume=250 mL.

6.2.2 Spray-coated 25 cm^2 GDE

The GDE production for the 25 cm^2 cell requires multiple and specific devices, not available in the ITC department. In order to overcome the necessity of such sophisticated tools, a spray-coated method was tested since it only requires a spray-coating gun. A feasibility study was made using the procedure described in *chapter 5.2* with the use of PTFE as binder.

These GDEs were made by using a carbon fiber-based gas diffusion layer (Sigracet 39 BB where BB indicate the presence of an MPL) that serve both as support (give more endurance) and as gas diffusion layer (GDL). In this case, it is preferably to use a carbon paper endowed with a micro-porous layer (MPL) to improve the GDE hydrophobicity in case of macroscopic cracks on the catalyst@AB layer.

The final GDE showed good performances during the experiment with FE_{FA} very similar to the dry-pressed one.

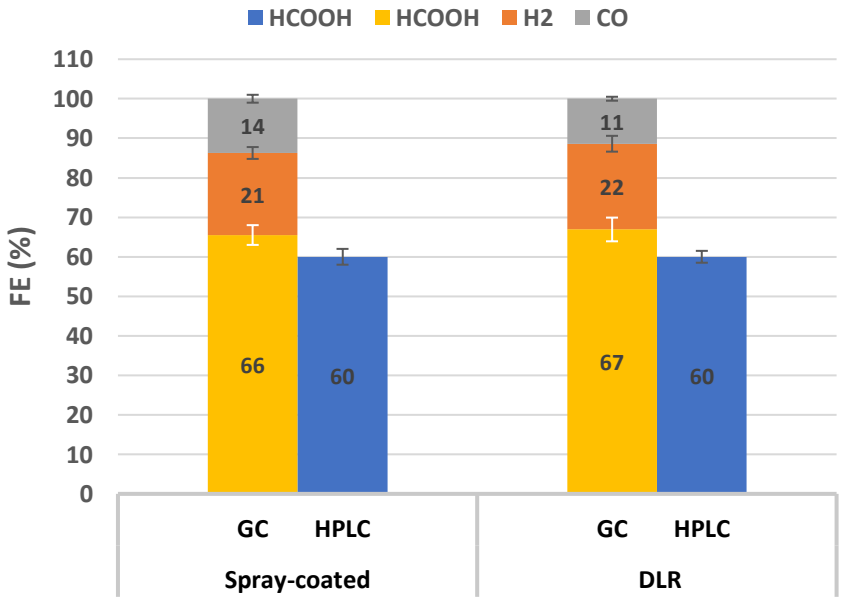

Figure 6.15. FEs comparison between spray-coated and dry-pressed GDE. CP=1.6 bar; CD=-100 mA/cm²; T~42°C; catholyte=0.5 M K_2SO_4; flowrate=20 mL/min; anolyte=bi-distilled water; t=120 min at CCE; catalyst: SnO_x@AB (2.62 wt.%) with; catholyte volume=250 mL.

On the other hand, a single GDE required 2 h for the manual spray-coating procedure only and - due to amount of material that needed to be deposited - a lot of cracks were formed *(Figure 6.16a)*. Also, low solubility of PTFE in isopropanol made the process problematic. Every ~15 min the ink needed to be ultrasonicated to avoid the precipitation of PTFE. The use of an automatic spray-coating machine (available in laboratory) was also hindered by the PTFE insolubility.

For this reason, a more soluble binder was tested. The KD-14 binder showed an excellent solubility into isopropanol allowing the use of the automatic spray-coating machine. Nevertheless, it did not show enough stability over the experiments with a detachment of catalyst from the carbon paper surface.

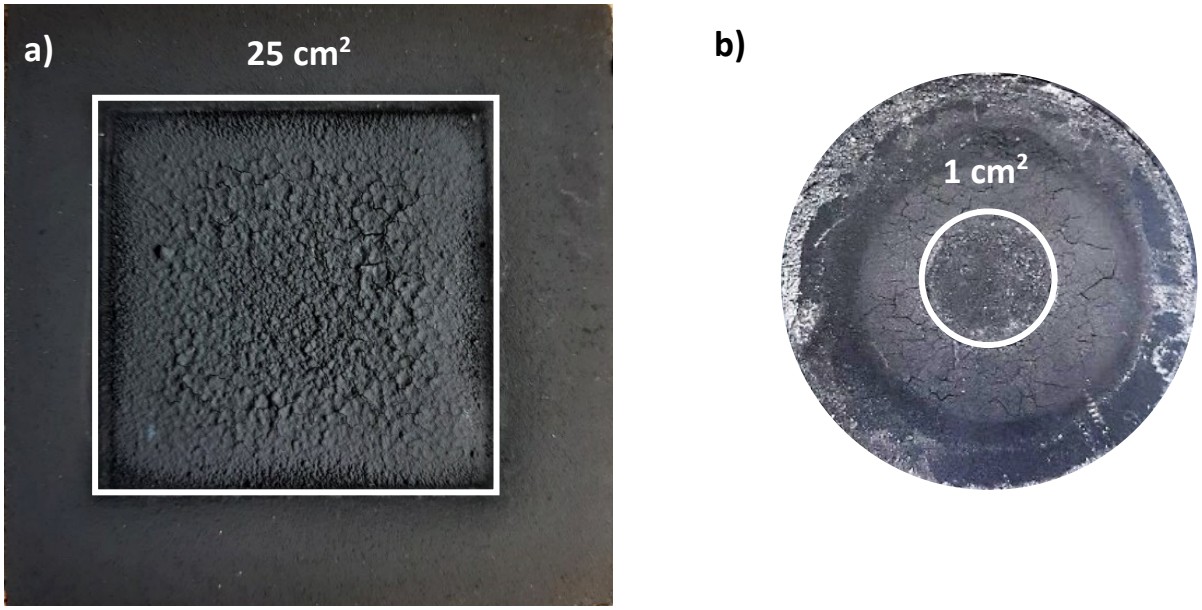

Figure 6.16. a) 25 cm^2 spray coated GDE (PTFE) b) 1 cm^2 spray coated GDE (KD-14).

6.2.3 Membrane

The FE mismatch between the GC and HPLC measurements indicated a FA loss which could be partially caused by its crossover through the membrane. The latter one should allow the passage of cationic species and block or limit the passage of the final products from the cathode to the anode. With the aim of establishing the most adequate one, 4 h long experiments were conducted with the following membranes: N117, N324, FKBPK130 and IrO_x@N115. While N117, N324 and FKBPK130 are commercially available, the IrO_x@N115 was custom made and it is characterised by the presence of an IrO_x layer directly applied to the membrane surface in order to improve the ZGA cell configuration.

A solution containing both 0.5 M K_2SO_4 and 0.25 M HCOOH was used as catholyte. FA was pre-added in order to observe the loss of product since the beginning. Every 30 min a 1 mL sample was collected and analysed through HPLC.

However, the pre-addition of FA caused the development of a strong acidic environment which led to an overwhelming hydrogen evolution. This resulted in the development of an excessive internal pressure which could have damaged the *P*-sensor and the GDE. Because of that, it was not possible to compare the result with the GC measurement analysis since the excessive pression forced to open the off gas valve with a consequent loss of the gaseous products (CO and H_2).

Consequently, the comparison of the membranes was performed considering the final amount of FA obtained since the same catalyst - from the same batch - was used. Therefore, the total quantity of product should depend just by the membrane used. In *Figure 6.17* are reported the total amounts of FA collected with each membrane (mmol).

The calculations were done assuming a constant volume of catholyte during all the experiment since it was observed that the initial (V_{in}) and final (V_{fin}) volumes maintained the same value of 250 mL. Indeed, part of the anodic water managed to flow through the cathode by osmosis, compensating for the missing volume taken for each sample.

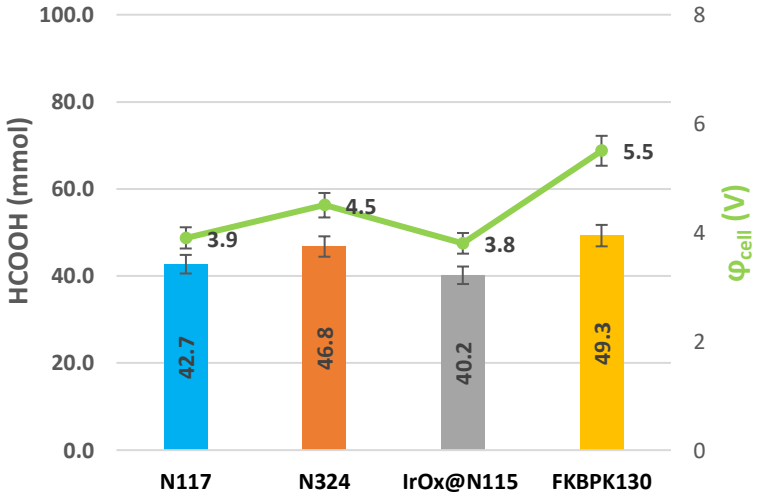

Figure 6.17 Total amount of HCOOH and φ_{cell} obtained per every membranes. FF=0.5 mm; CP=1.6 bar; CD=-100 mA/cm^2; T~42°C; catholyte=0.5 M K_2SO_4; flowrate=20 mL/min; anolyte=bi-distilled water; t=240 min at CCE; catalyst: Bi_2O_3@AB (17.0 and 20.6 wt.%); catholyte volume~250 mL.

Figure 6.18 report the concentration of formic acid as function of time. From this graph it can be seen that the membranes follow a common trend: over the time there is a decrease in slope which could indicate a higher membrane permeability when higher FA concentrations are reached. This phenomena was expected as higher product concentrations would result in higher concentration gradients at the membrane.[83] On the other hand, that could be caused by an increase of a competitive HER by means of a catholyte acidification.

As depicted by *Figure 6.18*, the membranes permeability shows very similar behaviour since their standard deviation bars overlap in a considerably way.

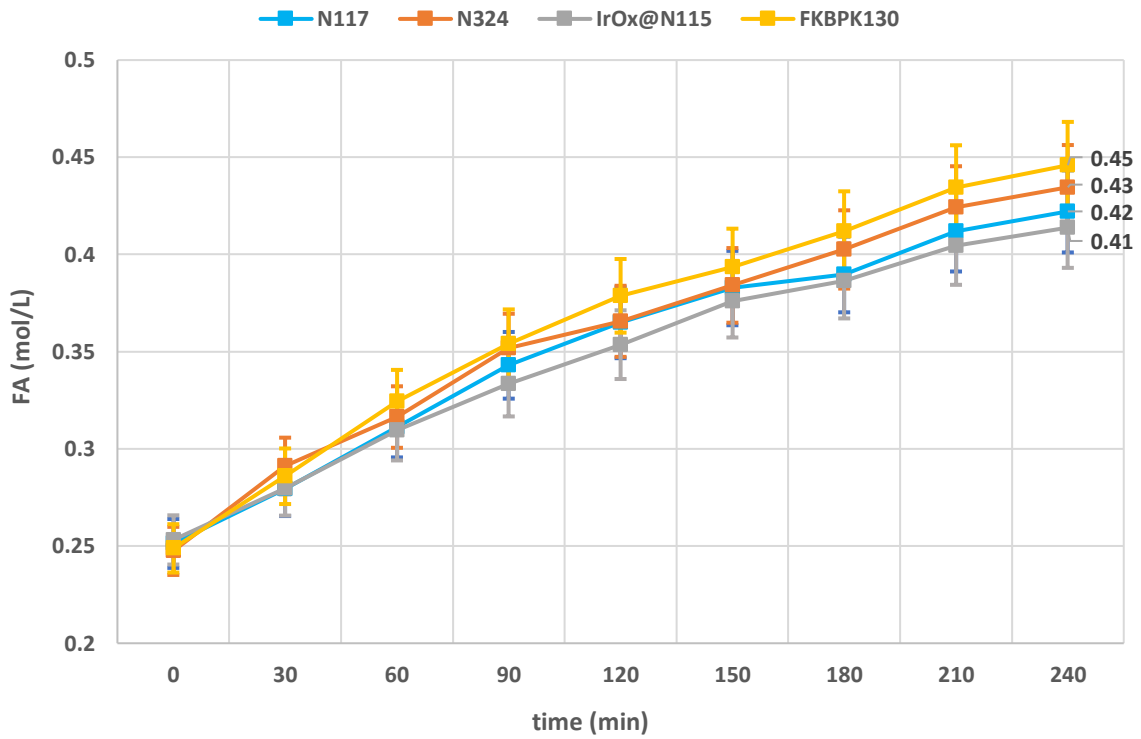

Figure 6.18. Formic acid concentration over time per every membrane. FF=0.5 mm; CP=1.6 bar; CD=-100 mA/cm^2; T~42°C; catholyte=0.5 M K_2SO_4; flowrate=20 mL/min; anolyte=bi-distilled water; t=240 min at CCE; catalyst: Bi_2O_3@AB (17.0 and 20.6 wt.%); catholyte volume=250 mL.

Despite its thicker structure (*table 5.2*), N117 did not exhibit much lower FA permeability than FKBPK130 and N324.

The decent performance of Nafion® N324 was in line with the analysis reported by Yang et al.[66] Such result was justified by its thickness and by the presence of very low water content compared to the other Nafion® membranes which should prevent the FA crossover at higher FA concentrations. On the other hand, a smaller amount of water made the membrane less conductive with a visible increase in φ_{cell} (*Figure 6.17)*.

FKBPK130 structure is not well defined by FUMATECH BWT GmbH but the φ_{cell} analysis suggests it has very little water amount which could also explain its ability to reduce the FA crossover.

Overall, the membranes exhibited very similar behaviour. This made choosing the most suitable one non-trivial. The energy efficiencies showed a value of ~8%.

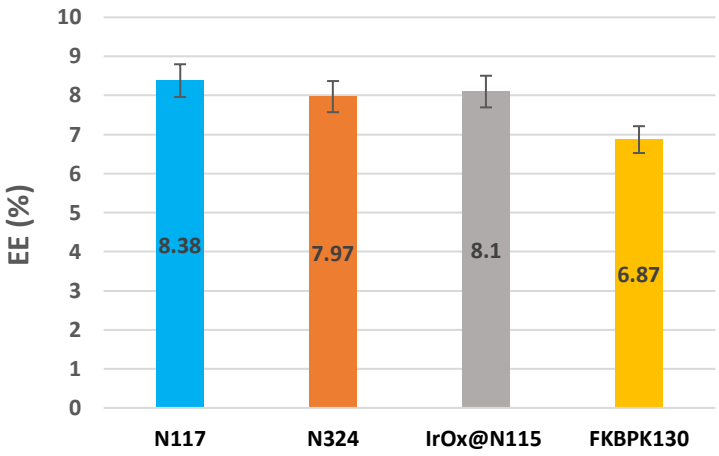

Figure 6.19. Energy efficiencies obtained per every membrane. FF=0.5 mm; CP=1.6 bar; CD=-100 mA/cm^2; T~42°C; catholyte=0.5 M K_2SO_4; flowrate=20 mL/min; anolyte=Bi-distilled water; t=240 min at CCE; catalyst: Bi_2O_3@AB (17.0 and 20.6 wt.%); catholyte volume=250 mL.

For the following experiments N324 was chosen because of its FA permeability and mechanical stability, guaranteed by the presence of a support grid (*Figure 6.19)*. This last aspect was taken in consideration in order to avoid the contact between GDE and membrane as described in the *clamping pressure* chapter. Also, a stiffer membrane resulted in lower probability of wrinkling and therefore a better anode-membrane contact.

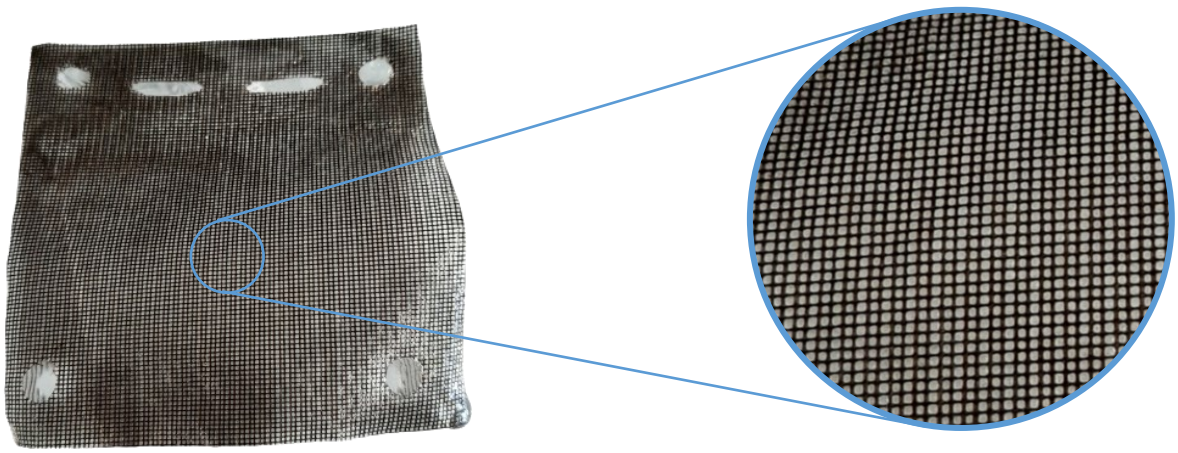

Figure 6.20 Photo and zoom-in of the Nafion® N324 membrane.

6.2.4 Flow rate & Temperature

The flow rate is defined as the speed at which the catholyte moves inside the cathodic compartment and it is fundamental to improve the solution homogeneity.

The temperature (*T*), on the other end, could influence both the solubility and the diffusion of CO_2. In detail, as explained in *chapter 4.4*, *T* could increase the product selectivity up to ~40%.

At first, the experiments were conducted using the unaltered setup described in *chapter 5.4*. The values of 10 mL/min and 30 mL/min were considered for the flow rate while values of 35 and 60°C were considered for the *T*.

The initial results indicated that a higher FE_{FA} could be achieved at a flow rate of 10 mL/min. However, it was also noticed that lower flow rates determined an inferior circulation of catholyte inside the thermostat and an increase of heat dispersion from the connecting pipes. Therefore that caused a decrease in the temperature of the catholyte. Because of that, it was unclear whether the FE_{FA} improvement was caused by a lower flow rate or a temperature decrease. To identify and differentiate their effects, the setup had to be modified. The cathodic reservoir was then immerged in a water bath and opportunely heated to the desired temperature by means of a heating plate. During the experiment, particular attention was paid to the inlet and outlet catholyte temperatures to ensure their constancy. Temperatures of 35°C and 60°C were studied at both 30 and 10 mL/min. The results are shown in *Figure 6.21.*

Flow rate and temperature show a similar effect on HER and FA production. In detail, the graph clearly shows that temperature and flow rate are inversely proportional to the FE_{FA}.

The results shows better performance at lower *T* (35°C) with ~12% improvement in FE_{FA}. In fact, as shown in *figure 6.22*, HER has a linear increase over time with a steeper slope at 60°C. This trend reflects the results reported in the literature (*Chapter 4.4*) as a temperature range of 35-50°C allows to operate at an optimal *S* and *D* compromise (*Figure 4.15*).[9,60] Nevertheless, only outermost temperatures of 35°C and 60°C were tested in this work making further investigation necessary. It should be pointed out that a larger cell size could lead to more rapid heat dispersion resulting in greater temperature inhomogeneity. Also, the temperature sensor was not placed directly in the cathode compartment (*figure 5.4*) but in the catholyte outlet tube. For this reason, the displayed temperatures may deviate from reality.

Finally, the literature mainly states that a lower flow rate generally leads to worse performance when a single-pass mode is adopted.[66] However, in this case, with a recirculating catholyte (batch mode), the opposite occurs and no relevant variations in pH were observed. The reason of such effect is not easy to determine as it could be mainly related to the design of the cell itself.

The energy efficiencies reported the same trend since different *T* and flow rates did not cause a voltage variation (*figure 6.23*).

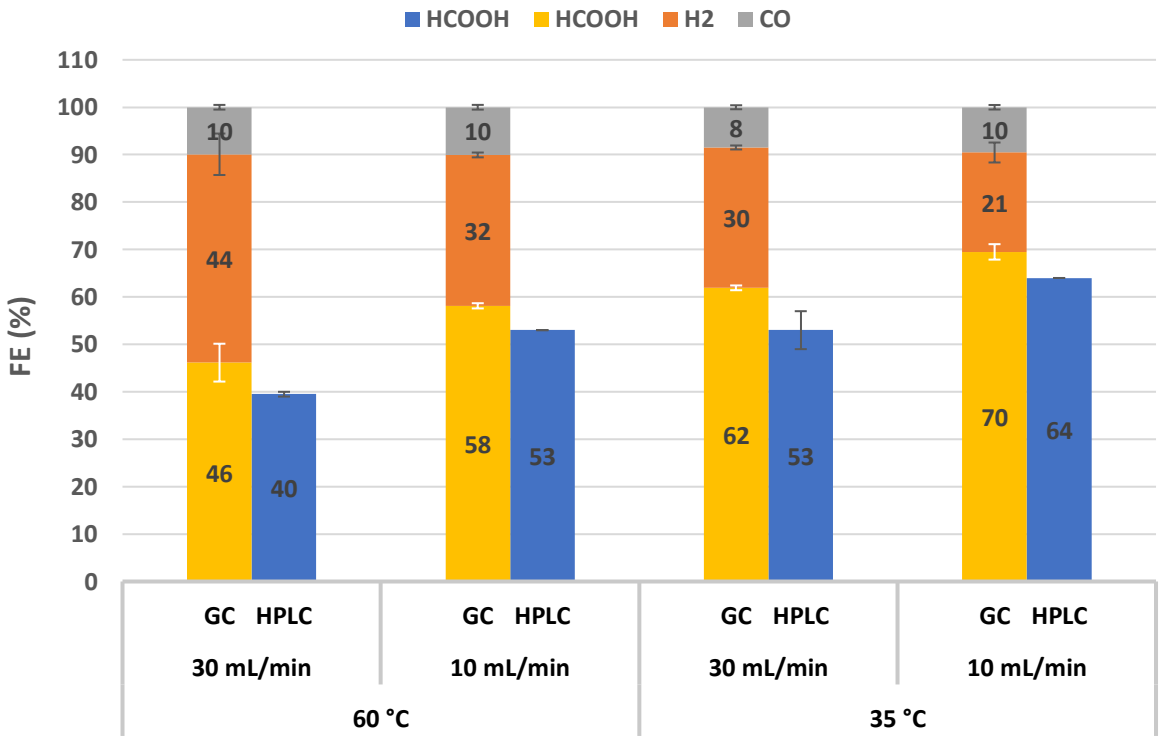

Figure 6.21. Effect of Temperature and flow rate on the CO_2RR. FF=0.5 mm; CP=1.6 bar; CD=-100 mA/cm^2; catholyte=0.5 M K_2SO_4; anolyte=bi-distilled water; t=120 min at CCE; catalyst: SnO_x@AB (2.76 and 2.84 wt.%); catholyte volume=250 mL.

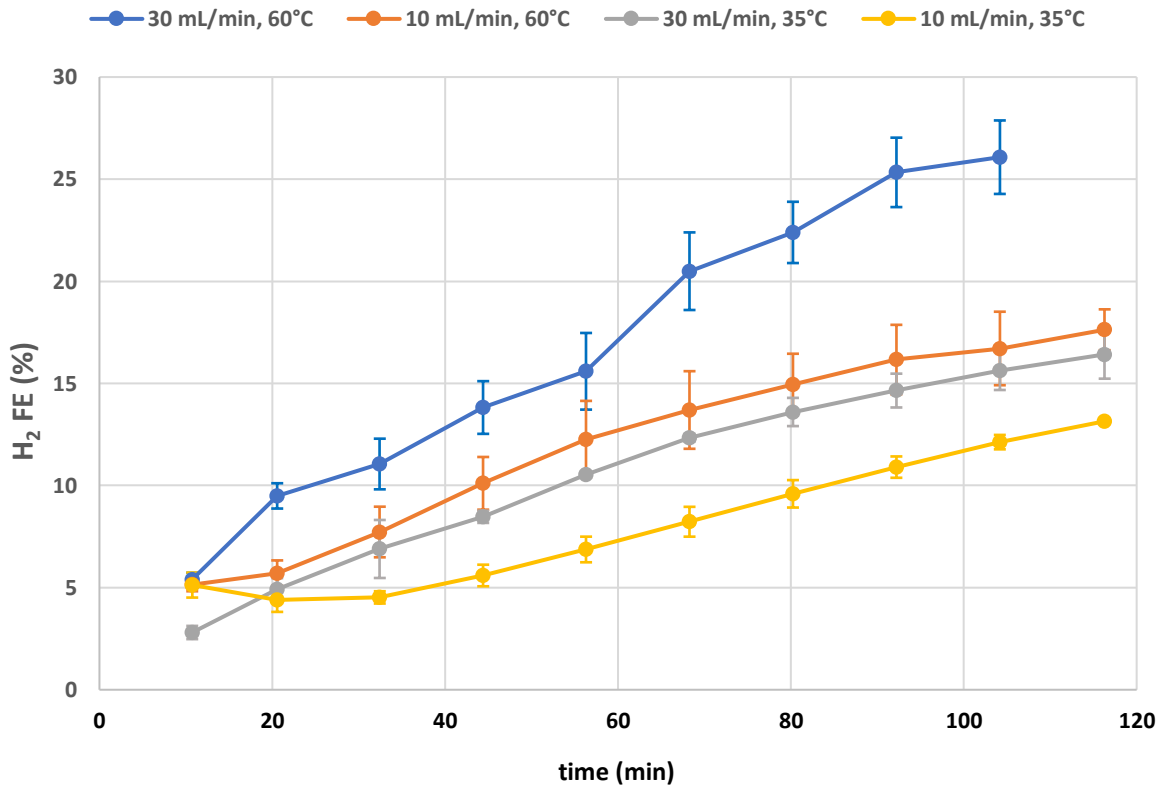

Figure 6.22. FE_{HER} over time. The experiments were conducted at different T and flow rate as indicated in the legend. FF=0.5 mm; CP=1.6 bar; CD=-100 mA/cm2; catholyte=0.5 M K_2SO_4; anolyte=bi-distilled water; t=120 min at CCE; catalyst: SnO_x@AB (2.76 and 2.84 wt.%); catholyte volume=250 mL.

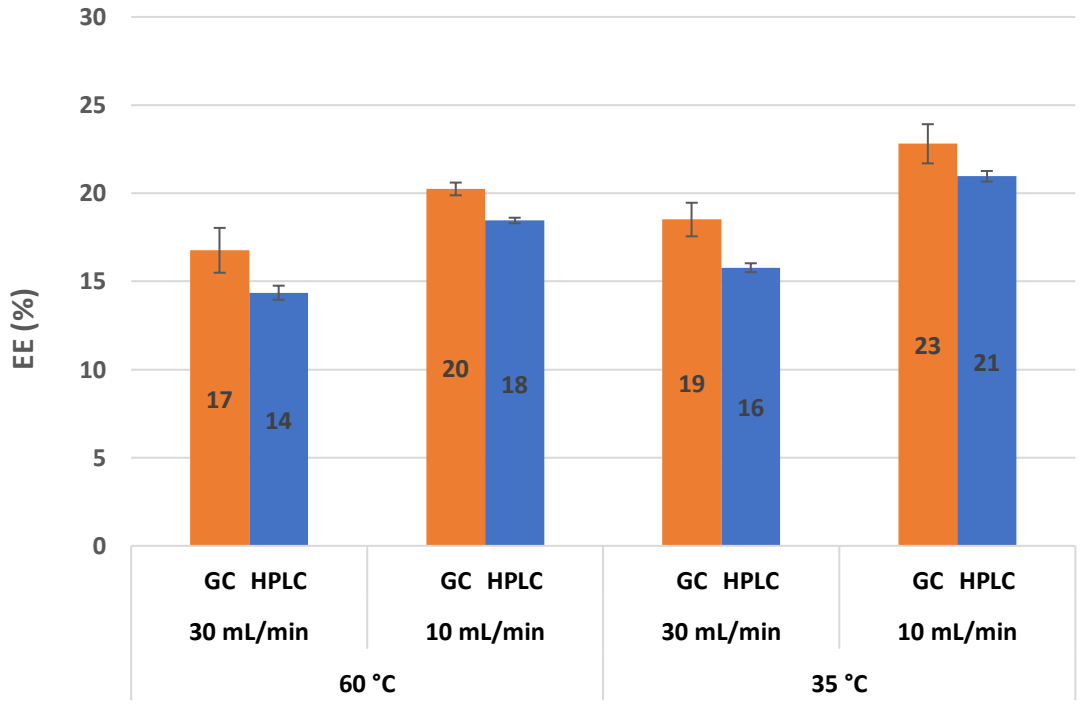

Figure 6.23. Energy efficiency vs T and Flow rate. CD=-100mA/cm^2; catholyte=0.5 K_2SO_4. FF=0.5 mm; CP=1.6 bar; anolyte=bi-distilled water; t=120 min at CCE; catalyst: SnO_x@AB (2.76 and 2.84 wt.%); catholyte volume=250 mL.

6.2.5 Current density

For the previous experiments, only CD of -100 mA/cm^2 were used. However, values below |CD|=200 mA/cm^2 should not be considered for industrial scale applications as they would lead to an inefficient process.[57] For that reason, higher current densities were tested with the aim of determining the 25 cm^2 cell limit.

Unsurprisingly, more negative current densities led to a lower FE_{FA} and higher φ_{cell}.[82] This caused an overall EE decrease of 7% when the CD was switched from -100 to -300 mA/cm^2.

With higher CD it was expected a greater H^+ production on the anodic compartment. That could eventually cause an excessive acidification of the catholyte and increase in HER. However, by looking at the pH trend in *figure 6.24c*, it appears that the catholyte show a pH difference of just ~0.2 which might be not enough to justify such increase in HER.

Therefore, at first instance, the reason of a higher HER is attributable to the CO_2 mass transport limitation at CD less negative than -100 mA/cm^2.

Alternatively, more negative current densities may also cause more negative potentials and a faster electrowetting, meaning that the electrolyte penetrates deeper into the GDE. That could lead to an excessive flooding with a consequent block of the CO_2 transport pores.

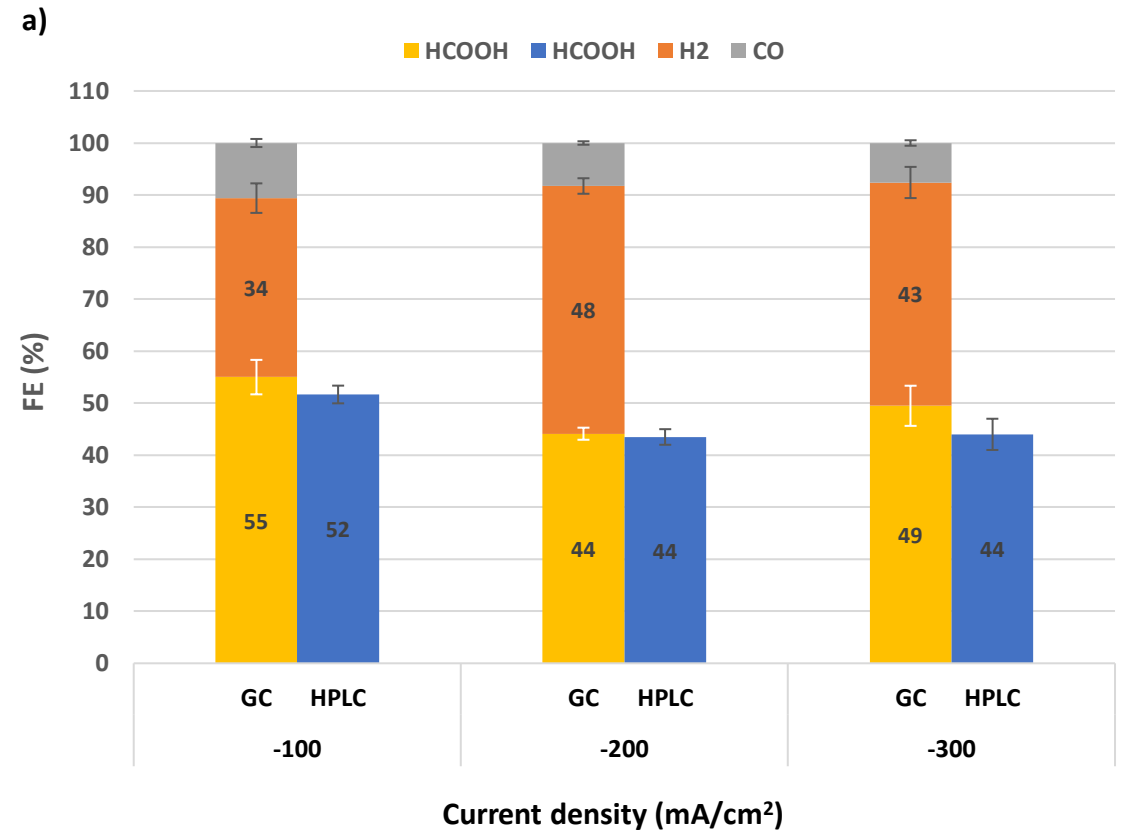
a)
HCOOH
HCOOH
H2
CO
FE (%)
110
100
90
80
70
60
50
40
30
20
10
0
34
55
52
48
44
44
43
49
44
GC
HPLC
GC
HPLC
GC
HPLC
-100
-200
-300
Current density (mA/cm²)

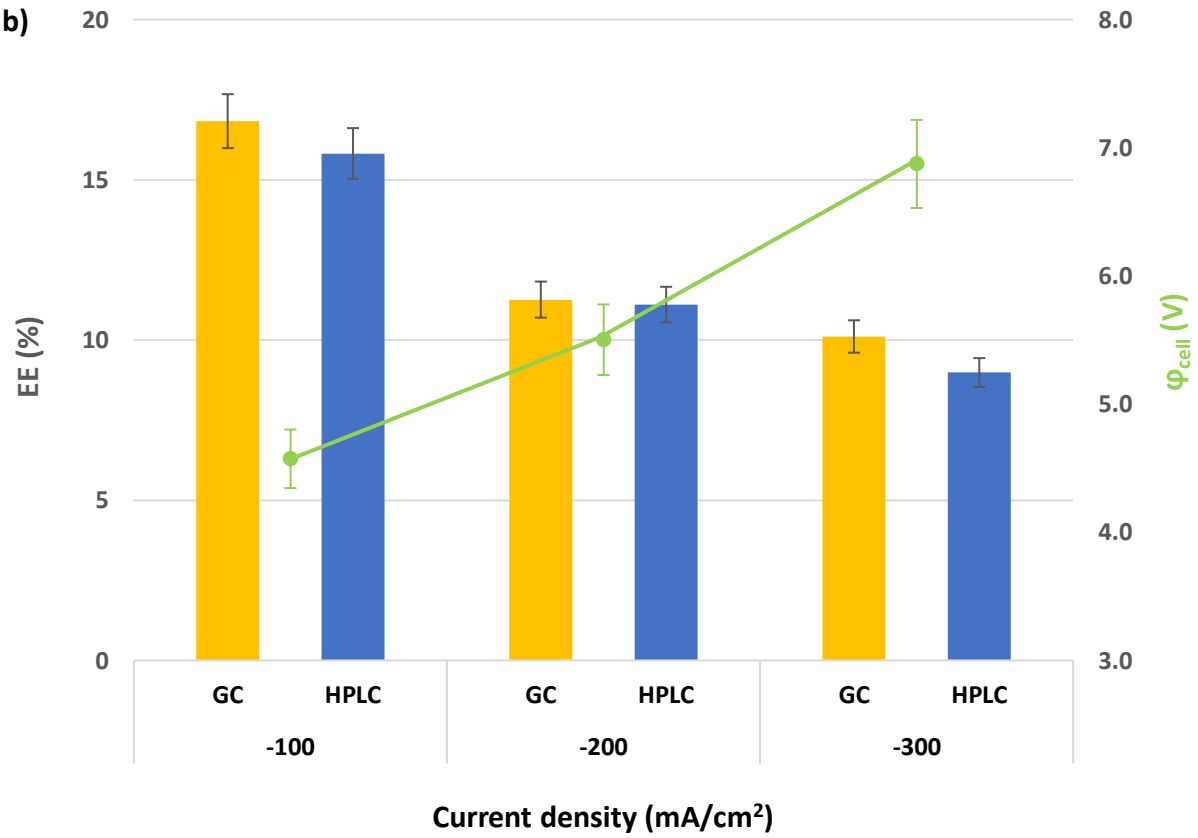
b)
EE (%)
20
15
10
5
0
8.0
7.0
6.0
5.0
4.0
3.0
φcell (V)
GC
HPLC
GC
HPLC
GC
HPLC
-100
-200
-300
Current density (mA/cm²)

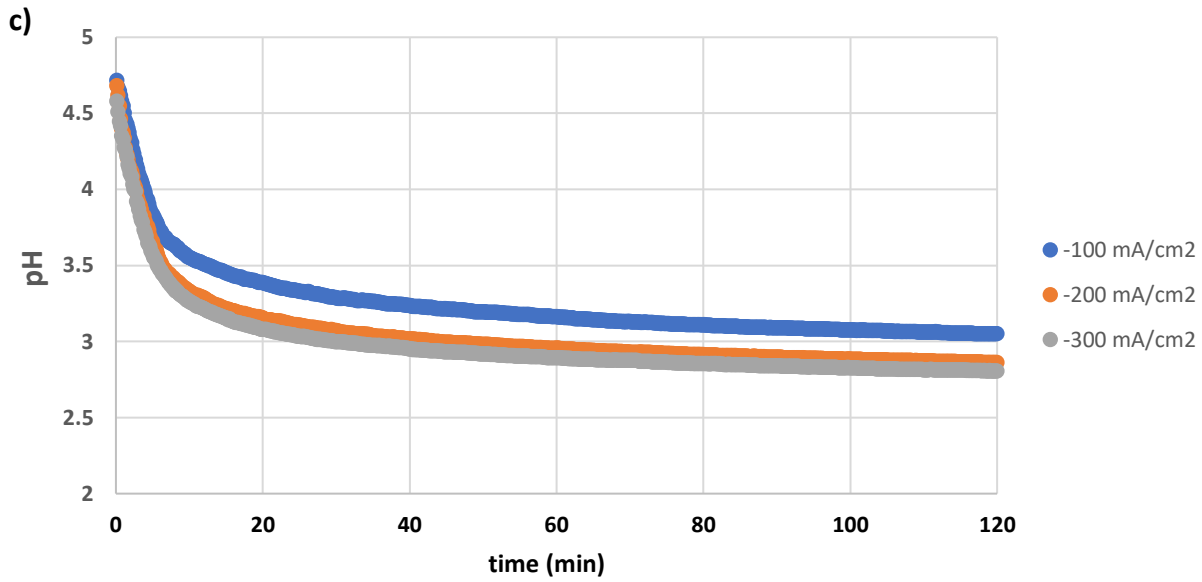

Figure 6.24. a) FE variation at different CD b) φ_{cell} and EE variation at different CD c) pH over time at different CD. FF=0.5 mm; CP=1.6 bar; T~42°C; catholyte=0.5 M K_2SO_4; flowrate=20 mL/min; anolyte=bi-distilled water; t=120 min at CCE; catalyst: SnO_x@AB (2.76 wt.%); catholyte volume=250 mL.

However, as expressed in *formula 3.9,* the overvoltage present a resistance contribution which depends on several features such membrane, electrolyte and electrodes. Because of that, part of the energy supplied is dissipated as heat (Joule effect). Consequently, when higher CD were used, the amount of dispersed heat increased with a consequent rise of the catholyte temperature. For that purpose, the catholyte T_{in} and T_{out} were measured through the use of sensors in proximity of the inlet and outlet channels. The results are reported in *Table 6.1* and demonstrate the presence of an actual variation of the inner cell catholyte temperature with different currents. For that reason, the real cause of decrease in FE_{FA} and EE, could be attributable to a limited solubility of CO_2 deriving from an excessive increase in the operating temperature.

Table 6.1. Approximative temperature variation from the inlet to the outlet at different current density.

Current density (mA/cm^2)	$\Delta T=T_{out}-T_{in}$ (°C)	T_{out} (°C)
-100	1	43
-200	10	52
-300	14	56

6.2.6 Electrolyte concentration

The eForFuel final aim is to produce renewable fuel by coupling the CO_2 electrochemical reduction to FA with the fermentation of FA by formatotrophic bacterias.[90] For that purpose, one of the most promising bacteria is the E. Coli which could be used to transform HCOOH into biofuel.[11,91] Even though the used sulphate salts are not toxic to microorganisms per se, a high salt concentration will negatively influence the growth rates, regardless of toxicity. For this reason, it was tested the possibility to conduct the experiments at lower K_2SO_4 amounts. Concentrations of 0.1, 0.25 and 0.5 M were examined but higher values could not be tested since a 0.5 M K_2SO_4 water solutions is nearly saturated.

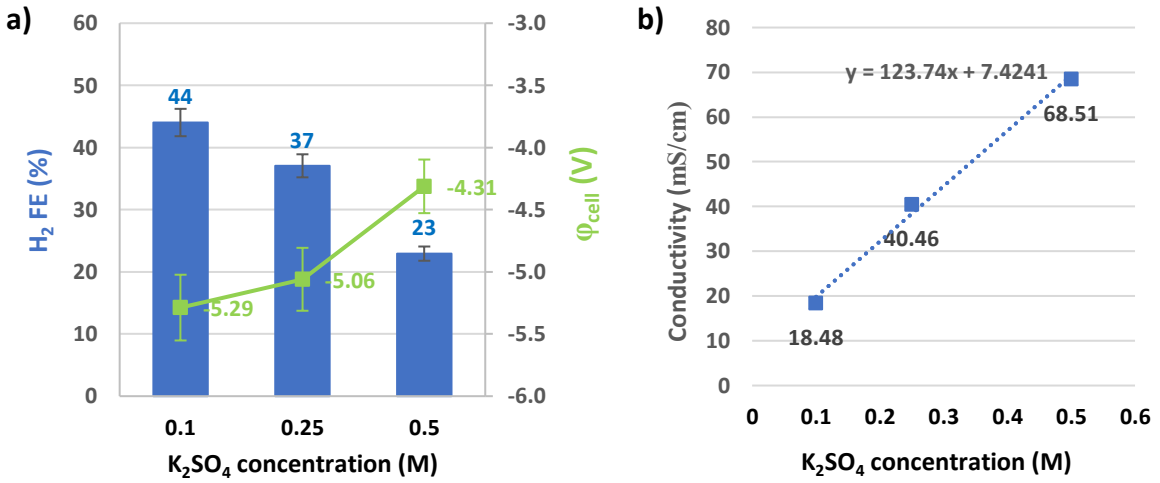

Figure 6.25. a) electrolyte concentration effects on φ_{cell} and HER. b) conductivity vs K_2SO_4 concentration. FF=0.5 mm; CP=1.6 bar; CD=-100 mA/cm^2; T~42°C; anolyte=bi-distilled water; flow rate=20 mL/min; t=120 min at CCE; catalyst: SnO_x@AB (2.62 and 2.67 wt.%); catholyte volume=250 mL.

A more negative cell voltage was observed when decreasing the electrolyte concentration since it led to a reduced catholyte conductivity and so to an increase in R_{cell} contribution.

Besides the voltage variation, an unexpected phenomenon was also noticed: when the electrolyte concentrations were increased, HER was observed to decrease instead. Such effect could be explained by the depletion of protons from K^+ ions near to the cathode surface which triggers CO_2 activation at the expense of H_2 formation.[92] In conclusion, the increase of salt concentration from 0.1 to 0.5 M determined an ECE increase of ~8%.

However, this part of the project is supposed to be better investigated by the Max-Planck-Institute of Molecular Plant Biology. Therefore, the actual benefits on the overall projects must be determined with the aim of defining the best compromise both for the production of FA and for its fermentation.

6.3 Catalysts and cells operability at single-pass mode

In the last part of this work, it was investigated the feasibility of a continuous single-pass operation mode for long-term CCE (8 h). The instrumentation was so adapted in order to allow the single passage of catholyte from a first reservoir to a "product collection reservoir".

The performances in the long run CCE were conducted for the Bi- and Sn-based catalyst in both the electrolyser. Also in this case, the catholyte amounts were adjusted according to the geometrical electrode surface and the chosen current density in order to obtain the same FA concentration in the final product collection reservoir. The flow rates were adapted at 6.25 mL/min and 0.25 mL/min respectively for the 25 cm^2 and 1 cm^2 cell. An actual comparison between the two cells could not be done since the scale up cell does not present any reference electrode, therefore, the *IR* compensation could not be applied.

In the 1 cm^2 cell, a CD of -100 mA/cm^2 was applied. The two catalyst performed very similarly both in product selectivity and cathodic voltage. Surprisingly, the ECE showed a value of ~20%, the same observed with a batch mode at CD of -400 mA/cm^2 (*catalyst reproducibility*).

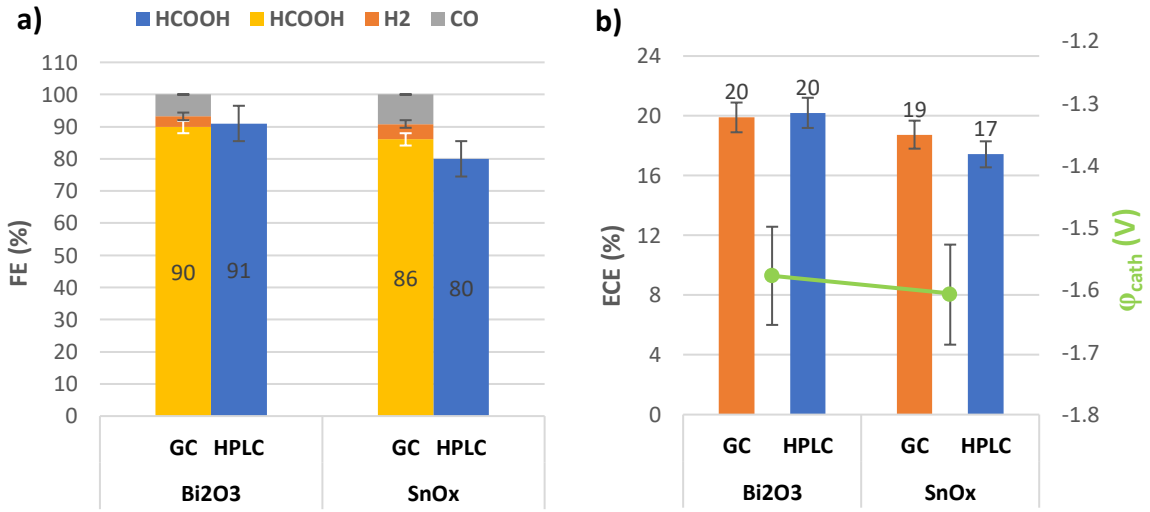

Figure 6.25. FE (a) and ECE (b) comparison between catalyst at single-pass modality in the 1 cm^2 cell. CD=-100 mA/cm^2; T=45°C; catholyte=0.5 M K_2SO_4; flowrate=0.25 mL/min; anolyte=bi-distilled water; flow rate=0.25 mL/min; t=480 min at CCE; catholyte volume=150 mL; catalysts: SnO_x@AB (2.44 and 2.32 wt%) and Bi_2O_3 (23.3 wt.%).

As concerns the scale up electrolyser, it showed a higher mismatch of selectivity between SnO_x@AB and Bi_2O_3@AB. In addition, an unprecedent FE_{FA} of ~90% could be achieved. On the other hand, the increase in φ_{cell} did not allow to reach EE above 19%. Such higher FA selectivity could be attributable to a lower acidification of the electrolyte due to the use of a larger volume (3L) and a single passage of the catholyte.

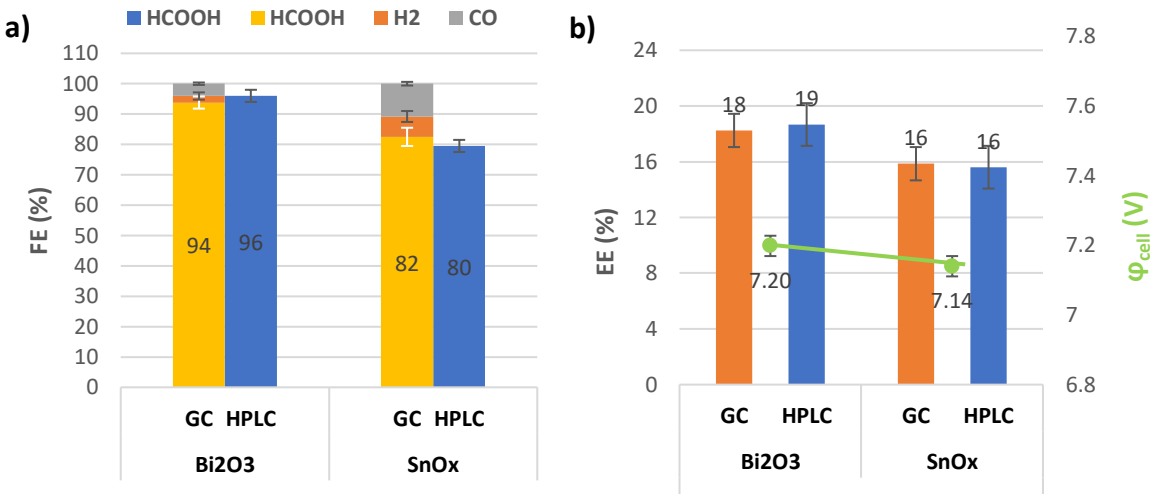

Figure 6.26. FE (a) and ECE (b)comparison between catalyst at single-pass modality in the 25 cm² cell. FF=0.5 mm; CP=1.6 bar; CD=-100 mA/cm²; T=45°C; catholyte=0.5 M K_2SO_4; flowrate=20 mL/min; anolyte=bi-distilled water; flow rate=6.25 mL/min; t=480 min at CCE; catholyte volume=3 L; catalysts: SnO_x@AB (2.44 and 2.32 wt%) and Bi_2O_3 (23.3 wt.%).

Overall, in accordance with the data depicted in *Chapter 6.1*, the Bi-based catalyst showed a higher FE_{FA} most likely because of its intrinsic higher selectivity to reduce CO_2 towards FA.[29,89] However, the ECE and EE - reported in *figure 6.25b* and *figure 6.26b* - indicate a negligible improvement to the cell efficiency as both SnO_x@AB and Bi_2O_3@AB presented very similar values.

Beside the high product selectivity, it is important to operate at pH lower than the pK_a of FA (pK_a =3.77) as we want the FA to be protonated. For that reason, it was analysed the pH of both the electrolyser at single-pass mode. As showed in *figure 6.26*, the catholyte present a much higher value compared to the batch mode (*figure 6.1 and 6.4c*) for both the electrolysers.

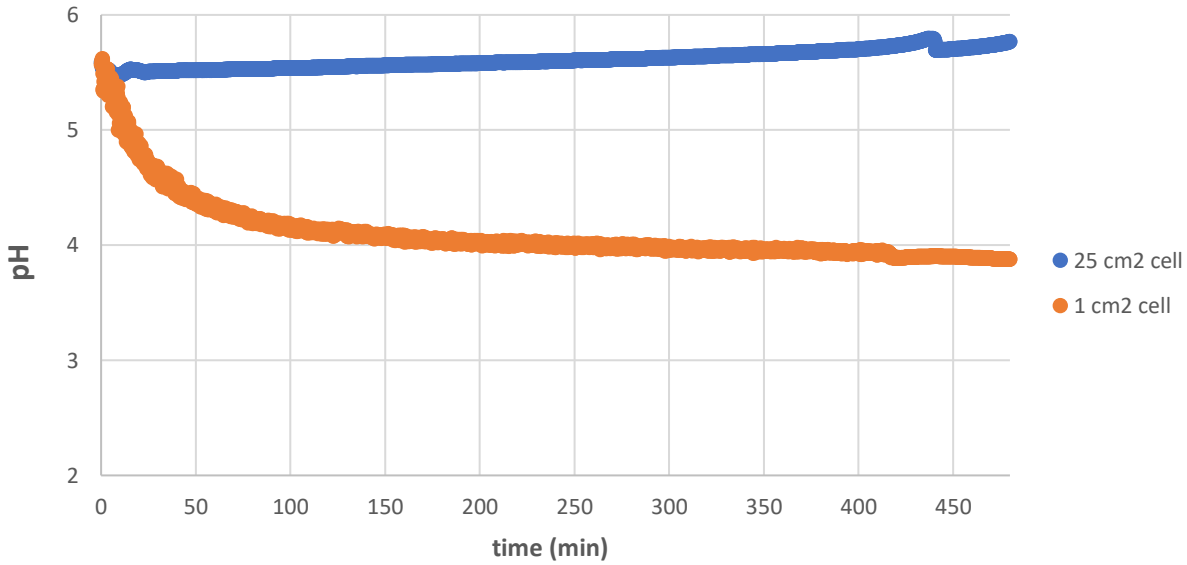

Figure 6.26. pH over time at single-pass mode in the 1 cm² cell (CD=-100 mA/cm²; T=45°C; catholyte=0.5 M K_2SO_4; anolyte=bi-distilled water; flow rate=0.25 mL/min; t=480 min at CCE; catholyte volume= 150 mL) and 25 cm² cell (FF=0.5 mm; CP=1.6 bar; CD=-100 mA/cm²; T=45°C; catholyte=0.5 M K_2SO_4; anolyte=bi-distilled water; flow rate=6.25 mL/min; t=480 min at CCE; catholyte volume= 3 L). Catalysts: SnO_x@AB (2.44 and 2.32 wt%) and Bi_2O_3 (23.3 wt.%).

From that point of view the single-pass mode failed as it did not show pH lower than 3.9. However, this could be adjusted with the use lower flow rates, as that could lead to an acidification of the catholyte.

7. Summary

Efforts were focused on the operability and scalability of CO_2RR under acidic conditions. As previously discussed, the importance of operating at low pH is a key aspect of the whole process as it would avoid the need for additional acidification steps which could compromise the overall efficiency.

The first part of this work aimed to define the performances and reproducibility of the catalysts by using a 1 cm^2 geometrical surface area electrolyser. Sn- and Bi-based GDEs were taken into account due to their great selectivity to FA production and low toxicity.[9,28,29] Both the catalysts performed successfully with FE_{FA} higher than 90% in the short period CCE (2 h) at CD=-400 mA/cm^2 and φ_{cath} of approximately -1.7 V. A slight superior FE_{FA} could be reached with the Bi-based catalyst because of its intrinsic product selectivity.[29,89] This allowed to reach values up to 95% even in the long run CCE (8 h) with a φ_{cath} of -1.7 V.

Consequently, it was investigated the feasibility to reach higher selectivity by increasing the amount of Bi-catalyst in the electrode but no relevant improvement could be achieved. For what concerns the catalyst loading reproducibility, while Sn wt.% showed similar values, not so reproducible Bi-loadings cold be achieved. Beside that, all the different batches performed in a very similar way with almost identical results both in product selectivity and cathodic voltage.

The central part of this work was instead the analysis of the scale up cell, characterised by the use of a 25 cm^2 geometrical surface area. As explained in *Chapter 5.2,* the electrolyser was designed with the concept of adjusting several design parameters in order to delineate the best configuration for future scale up developments. The multi-parameter nature of the system made its analysis challenging since a single variation led to an unpredictable response of the cell as result of different cause-effect events.

The first parameter investigated was the role played by different clamping pressures as a variation of the membrane-anode contact which could be suitably altered by using appropriate clamps. A CP increase led to lower φ_{cell} and FE_{FA}: while the anode-membrane contact resulted improved, on the other side of the cell, it determined a GDE damage and/or it caused a GDE-membrane contact with a consequent easing of the proton migration to the active sites. The best compromise was recorded at 1.6 bar, later used for the following experiments.

Similarly, it was noted that the GDE-membrane distance - and therefore the catholyte layer thickness - has a significant impact on the overall efficiency. For that purpose, appropriate spacers (flow field or FF) were used to examine it. The results depicted an overall decrease in both φ_{cell} and FE_{FA} when a thinner catholyte layer is employed. The 2 mm FF required the same cell voltage as the 1.3 mm FF, with an actual FE_{FA} improvement. Overall, it could be defined a strong dependence of HER from the cathode-membrane distance: with thinner flow fields - despite the nearly unchanged pH values - the H_2 evolution showed much higher values. It is supposed that the presence of a smaller inner cell electrolyte layer could cause an acidification of the GDE local pH and so a higher probability for the protons to reach

the catalyst surface. An attempt to prevent an excessive acidification was made by using a higher flow rate of 30 mL/min without any significant result.

In this work, most of the experiments were conducted in a batch mode, so the necessity of an adequate membrane was fundamental in order to avoid the product reoxidation. For that purpose, four different CEM were tested. Decent performances were observed with the FUmA-Tech® FKBPK130 and the Nafion® N324. Both the membranes showed a resistance to the FA crossover due to the presence of a dehydration layer which, on the other hand determined a conductivity reduction and a consequent increase of the total cell voltage. Specifically for this setup, the Nafion® N324 turned out to be the most suitable as it presented an adequate compromise between FA permeation and φ_{cell}. It was also distinguished by the presence of an integrated grid which served as structural support.

Afterwards, the electrolyte properties were tested with a particular attention to its temperature and flow rate. The first one turned out to play a key role due its connection with the CO_2 solubility and diffusion. As stated by literature, the best *T* compromise seems to be placed in the range 35-50°C [9,60] as lower and higher temperatures would cause a decrease in CO_2 diffusion and solubility respectively. For this reason, the 25 cm^2 electrolyser worked best at 35°C instead of 60°C. Regarding the electrolyte flow rate, a general drop in HER was noticed at lower values. The reason for this behaviour is still unclear and difficult to define as it could be mainly related to the cell design.

For what concerns the overall eForFuel project, the FA produced must then be converted into renewable fuels using specific formatothropic bacteria which could be particularly sensitive to the presence of electrolytes such sulphates. In this work, K_2SO_4 was used to increase the catholyte conductivity, therefore concentrations of 0.1, 0.25 and 0.5 M were compared to better understand if its amount could possibly be lowered. However, the catholyte showed 4 time higher conductivity when a 0.5 M solution was used instead of 0.1 M one. This resulted in a FE_{HER} decrease of 21%, with a consequent increase of 8% in energy efficiency. Such effect could be justified by the formation of a K^+ layer which inhibit the H^+ adsorption and reduction into the catalyst surface. In conclusion, the presence of electrolyte turned out to be essential, making it difficult to work at lower K_2SO_4 concentrations.

It has to be reminded that most of the scale up cell experiments were conducted at CD of -100 mA/cm^2. Yet, for sustainable industrial application, high cell efficiencies should be reached with $|CD| \geq 200$ mA/cm^2. Therefore, values of -100, -200 and -300 mA/cm^2 were tested and compared. The results defined a linear φ_{cell} increase (from 4.57 to 6.87 V) and a less uniform FE_{FA} decrease when switching from -100 to -300 mA/cm^2. Also, the cell EE reported a decrease of 7%. More negative CD determined more negative potentials and a faster electrowetting. That could have lead to an excessive flooding with a consequent block of the CO_2 transport pores. Also, it was observed a *T* catholyte increase of 10 and 14°C at CD of -200 and -300 mA/cm^2 respectively which brought the catholyte *T* at values of 52 and 56°C with possible negative effects on the CO_2 solubility and so FE_{FA}.

Finally, a single-pass mode allowed to reach FE_{FA} up to 90% for both setups but sufficient acidification could not be achieved in both the electrolysers (pH>3.77). Because of that, formate was produced instead of FA making this continuous operation not compatible with the project.

8. Outlook

The development of an industrial scale CO_2RR electrolyser still require major efforts before being sustainable both from a economic and technical point of view. Some of the key points that will have to be taken into consideration for future analysis are described in this chapter.

Still, the catalyst analysis will be of paramount importance. So far the Bi-based catalyst showed the most promising performances for the FA production under acidic conditions. Nevertheless, further analysis should be done with particular attention to its loading and reproducibility. Also, further considerations over the higher mismatch between the online GC and offline HPLC measurement are needed since the product loss could represent a big limitation of the catalyst itself. Alternative substrate should also be examined in order to increase the overall GDE durability.

Despite the scale up electrolyser allowed to achieve FE_{FA} up to 90%, the potential needed to reach it turned out to be the main limit. For a relevant decrease of the cell energy consumption it will be essential to pay a particular attention at the different materials which make up the electrolyser. For that purpose, beside the cathodic materials, alternative anodes should be studied as reported in recent researches.[93] Further analysis over of the electrolyte type and concentration could also be relevant since, as previously mentioned, the catholyte allow a substantial EE improvement due to a increase of conductivity. Given the scope of the project, the choice of the electrolyser should be found in cooperation with the Max-Plank-Institute in view of facilitating the bacteria operability.[90]

Other 'electrolyte-linked' variables include the temperature and flow rate. The first one should be investigated at multiple values in the 35-50 °C range and eventually introduce an 'internal' T sensor in order to have a more accurate measurement. On the other hand, the flow rate analysis should also be deepened both for the batch and single-pass mode.

In future investigations, the scale up design should be able to improve the anode-membrane contact by supporting higher CP. In order to achieve that, the flow field structure should be redesigned in such a way as to prevent GDE damages. Concomitantly, the role of the FF thickness should be further investigated to define an optimal distance between electrode and membrane without leading to excessive cell voltage. Nevertheless, the GDE-membrane distance demonstrated to be an important feature to consider when designing an electrolyser. The adequate value must be defined in order to improve both the product selectivity and the cell voltage.

Finally, the single-pass operation mode will need to be reconsidered for the scale up cell. In detail an acidic environment must be reached while maintaining an adequate FE_{FA} and φ_{cell}. This could be achieved by adopting a lower catholyte flow rate as described in similar cell configurations.[66] In alternative, pre-acidified electrolytes could be considered.

Overall, the scale up cell design described here indicated a potential pathway for further cell enlargement. In view of this, the considerations presented in this work want to make a contribution to its development.

9. BIBLIOGRAPHY

1. Lamb, W. F. *et al.* A review of trends and drivers of greenhouse gas emissions by sector from 1990 to 2018. *Environ. Res. Lett.* **16**, (2021).
2. Ahmad, T. & Zhang, D. A critical review of comparative global historical energy consumption and future demand: The story told so far. *Energy Reports* **6**, 1973–1991 (2020).
3. eurostat energy. https://ec.europa.eu/eurostat/cache/infographs/energy/bloc-2a.html?lang=en.
4. Velasquez, C. E., e Estanislau, F. B. G. L., Costa, A. L. & Pereira, C. Assessment of the French nuclear energy system – A case study. *Energy Strateg. Rev.* **30**, (2020).
5. Fyke, A. The Fall and Rise of Gravity Storage Technologies. *Joule* **3**, 625–630 (2019).
6. Gravitricitry. https://gravitricity.com/technology/.
7. Ambri. https://ambri.com/technology/.
8. Bienen, F. *et al.* Degradation study on tin- and bismuth-based gas-diffusion electrodes during electrochemical CO2 reduction in highly alkaline media. *J. Energy Chem.* **62**, 367–376 (2021).
9. Löwe, A. *et al.* Influence of Temperature on the Performance of Gas Diffusion Electrodes in the CO2 Reduction Reaction. *ChemElectroChem* **6**, 4497–4506 (2019).
10. Burdyny, T. & Smith, W. A. CO2 reduction on gas-diffusion electrodes and why catalytic performance must be assessed at commercially-relevant conditions. *Energy Environ. Sci.* **12**, 1442–1453 (2019).
11. eForfuel. https://www.eforfuel.eu/.
12. Kopljar, D., Wagner, N. & Klemm, E. Transferring Electrochemical CO2 Reduction from Semi-Batch into Continuous Operation Mode Using Gas Diffusion Electrodes. *Chem. Eng. Technol.* **39**, 2042–2050 (2016).
13. Oßkopp, M. *et al.* Producing formic acid at low pH values by electrochemical CO2 reduction. *J. CO2 Util.* (2021) doi:10.1016/j.jcou.2021.101823.
14. *Allen J. Bard and Larry R. Faulkner, Electrochemical Methods: Fundamentals and Applications, New York: Wiley, 2001, 2nd ed.*.
15. Kear, Gareth and Frank C. Walsh. “The characteristics of a true Tafel slope.” (2005).
16. Luckarift, H. R., Atanassov, P. & Johnson, G. R. *Enzymatic Fuel Cells: From Fundamentals to Applications*. *Enzymatic Fuel Cells: From Fundamentals to Applications* vol. 9781118369 (2014).
17. Gschwend, G. C. & Girault, H. H. Discrete Helmholtz model: a single layer of correlated counter-ions. Metal oxides and silica interfaces, ion-exchange and biological membranes. *Chem. Sci.* **11**, 10304–10312 (2020).
18. Matsumoto, M, ‘Electrocapillarity and double layer structure,’ in Electrical phenomena at interfaces: fundamentals, measurements, and applications, vol. 76, Surfactant science series, H. Ohshima, & Furusawa, K., Ed., 2nd ed. New York: Marcel Dekker, Inc.,. in.
19. Gamry. https://www.gamry.com/application-notes/instrumentation/understanding-ir-

compensation/.

20. Sun, Y. *et al. Applications of MXenes and their composites in catalysis and photoelectrocatalysis*. *MXenes and their Composites: Synthesis, Properties and Potential Applications* (INC, 2021). doi:10.1016/B978-0-12-823361-0.00007-1.

21. Zhao, J. *et al.* An overview of Cu-based heterogeneous electrocatalysts for CO2 reduction. *J. Mater. Chem. A* **8**, 4700–4734 (2020).

22. Kopljar, D., Inan, A., Vindayer, P., Wagner, N. & Klemm, E. Electrochemical reduction of CO2 to formate at high current density using gas diffusion electrodes. *J. Appl. Electrochem.* **44**, 1107–1116 (2014).

23. Liu, X., Zhong, H., Wang, C., He, D. & Jin, F. CO2 reduction into formic acid under hydrothermal conditions: A mini review. *Energy Sci. Eng.* 1–13 (2022) doi:10.1002/ese3.1064.

24. Sun, D., Xu, X., Qin, Y., Jiang, S. P. & Shao, Z. Rational Design of Ag-Based Catalysts for the Electrochemical CO2 Reduction to CO: A Review. *ChemSusChem* **13**, 39–58 (2020).

25. Hori, Y., Wakebe, H. H. I., Tsukamoto, T. & Koga, O. 堀先生：金属電極における二酸化炭素還元２. *Electrochim. Acta* **39**, 1833–1839 (1994).

26. Pander, J. E., Baruch, M. F. & Bocarsly, A. B. Probing the Mechanism of Aqueous CO2 Reduction on Post-Transition-Metal Electrodes using ATR-IR Spectroelectrochemistry. *ACS Catal.* **6**, 7824–7833 (2016).

27. Wu, D., Hao, J., Song, Z., Fu, X. Z. & Luo, J. L. All roads lead to Rome: An energy-saving integrated electrocatalytic CO2 reduction system for concurrent value-added formate production. *Chem. Eng. J.* **412**, 127893 (2021).

28. U.S.G.S. *Mineral Commodity Summaries 2022 - Zeolites*. (2022).

29. An, X. *et al.* Common strategies for improving the performances of tin and bismuth-based catalysts in the electrocatalytic reduction of CO2 to formic acid/formate. *Renew. Sustain. Energy Rev.* **143**, 110952 (2021).

30. Hoflund, G. B. & Corallo, G. R. Electron-energy-loss study of the oxidation of polycrystalline tin. *Phys. Rev. B* **46**, 7110–7120 (1992).

31. Baruch, M. F., Pander, J. E., White, J. L. & Bocarsly, A. B. Mechanistic Insights into the Reduction of CO2 on Tin Electrodes using in Situ ATR-IR Spectroscopy. *ACS Catal.* **5**, 3148–3156 (2015).

32. Chen, Y. & Kanan, M. W. Tin oxide dependence of the CO 2 reduction efficiency on tin electrodes and enhanced activity for tin/tin oxide thin-film catalysts. *J. Am. Chem. Soc.* **134**, 1986–1989 (2012).

33. Kapusta, S. & Hackerman, N. The Electroreduction of Carbon Dioxide and Formic Acid on Tin and Indium Electrodes. *J. Electrochem. Soc.* **130**, 607–613 (1983).

34. Luc, W. W. *et al.* Subscriber access provided by UNIV OF CALIFORNIA SAN DIEGO LIBRARIES Ag-Sn Bimetallic Catalyst with a Core-Shell Structure for CO 2 Reduction. *J. Am. Chem. Soc., Just Accept. Manuscr. • Publ. Date* 17 (2017).

35. Lee, C. W., Cho, N. H., Yang, K. D. & Nam, K. T. Reaction Mechanisms of the Electrochemical Conversion of Carbon Dioxide to Formic Acid on Tin Oxide Electrodes. *ChemElectroChem* **4**, 2130–2136 (2017).

36. Li, F., Chen, L., Knowles, G. P., MacFarlane, D. R. & Zhang, J. Hierarchical Mesoporous

SnO2Nanosheets on Carbon Cloth: A Robust and Flexible Electrocatalyst for CO2Reduction with High Efficiency and Selectivity. *Angew. Chemie - Int. Ed.* **56**, 505–509 (2017).

37. Sen, S., Brown, S. M., Leonard, M. L. & Brushett, F. R. Electroreduction of carbon dioxide to formate at high current densities using tin and tin oxide gas diffusion electrodes. *J. Appl. Electrochem.* **49**, 917–928 (2019).

38. Zhang, R., Lv, W. & Lei, L. Role of the oxide layer on Sn electrode in electrochemical reduction of CO 2 to formate. *Appl. Surf. Sci.* **356**, 24–29 (2015).

39. Won, D. H. *et al.* Rational Design of a Hierarchical Tin Dendrite Electrode for Efficient Electrochemical Reduction of CO2. *ChemSusChem* **8**, 3092–3098 (2015).

40. Kumar, B. *et al.* Reduced SnO2 Porous Nanowires with a High Density of Grain Boundaries as Catalysts for Efficient Electrochemical CO2-into-HCOOH Conversion. *Angew. Chemie - Int. Ed.* **56**, 3645–3649 (2017).

41. Qiu, Y., Du, J., Dai, C., Dong, W. & Tao, C. Bismuth Nano-Flowers as a Highly Selective Catalyst for Electrochemical Reduction of CO 2 to Formate . *J. Electrochem. Soc.* **165**, H594–H600 (2018).

42. Miao, C. C. & Yuan, G. Q. Morphology-Controlled Bi2O3 Nanoparticles as Catalysts for Selective Electrochemical Reduction of CO2 to Formate. *ChemElectroChem* **5**, 3741–3747 (2018).

43. Pourbaix, M., Zhang, H. & Pourbaix, A. Presentation of an Atlas of chemical and electrochemical equilibria in the presence of a gaseous phase. *Mater. Sci. Forum* **251**–**254**, 143–148 (1997).

44. Vivier, V. *et al.* Electrochemical Study of Bi[sub 2]O[sub 3] and Bi[sub 2]O[sub 2]CO[sub 3] by Means of a Cavity Microelectrode. I. Observed Phenomena and Direct Analysis of Results. *J. Electrochem. Soc.* **147**, 4252 (2000).

45. Koh, J. H. *et al.* Facile CO2 Electro-Reduction to Formate via Oxygen Bidentate Intermediate Stabilized by High-Index Planes of Bi Dendrite Catalyst. *ACS Catal.* **7**, 5071–5077 (2017).

46. Methods, O. *Edition 95*. *Journal of the American Pharmaceutical Association* (1942).

47. Löwe, A. *et al.* Optimizing Reaction Conditions and Gas Diffusion Electrodes Applied in the CO2Reduction Reaction to Formate to Reach Current Densities up to 1.8 A cm-2. *ACS Sustain. Chem. Eng.* **9**, 4213–4223 (2021).

48. Martínez-Rodríguez, M. J. *et al.* Effect of microporous layer on MacMullin number of carbon paper gas diffusion layer. *J. Power Sources* **207**, 91–100 (2012).

49. Liang, S., Altaf, N., Huang, L., Gao, Y. & Wang, Q. Electrolytic cell design for electrochemical CO2 reduction. *J. CO2 Util.* **35**, 90–105 (2020).

50. Liu, L. X. *et al.* Tuning Sn3O4 for CO2 reduction to formate with ultra-high current density. *Nano Energy* **77**, 105296 (2020).

51. Li, J. *et al.* Two-Dimensional SnO 2 Nanosheets for Efficient Carbon Dioxide Electroreduction to Formate . *ACS Sustain. Chem. Eng.* **8**, 4975–4982 (2020).

52. Yu, J., Yoshikawa, Y., Matsuura, T., Islam, M. N. & Hori, M. Preparing gas-diffusion layers of PEMFCs with a dry deposition technique. *Electrochem. Solid-State Lett.* **8**, 152–155 (2005).

53. Bienen, F. *et al.* Importance of Time-Dependent Wetting Behavior of Gas-Diffusion

Electrodes for Reactivity Determination. *Chemie-Ingenieur-Technik* **93**, 1015–1019 (2021).

54. Braverman, S., Cherkinsky, M. & Birsa, M. L. Reduction of Carbon Dioxide. *Four Carbon-Heteroatom Bond.* 1 (2005) doi:10.1055/sos-sd-018-00074.

55. Rabiee, H. *et al.* Gas diffusion electrodes (GDEs) for electrochemical reduction of carbon dioxide, carbon monoxide, and dinitrogen to value-added products: A review. *Energy Environ. Sci.* **14**, 1959–2008 (2021).

56. Detailing, G. H-Cell Product Information. **10059**, 2016–2017 (2017).

57. Weekes, D. M., Salvatore, D. A., Reyes, A., Huang, A. & Berlinguette, C. P. Electrolytic CO2 Reduction in a Flow Cell. *Acc. Chem. Res.* **51**, 910–918 (2018).

58. Ma, D., Jin, T., Xie, K. & Huang, H. An overview of flow cell architecture design and optimization for electrochemical CO2reduction. *J. Mater. Chem. A* **9**, 20897–20918 (2021).

59. Mahmood, M. N., Masheder, D. & Harty, C. J. Use of gas-diffusion electrodes for high-rate electrochemical reduction of carbon dioxide. II. Reduction at metal phthalocyanine-impregnated electrodes. *J. Appl. Electrochem.* **17**, 1223–1227 (1987).

60. Dufek, E. J., Lister, T. E. & McIlwain, M. E. Bench-scale electrochemical system for generation of CO and syn-gas. *J. Appl. Electrochem.* **41**, 623–631 (2011).

61. Whipple, D. T., Finke, E. C. & Kenis, P. J. A. Microfluidic reactor for the electrochemical reduction of carbon dioxide: The effect of pH. *Electrochem. Solid-State Lett.* **13**, 109–111 (2010).

62. Lu, X., Leung, D. Y. C., Wang, H. & Xuan, J. A high performance dual electrolyte microfluidic reactor for the utilization of CO2. *Appl. Energy* **194**, 549–559 (2017).

63. Lu, X., Leung, D. Y. C., Wang, H., Maroto-Valer, M. M. & Xuan, J. A pH-differential dual-electrolyte microfluidic electrochemical cells for CO2 utilization. *Renew. Energy* **95**, 277–285 (2016).

64. Lu, X., Leung, D. Y. C., Wang, H. & Xuan, J. Microfluidics-based pH-differential reactor for CO2 utilization: A mathematical study. *Appl. Energy* **227**, 525–532 (2018).

65. Lee, W., Kim, Y. E., Youn, M. H., Jeong, S. K. & Park, K. T. Catholyte-Free Electrocatalytic CO2 Reduction to Formate. *Angew. Chemie - Int. Ed.* **57**, 6883–6887 (2018).

66. Yang, H., Kaczur, J. J., Sajjad, S. D. & Masel, R. I. Electrochemical conversion of CO2 to formic acid utilizing Sustainion™ membranes. *J. CO2 Util.* **20**, 208–217 (2017).

67. Yang, H., Kaczur, J. J., Sajjad, S. D. & Masel, R. I. Performance and long-term stability of CO2conversion to formic acid using a three-compartment electrolyzer design. *J. CO2 Util.* **42**, 101349 (2020).

68. Covestro OCD. https://www.covestro.com/-/media/covestro/corporate/sustainability/flagship-solutions/oxygen-depolarized-cathode/documents/3_6_covestro_produktblatt_oxygendepolarized_cathode_en_2017_te_v02.pdf?la=en&hash=6099CDF7D4CD229E68CF03BBE4E5D36AE73E2C5C.

69. Anonymous. CO2 for a Clean Performance: Rheticus Research Project Enters Phase 2. *Evonik* 2–5 (2019).

70. Wu, J., Risalvato, F. G., Ma, S. & Zhou, X. D. Electrochemical reduction of carbon dioxide III. the role of oxide layer thickness on the performance of Sn electrode in a full

electrochemical cell. *J. Mater. Chem. A* **2**, 1647–1651 (2014).

71. Bondue, C. J., Graf, M., Goyal, A. & Koper, M. T. M. Suppression of Hydrogen Evolution in Acidic Electrolytes by Electrochemical CO2Reduction. *J. Am. Chem. Soc.* **143**, 279–285 (2021).

72. Sigma aldrich. https://www.sigmaaldrich.com/IT/it/product/sigma/s5761.

73. Prakash, G. K. S., Viva, F. A. & Olah, G. A. Electrochemical reduction of CO 2 over Sn-Nafion ® coated electrode for a fuel-cell-like device. *J. Power Sources* **223**, 68–73 (2013).

74. Kim, H. Y. *et al.* Analysis on the effect of operating conditions on electrochemical conversion of carbon dioxide to formic acid. *Int. J. Hydrogen Energy* **39**, 16506–16512 (2014).

75. Tasic, G. S., Maslovara, S. P., Zugic, D. L., Maksic, A. D. & Marceta Kaninski, M. P. Characterization of the Ni-Mo catalyst formed in situ during hydrogen generation from alkaline water electrolysis. *Int. J. Hydrogen Energy* **36**, 11588–11595 (2011).

76. Mizuno, T. *et al.* Effect of temperature on electrochemical reduction of high-pressure CO2 with In, Sn, and Pb electrodes. *Energy Sources* **17**, 503–508 (1995).

77. Tamimi, A., Rinker, E. B. & Sandall, O. C. Diffusion Coefficients for Hydrogen Sulfide, Carbon Dioxide, and Nitrous Oxide in Water over the Temperature Range 293–368 K. *J. Chem. Eng. Data* **39**, 330–332 (1994).

78. Cadogan, S. P., Maitland, G. C. & Trusler, J. P. M. Diffusion coefficients of CO2 and N2 in water at temperatures between 298.15 K and 423.15 K at pressures up to 45 MPa. *J. Chem. Eng. Data* **59**, 519–525 (2014).

79. Unver, A. A. & Himmelblau, D. M. Diffusion Coefficients of CO2, C2H4, C3H6, and C4H8 in Water from 6° to 65° C. *J. Chem. Eng. Data* **9**, 428–431 (1964).

80. Harneo, H. S. & Davis, R. The Ionization Constant of Carbonic Acid in Water and the Solubility of Carbon Dioxide in Water and Aqueous Salt Solutions from 0 to 50°. *J. Am. Chem. Soc.* **65**, 2030–2037 (1943).

81. Duan, Z. & Sun, R. An improved model calculating CO 2 solubility in pure water and aqueous NaCl solutions from 273 to 533 K and from 0 to 2000 bar. *Chem. Geol.* **193**, 257–271 (2003).

82. Zhang, Z. *et al.* pH Matters When Reducing CO2in an Electrochemical Flow Cell. *ACS Energy Lett.* **5**, 3101–3107 (2020).

83. Jeong, K. J. *et al.* Fuel crossover in direct formic acid fuel cells. *J. Power Sources* **168**, 119–125 (2007).

84. Rhee, Y. W., Ha, S. Y. & Masel, R. I. Crossover of formic acid through Nafion® membranes. *J. Power Sources* **117**, 35–38 (2003).

85. Grot, W. Commercial Membrane Types. *Fluorinated Ionomers* 185–199 (2011) doi:10.1016/b978-1-4377-4457-6.10007-x.

86. Rice, C. *et al.* Direct formic acid fuel cells. *J. Power Sources* **111**, 83–89 (2002).

87. N D-S P Ul t ra s o n i c L A B.

88. Fkbpk130. https://www.fuelcellstore.com/fumasep-fkb.

89. Lee, C. W. *et al.* Selective Electrochemical Production of Formate from Carbon Dioxide with Bismuth-Based Catalysts in an Aqueous Electrolyte. *ACS Catal.* **8**, 931–937 (2018).

90. Oßkopp, M., Löwe, A. & Klemm, E. Acidic CO 2 electrolysis to formic acid for microbial conversion towards chemicals . *Chemie Ing. Tech.* **92**, 1275–1276 (2020).

91. Kim, S. J., Yoon, J., Im, D. K., Kim, Y. H. & Oh, M. K. Adaptively evolved Escherichia coli for improved ability of formate utilization as a carbon source in sugar-free conditions. *Biotechnol. Biofuels* **12**, 1–12 (2019).

92. Huang, J. E. *et al.* CO2 electrolysis to multicarbon products in strong acid. *Science (80-.).* **372**, 1074–1078 (2021).

93. Ma, S., Luo, R., Moniri, S., Lan, Y. & Kenis, P. J. A. Efficient Electrochemical Flow System with Improved Anode for the Conversion of CO 2 to CO . *J. Electrochem. Soc.* **161**, F1124–F1131 (2014).